NAVAL POSTGRADUATE SCHOOL

MONTEREY, CALIFORNIA

THESIS

EVALUATING EFFECTIVENESS OF DIRECTIONAL ACOUSTIC MODEMS INTEGRATED ONTO AUTONOMOUS PLATFORMS

by

Leander J. C. van Schriek

June 2018

Thesis Advisor: Kevin B. Smith
Co-Advisor: Douglas P. Horner

THIS PAGE INTENTIONALLY LEFT BLANK

REPORT DOCUMENTATION PAGE			*Form Approved OMB No. 0704-0188*

1. AGENCY USE ONLY *(Leave blank)*	**2. REPORT DATE** June 2018	**3. REPORT TYPE AND DATES COVERED** Master's thesis

4. TITLE AND SUBTITLE EVALUATING EFFECTIVENESS OF DIRECTIONAL ACOUSTIC MODEMS INTEGRATED ONTO AUTONOMOUS PLATFORMS	**5. FUNDING NUMBERS** NRP/CRUSER
6. AUTHOR(S) Leander J. C. van Schriek	
7. PERFORMING ORGANIZATION NAME(S) AND ADDRESS(ES) Naval Postgraduate School Monterey, CA 93943-5000	**8. PERFORMING ORGANIZATION REPORT NUMBER**
9. SPONSORING / MONITORING AGENCY NAME(S) AND ADDRESS(ES) N/A	**10. SPONSORING / MONITORING AGENCY REPORT NUMBER**

11. SUPPLEMENTARY NOTES The views expressed in this thesis are those of the author and do not reflect the official policy or position of the Department of Defense or the U.S. Government.

12a. DISTRIBUTION / AVAILABILITY STATEMENT Approved for public release. Distribution is unlimited.	**12b. DISTRIBUTION CODE** A

13. ABSTRACT (maximum 200 words)

Navies have been operating with unmanned underwater vehicles (UUVs) for decades. Recently, these platforms are assigned more and more complicated tasks. Compared to other domains, the underwater domain offers substantial additional challenges. One of these challenges is accurate navigation of these UUVs.

In this thesis, the use of directional acoustic modems integrated onto autonomous platforms is evaluated, specifically in the role they can play in improving underwater navigation accuracy of submerged assets. The main research effort within this thesis was the evaluation of data from sea trials in the shallow parts of Monterey Bay in September 2017 and April 2018. Two directional acoustic modems were installed in tow bodies that were tethered to two unmanned surface vehicles (USVs). These USVs were then directed on multiple missions in an area surrounding the deployment of a bottom-moored acoustic echo repeater, which acted as a surrogate underwater platform.

Data collected during the sea trials is then compared between measured and best-estimated ranges and bearings. Using the Bellhop ray-tracing model and beam pattern analysis, the actual accuracy of these systems was extensively evaluated. Results indicate that, when operating properly, these modems can provide accurate data to assist in underwater navigation.

14. SUBJECT TERMS effectiveness, acoustic, modem, navigation, underwater, sea trial, Monterey Bay, wave glider, tow body, Teledyne	**15. NUMBER OF PAGES** 131
	16. PRICE CODE

17. SECURITY CLASSIFICATION OF REPORT	**18. SECURITY CLASSIFICATION OF THIS PAGE**	**19. SECURITY CLASSIFICATION OF ABSTRACT**	**20. LIMITATION OF ABSTRACT**
Unclassified	Unclassified	Unclassified	UU

NSN 7540-01-280-5500 Standard Form 298 (Rev. 2-89) Prescribed by ANSI Std. 239-18

THIS PAGE INTENTIONALLY LEFT BLANK

Approved for public release. Distribution is unlimited.

EVALUATING EFFECTIVENESS OF DIRECTIONAL ACOUSTIC MODEMS INTEGRATED ONTO AUTONOMOUS PLATFORMS

Leander J. C. van Schriek
Lieutenant, Royal Netherlands Navy
Diploma, Royal Netherlands Naval College, 2004

Submitted in partial fulfillment of the
requirements for the degree of

MASTER OF SCIENCE IN APPLIED PHYSICS

from the

NAVAL POSTGRADUATE SCHOOL
June 2018

Approved by: Kevin B. Smith
Advisor

Douglas P. Horner
Co-Advisor

Kevin B. Smith
Chair, Department of Physics

THIS PAGE INTENTIONALLY LEFT BLANK

ABSTRACT

Navies have been operating with unmanned underwater vehicles (UUVs) for decades. Recently, these platforms are assigned more and more complicated tasks. Compared to other domains, the underwater domain offers substantial additional challenges. One of these challenges is accurate navigation of these UUVs.

In this thesis, the use of directional acoustic modems integrated onto autonomous platforms is evaluated, specifically in the role they can play in improving underwater navigation accuracy of submerged assets. The main research effort within this thesis was the evaluation of data from sea trials in the shallow parts of Monterey Bay in September 2017 and April 2018. Two directional acoustic modems were installed in tow bodies that were tethered to two unmanned surface vehicles (USVs). These USVs were then directed on multiple missions in an area surrounding the deployment of a bottom-moored acoustic echo repeater, which acted as a surrogate underwater platform.

Data collected during the sea trials is then compared between measured and best-estimated ranges and bearings. Using the Bellhop ray-tracing model and beam pattern analysis, the actual accuracy of these systems was extensively evaluated. Results indicate that, when operating properly, these modems can provide accurate data to assist in underwater navigation.

THIS PAGE INTENTIONALLY LEFT BLANK

TABLE OF CONTENTS

THIS PAGE INTENTIONALLY LEFT BLANK

LIST OF FIGURES

THIS PAGE INTENTIONALLY LEFT BLANK

LIST OF TABLES

THIS PAGE INTENTIONALLY LEFT BLANK

LIST OF ACRONYMS AND ABBREVIATIONS

ATM	Acoustic Telemetry Modem
BS …, etc.	Bottom Surface …, etc., bounce
CTD	Conductivity Temperature Depth
DAT	Directional Acoustic Transponder
DP	Direct Path
ER	Echo Repeater
FCC	Federal Communications Commission
GPS	Global Positioning System
HFM	Hyperbolic Frequency Modulated
MLLW	Mean Low Low Water
NOAA	National Oceanic and Atmospheric Administration
RX	Receive
SB …, etc.	Surface Bottom …, etc., bounce
SSP	Sound Speed Profile
TB	Tow Body
TX	Transmission
UUV	Unmanned Underwater Vehicle

THIS PAGE INTENTIONALLY LEFT BLANK

I. INTRODUCTION

A. CONTEXT

Since the 1970s, several institutions have been involved in the development of unmanned underwater vehicles (UUVs). Soon after, this development gained the interest of navies worldwide. During the last 10–15 years, however, these platforms became commercially available, which led to a push improving the potential of these underwater platforms [1]. As a result these platforms became capable of executing more and more complicated tasks. In order to be able to execute these tasks, accurate navigation is paramount and will increasingly become more important when underwater operations with these platforms become even more complex. This is especially true, since there is a desire for UUVs to operate with multiple platforms, farther away from its operator, more autonomously, and in more challenging environments. Under these circumstances a need arises to be able to check and update the platform's navigation, if required. Accurate ranging, for example towards navigation aids, could assist in this process.

Compared to other domains, the underwater environment offers a great deal of additional challenges. The complexity of the (underwater) medium is the root cause of this challenge. Reverberations, boundary interactions, multi-paths and ambient noise all cause distortions in transmitted signals and therefore reduce the chance of interpreting a received ranging signal correctly.

B. OBJECTIVE

This thesis will discuss the role acoustic modems (integrated onto autonomous platforms) can play in improving underwater navigation accuracy of submerged assets. It will do so by thoroughly evaluating a system which could potentially support the proposed ranging solution to the UUV navigation problem.

For this purpose, the Naval Postgraduate School procured two Teledyne Benthos DAT-903 Directional Acoustic Transponders (DAT), which are associated with the ATM-900 series Acoustic Telemetry Modems (ATM). These acoustic modems are primarily built for underwater communications. As such they are capable of transmitting data packages

between nodes. The ATM-900 series modems can transmit data over the acoustic link at bit rates as high as 15,360 bits/s, and receive data at bit rates as high as 2400 bits/s [2]. According to its manual [2], typical applications of the Teledyne Benthos modems are: remote data acquisition, periodic acquisition of stored data, and UUV or wellhead command and control. Figure 1 illustrates the aforementioned applications in clockwise order, starting in the upper-left corner.

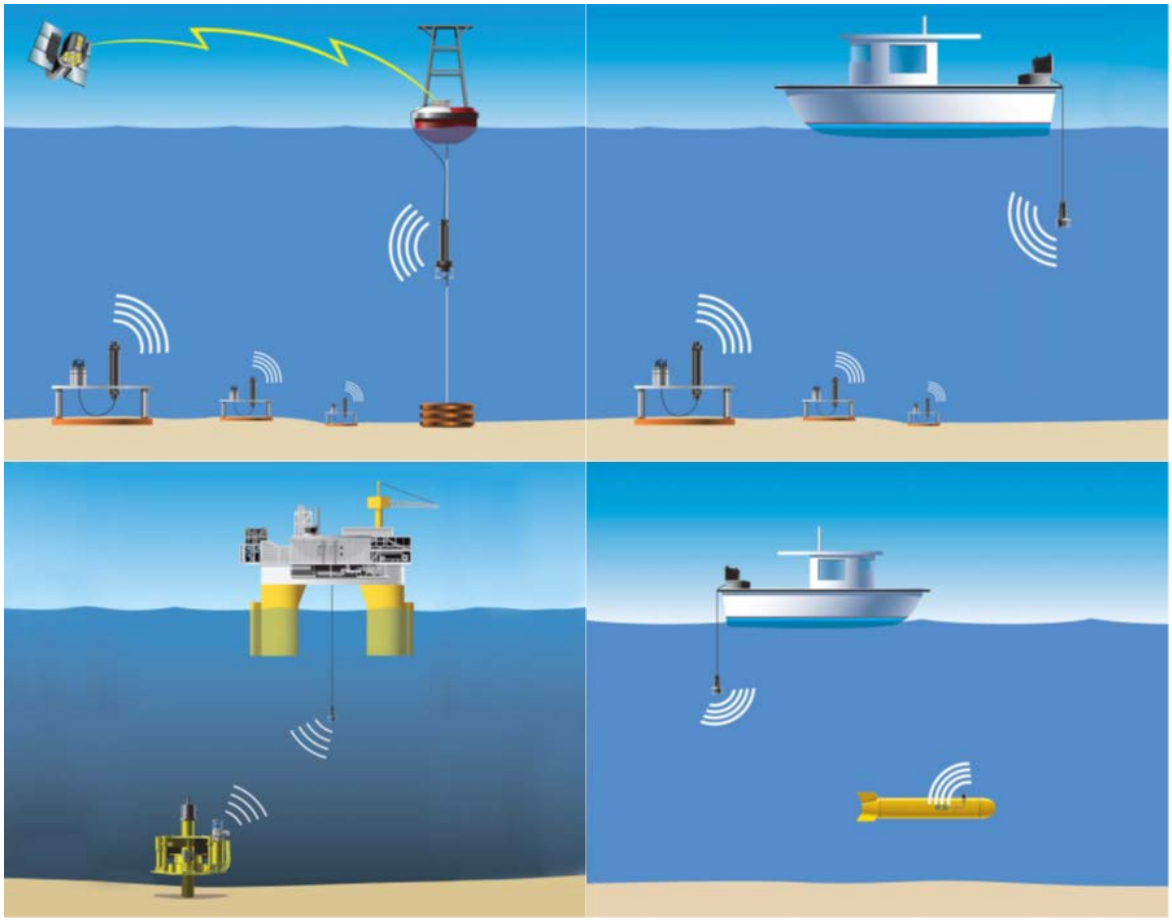

Figure 1. Typical Applications Teledyne Benthos Modems. Source: [2].

Besides the previously mentioned applications, they can also be used as ranging instruments, which can determine the range between two nodes. As mentioned before, this is the feature of interest for this thesis.

Besides ranging, the DAT transponder possesses a directional receiver, which can determine bearing information. This bearing information could, just as the ranging routine, assist in the UUV navigation problem.

The objective of this thesis is to execute an extensive evaluation of this underwater sensor and investigate how these sensors can contribute to improving UUV underwater navigation.

C. RESEARCH QUESTIONS

Taking into account the objective of this study, the following research questions were formulated.

- How well does the range estimate provided by a single, directional modem compare with the real range?
- How well does the bearing estimate provided by a single, directional modem compare with the real bearing?
- How well can the modem acquired ranges be predicted using the Bellhop ray tracing model?

D. RESEARCH

The main research effort within this thesis was the evaluation of data from actual sea trials in the shallow parts of Monterey Bay in September 2017. Two Teledyne-Benthos DAT modems were installed in tow bodies that were tethered to two Liquid Robotics Wave Glider unmanned surface vehicles (USVs). These USVs were then directed on multiple missions in an area surrounding the deployment of a bottom moored acoustic echo repeater. The echo repeater acted as a surrogate underwater platform. In April 2018, a second, very comparable trial was executed in the same area. Several suggestions to improve the results of the September trial were implemented. In addition to acoustic modem performance data, environmental data (e.g., sound speed profiles) were collected in the area to better interpret the performance results.

Data collected during the sea trials was then compared between measured and best estimated (GPS-based) ranges and bearings. Using the Bellhop ray-tracing model and beam pattern analysis, the actual accuracy of these systems was extensively evaluated.

E. THESIS OUTLINE

After this introduction, the theoretical background of acoustic ranging and the Bellhop ray tracing model will be discussed. The third chapter then describes the September sea trial, which was executed to evaluate the effectiveness of the acoustic modems in a real-world scenario. Before discussing the results of the sea trial, the necessary pre-analysis process, during which the acquired data is manipulated in order to be interpreted, will be addressed. Next, the results of the September sea trial will be discussed. The chapter following will briefly discuss the trial executed in April, and will compare the results with the September trial. Thereafter, the beam pattern measurements collected in one of the NPS water tanks will be discussed. In the final chapter, conclusions will be drawn and the research questions will be answered.

II. THEORETICAL BACKGROUND

In this chapter, the theoretical background and methods used in this thesis will be discussed.

A. COMPUTING THE RANGE PROBLEM

One of the important problems addressed in this thesis is the method to determine the range between a transmitter and a receiver. In short, this is executed by estimating the travel time of the signal between transmission and receipt. This chapter will discuss this estimation process. In his dissertation, R.P. Vio [3] provides a good review of this process. The next sections are based on his review.

1. Cross Correlation and Matched Filter

In order to estimate the travel time between, in the case of this thesis, two modems, a waveform is sent from source to receiver. The transmit time of this waveform will be accurately determined and recorded. Next the time of arrival of the received waveform at the target needs to be determined. This is done by cross-correlation of the known transmitted waveform with the received signal. In a real-world scenario the received waveform will be distorted (due to reverberations, Doppler, multi-paths, boundary interactions, etc.). Furthermore, the receiver will receive both noise and the signal. A matched filter executes a cross-correlation between the transmitted and received signal. (The output of this matched filter is maximized when the cross-correlation between transmitted and received signal maximizes.) The matched filter process effectively maximizes the signal-to-noise ratio within the band of the signal. The time at which this maximum occurs can be accurately determined and is considered the receive time of the signal.

Vio [3] explains how Doppler can distort the matched filter output when a modem is mounted on a moving platform. This distortion manifests itself by widening of the matched filter output response. This widening makes it harder to accurately estimate the receive time. In order to fight this type of distortion, most ranging applications, like the

one discussed in this thesis, use a hyperbolic frequency modulated (HFM) pulse. This is a pulse that sweeps through a frequency band, as shown in Figure 2. The result in the matched filter output will be a desired sharp peak. However, there will be a temporal offset due to the Doppler shift. This Doppler shift can be measured and compensated for, as will be discussed below.

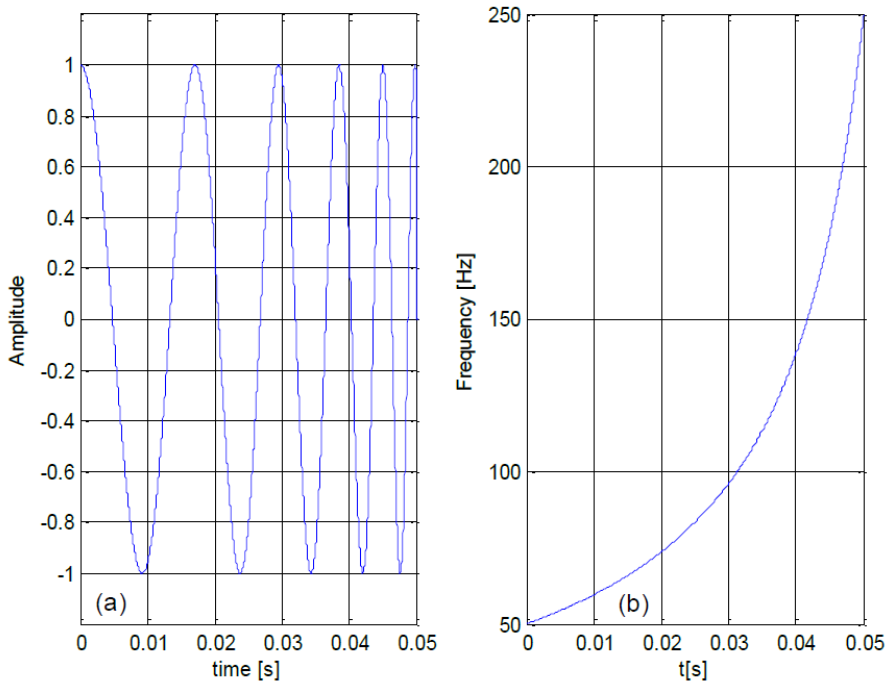

Figure 2. Example of a 50 ms HFM Pulse. Source: [3].

2. Acoustic Modem Ranging Routine

As noted in Chapter I, Teledyne-Benthos ATM-900 series acoustic modems have been used for this thesis. These acoustic modems are integrated into tow bodies and can make use of a built-in ranging routine to estimate the range between two nodes. This section will describe the sequence of events of this Teledyne-Benthos built-in routine, which is illustrated in Figure 3.

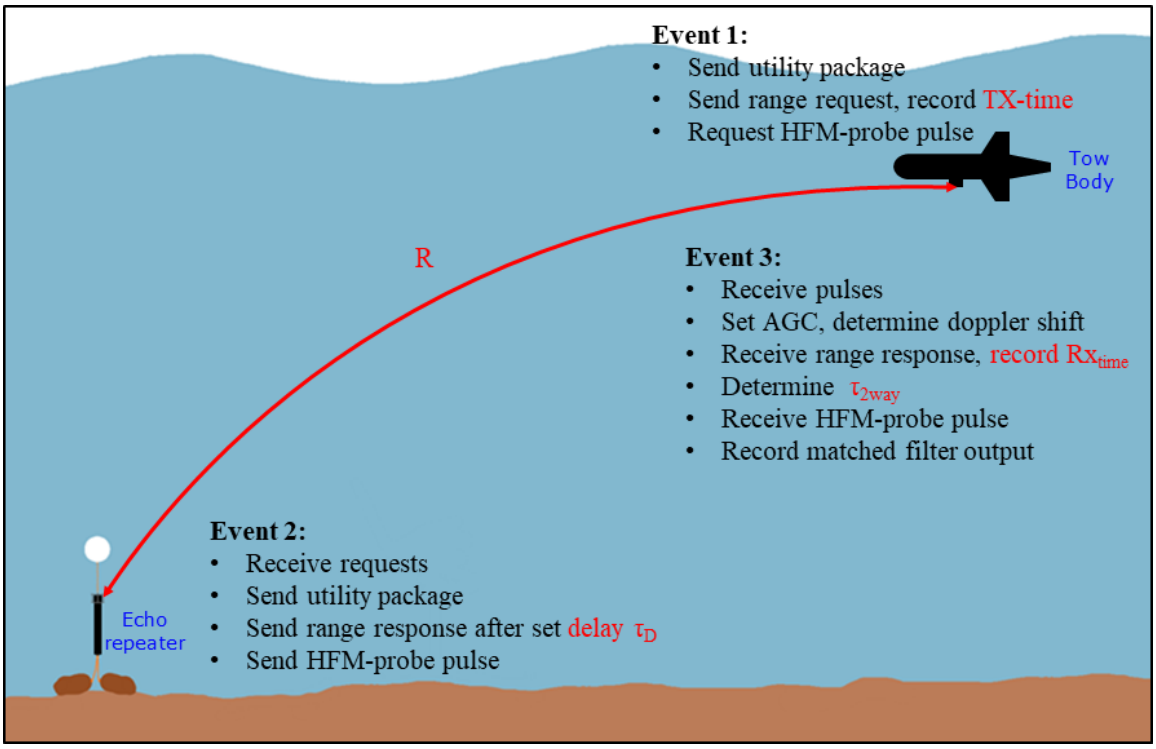

Figure 3. Teledyne-Benthos Ranging Routine

The tow body and echo repeater are separated by distance R. Initially, the tow body transmits a utility package to the echo repeater. This utility package contains, among other things, a single frequency pulse to assess the Doppler shift. This assessment will be used to compensate for the temporal shift as explained in Section 1. Furthermore, the utility package contains a noise pulse to set the tow body's automated gain control. This is required to prevent clipping of the range request signal at the echo repeater's end [4]. Shortly after the utility package is sent, a range and probe pulse request are transmitted. The modem will accurately record the time of this transmission (TX_{time}). Using a matched filter, the incoming signal is detected at the echo repeater. An estimate of the time of arrival is then made, based on the highest peak in the matched filter output. The echo repeater replies to the range request, after a fixed time delay (τ_D) and first sends a utility package again. After the utility package is sent, a range response message (including the time delay τ_D) is sent to the tow body. Again, matched filtering is used to estimate the time of arrival (RX_{time}) of the highest peak in the match filter output [3]. From the time difference between

RX_{time} and TX_{time} (minus τ_D), the two-way travel time (τ_{2way}) is estimated by the tow body using Equation 1 [5].

$$\tau_{2way} = (RX_{time} - TX_{time}) - \tau_D \quad (1)$$

At this point, the tow body's modem provides a rough estimate of the range R by multiplying the one-way travel time (which is half of the two-way travel time), by the (user) specified sound speed of the medium [2].

Shortly after the ranging routine is executed, the requested 50 ms HFM-probe pulse is sent from the echo repeater to the tow body. The matched filter output of this probe pulse is a very good estimate of the matched filter output produced by the ranging routine. The modem continuously buffers 50 ms worth of matched filter output data. Once a peak has been detected in one of those 50 ms "data chunks," recording is started, and 1 s of matched filter output data is saved as a wavfile [6].

B. RAY TRACING

In an "isospeed" environment, where the sound speed is approximately constant over a specified range and with depth, the distance between source and receiver may simply be estimated by multiplying the characteristic sound speed of the medium with the estimated one-way travel time. In underwater acoustics, however, the sound speed is rarely spatially constant. The sound speed in water increases with pressure, temperature and salinity [7]. Even in a range-independent environment, temperature and pressure change with depth. As a result, the propagating sound wave is refracting and therefore not propagating in a straight line.

A second important characteristic in underwater acoustics is the occurrence of multi-paths. In a multi-path environment, multiple arrivals reach the receiving transducer at different times by following different propagation paths, causing several peaks in the matched filter output. As discussed previously, an approach to estimate the travel time is to measure the arrival time of the highest peak in the matched filter output. However, as was explained in [3] the highest peak in this output will not always correspond to the direct path. The highest peak could be from a bottom or surface bounce path. Also, due to these

multiple arrivals, constructive (and destructive) interference could occur, which will influence the received amplitude of a specific path.

As a result of these two characteristics of the underwater medium, ray path modeling was introduced to better understand the way sound propagates underwater. Historically ray theory was used in optics and later adapted for underwater use. Especially during the Cold War these models were extensively studied and improved. Ray tracing became a popular way to model underwater sound propagation, because of its ease of use and relatively high processing speed. Nowadays more and more processing power is available, which has resulted in more modern (computationally intensive) acoustic propagation models. Since ray tracing models inherently assume a high frequency, these modern models perform better at lower frequencies than ray tracing can. For the frequencies used during the sea trials, however, a ray tracing model can produce an accurate representation of the acoustic ray paths.

1. Bellhop Beam Tracing Model

The ray tracing code used in this thesis is Bellhop, which was developed by Michael B. Porter and is available in the Ocean Acoustic Library website [8]. According to its manual:

> Bellhop is a beam tracing model for predicting acoustic pressure fields in ocean environments, where several types of beams may be implemented with both geometric and physics-based spreading laws. Bellhop can generate a variety of outputs including transmission loss, eigenrays, and predict arrival times. It allows for range-dependence in the top and bottom boundaries (altimetry and bathymetry), as well as in the sound speed profile. Additional input files permit the specification of directional sources as well as geo-acoustic properties for the bounding media. Top and bottom reflection coefficients may also be included. [9]

This thesis mainly uses the arrival prediction and eigenray modules of Bellhop. An eigenray is a ray path that connects source and receiver. The computation of eigenrays by Bellhop is done exactly the same way as it calculates regular ray traces. However, Bellhop only saves those rays whose associated beams contribute to the specified receiver location.

2. Ray Tracing Using Bellhop in Combination with Matched Filtering

Using the Bellhop beam tracing model, an estimate can be made of the actual acoustic path in the specific scenario. Bellhop uses the environment (Sound Speed Profile (SSP), bottom properties), source, and receiver details to calculate the eigenrays.

During the sea trial of September 2017, a total of 592 range requests were sent from the towed bodies to the echo repeater. Nearly 40 percent (218) of those range requests were successful, meaning that the echo repeater generated a response and sent this to the towed bodies. The ranging routine in the acoustic modem (see Section A.2) then estimated the range between tow body and echo repeater and stored the matched filter output.

Figure 4 shows this matched filter output within the appropriate one-second range gate. The y-axis indicates the normalized amplitude level in decibels. The left graph shows the entire processed one-second output, the right graph shows only the first 100 milliseconds. Note that in the zoomed figure, several amplitude peaks become apparent showing different arrivals of the probe signal at the modem in the tow body.

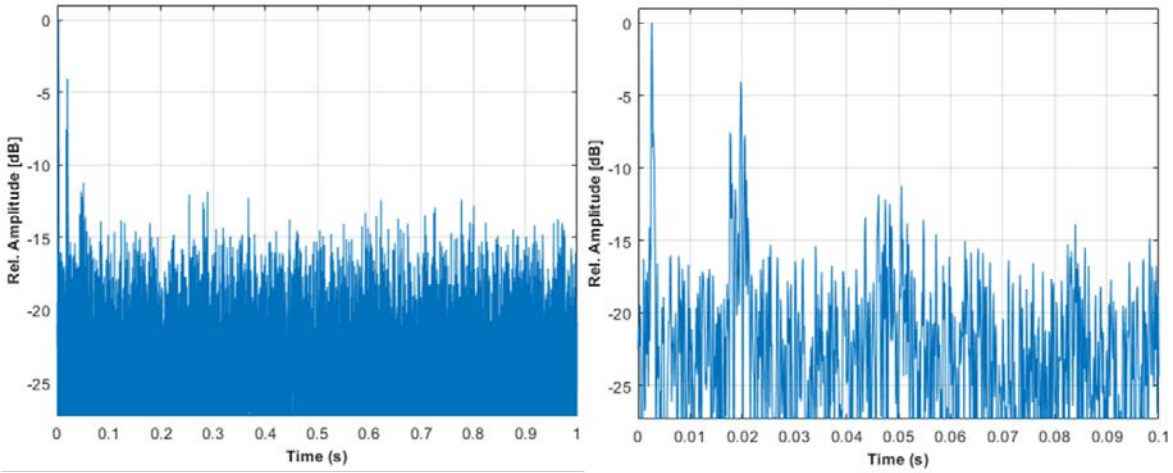

Figure 4. Unzoomed (left) and Zoomed (right) Matched Filter Output

The different arrivals are due to multi-paths, meaning that the sound bounced off the surface or the bottom first before it arrived at the tow body. Using Bellhop, the rays connecting source and receiver can be visualized. Figure 5 is an example that shows the

direct path in red, the single surface bounce path in blue, and the single bottom bounce path in green. The other colors (light blue, black and black dashed) show rays with multiple boundary interactions.

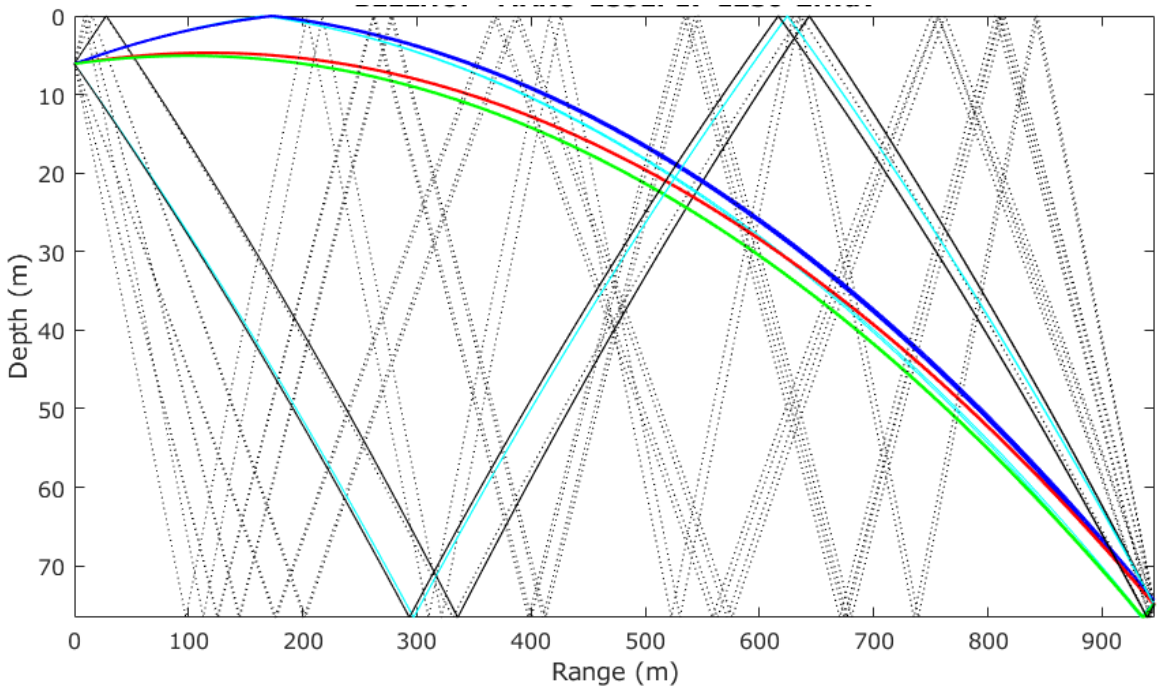

Figure 5. Example of Eigenrays between Tow Body and Echo Repeater

Using the environmental data, Bellhop can estimate both the arrival time and the transmission loss (due to spreading and boundary interactions) of the signal using the different paths. For the same data set as the previous figure, the arrival visualization is shown in Figure 6 on the left. On the right, this same arrival plot has been integrated into the appropriate matched filter output. This provides a good comparison between actual and predicted arrivals.

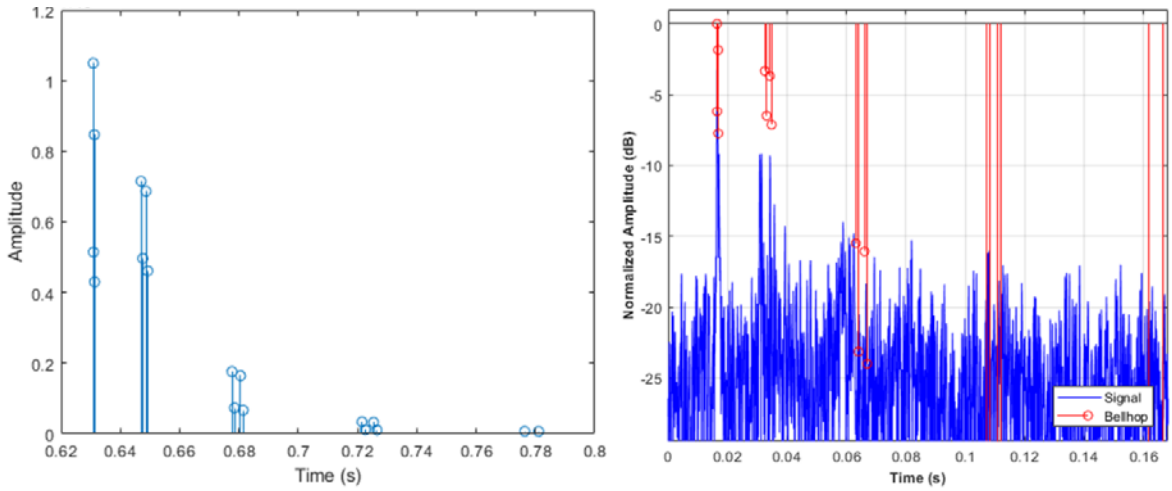

Figure 6. Bellhop Arrival File (left), Integrated in Matched Filter Output (right)

III. SEPTEMBER SEA TRIAL

A. INTRODUCTION

From 11 to 15 September 2017, a sea trial was conducted in Monterey Bay. Key assets for this trial were two Liquid Robotics Wave Gliders towing a body (including a directional modem), and an omni-directional modem (acting as an echo repeater) anchored near the bottom of the bay. The NOOA research vessel Fulmar operated as a command ship from which the trial was coordinated and the assets were deployed. After the echo repeater was deployed, a Remus UUV executed several side scan sonar runs near the bottom anchored echo repeater in order to accurately determine its position. Figure 7 shows the general set up of the trial (Note this figure is not to scale.).

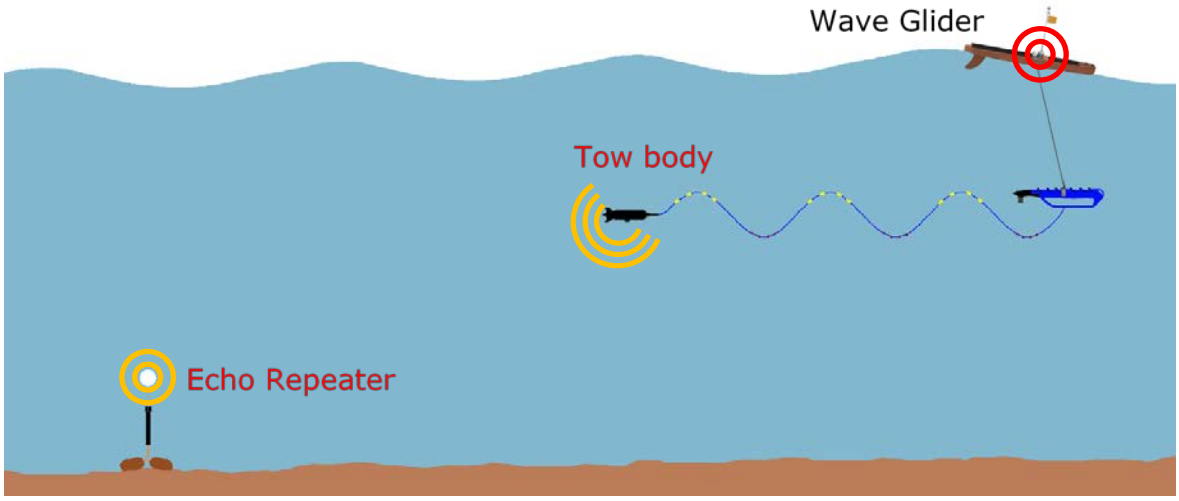

Figure 7. General Sea Trial Set Up

During the sea trial, several runs were executed by two similar Wave Gliders. One will be referred to as Mako (since the end of 2017 re-named Thresher), the second as Tiburon. After the initial set up, two complete data sets were gathered for each Wave Glider. These data sets covered the following time periods (all times are local);

- 13 September 2017
    - Mako: 10:54 until 20:54
    - Tiburon: 11:38 until 21:00
- 14 September 2017
    - Mako: 11:16 until 21:16
    - Tiburon: 11:04 until 21:04

B. KEY ASSETS

This section will describe the key assets used during the sea trial.

1. The Wave Gliders

The Liquid Robotics SV2 Wave Glider (shown in Figure 8) is an Unmanned Surface Vehicle (USV), which is composed of a float unit and a sub unit. The float unit houses vehicle controls, data logging, as well as a GPS-receiver (for accurate position information), an Iridium communication system (for commands), solar panels and a battery pack (to power all on board systems). The sub unit converts wave motion into forward movement using its cantilevered wings. As such, the sub unit is pulling the float unit forward with speeds (depending on the wave height) up to 2 knots [10]. The sub unit also has the capability to tow a tow body. Part of the sub unit is the rudder, which steers the Wave Glider system along the predetermined trajectory. Attached to the sub unit is the compliant tow cable, which consists of light floating and heavy sinking elements. These elements create a wave like shape in the tow cable, intended to decouple the impulsive motion of the sub unit and produce smooth motion of the tow body. The float unit and sub

unit are connected via an umbilical cable, which acts as a tow cable, as well as a data command cable.

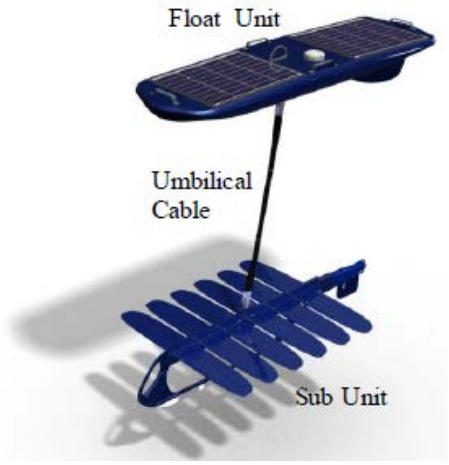

Figure 8. Liquid Robotics SV2 Wave Glider. Source: [10].

2. The Tow Body

As mentioned above, the sub unit of the Wave Glider pulls both the float unit as well as the tow body (Figure 9) forward. The tow body can house a payload. During the September sea trial, a Teledyne Benthos ATM-900 series acoustic modem along with a 900-series directional transducer were mounted in the tow body. Data logging also occurred inside the tow body.

Figure 9. The Tow Body, Compliant Tow Cable and Transducer

3. The Teledyne Benthos Transponder and Modem

The tow body houses a Teledyne Benthos ATM-900-series acoustic modem and DAT-903 directional transponder.

The DAT transducer actually consist of two parts. Acoustic transmissions are done by a ceramic ring that is located close to the base of the transducer. The same ceramic ring is used in the omni-directional transducer in the ATM-925 model, which was used as an echo repeater during the September sea trial. Above the transmit ring, a set of four small receiving elements, constructed in a tetrahedral shape, are situated. These four elements are only used to calculate the bearing and inclination of the incoming signal.

During the sea trial, the acoustic modems sent range requests towards the echo repeater. It logged transmit and receive times of these requests, along with the determined range (based on two way travel time), and bearing toward the echo repeater. Two range requests, separated by 30 seconds, were sent every 8 minutes. With every range request, a probe pulse request was sent. The matched filter output of this probe pulse (50 ms HFM pulse) was recorded and stored in the modem.

4. The Echo Repeater Assembly

The echo repeater assembly, which was deployed near the sea floor, consisted of a Teledyne Benthos ATM-925 modem and omni-directional LF (Low Frequency) transducer, two sand bags, a floating buoy, and an acoustic release mechanism (see Figure 10). After deployment, the heavy sand bags and the floating buoy kept the echo repeater up straight. The acoustic center of the modem was assessed to be about 1.65 m above the sea floor. The depth (above MLLW[1]) at the echo repeater location was determined to be 75.6 m, leaving the acoustic center at 74.0 m depth. During the September sea trial, the echo repeater only responded to requests by the tow body. It did not record data like the modems on board the tow body. A Remus UUV with a side scan sonar from the NPS Center for Autonomous Vehicle Research was utilized, and determined the echo repeater's

[1] MLLW = Mean Low Low Water, which is the chart datum used for the nautical chart 18685 of Monterey Bay.

location with one-meter accuracy after deployment. During the sea trial the echo repeater acted as a surrogate underwater platform, although its location remained stationary.

Figure 10. The Echo Repeater Assembly Before Deployment

C. AREA OF OPERATION

The September sea trial was executed in a relatively flat area just north of the Monterey Bay Canyon about 7.5 km west of Moss Landing (see Figure 11). This section will describe the properties of this area during the sea trial.

1. The Sea Floor

As mentioned, the sea floor within the operating area was relatively flat. The shallowest part, north of the echo repeater's location, was about 70 m deep. The southern part of the area was just north of the Monterey Bay Canyon, where the depth was about 130 m. From east to west the depth was flatter, with 75 m in the far east section and 77 m in the far west section of the operating area.

The sea floor at the area of operation consists of silt-clay and sand-silt-clay sediments. It was modeled in Bellhop, according to [11], as a fluid half space with the following properties:

- Sound speed: 1560 m/s;
- Density: 1.6 kg/m3;
- Attenuation: 1 dB/m.

Figure 11. Area of Operation

2. Weather During the Trial

During the sea trial, fair weather was experienced with good swell conditions to operate the Wave Gliders. Table 1 shows the most important weather conditions.

Table 1. Weather Conditions During the September Sea Trial

Weather	13 September	14 September
Wind	Southwest – 5 to 15 kts	West – 10–20 kts
Waves	1 to 3 ft	2 to 4 ft, increasing 3 to 4 ft
Swell	West – 2 to 3 ft, 10 s period	Northwest – 5 to 6 ft, 9 s period
Temperature (measured by float unit)	21-23 °C	21-23 °C

The experienced swell resulted in an average speed over ground for both Wave Gliders of 0.6 kts on 13 September and 1.0 kts on 14 September.

3. Tides

The water level above the chart datum (MLLW) increases the vertical distance between the tow body and the echo repeater and will therefore influence the path length of the sound waves. Notice in Figure 12 and Figure 13, there was about 80 cm of tidal variation during the trial.

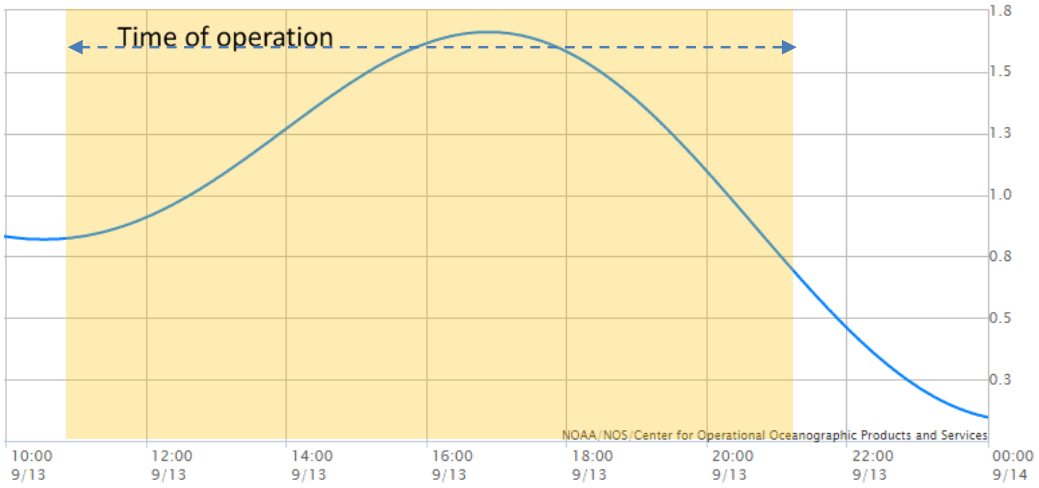

Figure 12. Tides Predicted on 13 September 2017. Source: [12].

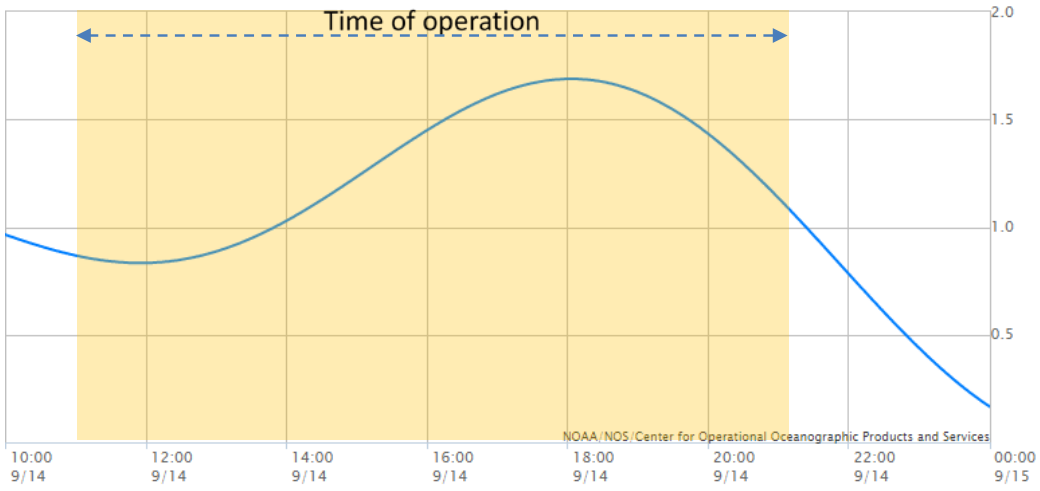

Figure 13. Tides Predicted on 14 September 2017. Source: [12].

4. Sound Speed Profiles (SSP)

During the sea trial, a handheld Sontek CastAway Conductivity Temperature Depth (CTD) profiler was used to measure 28 sound profiles within the area of operation. The advantage of this handheld device was that frequent CTD-casts could be taken. However, the maximum depth obtained by the CastAway was about 57 meters, due to the available

line, and therefore the SSP needed to be extrapolated down to the bottom. The CTD-casts were taken during the time frames that the R/V Fulmar was in the area of operation. As a result, there are no SSP measurements in the late afternoon or early evening. The SSPs were taken during the entire trial period (12-15 September). Figure 14 shows how the CTD-casts were spread over the time of day.

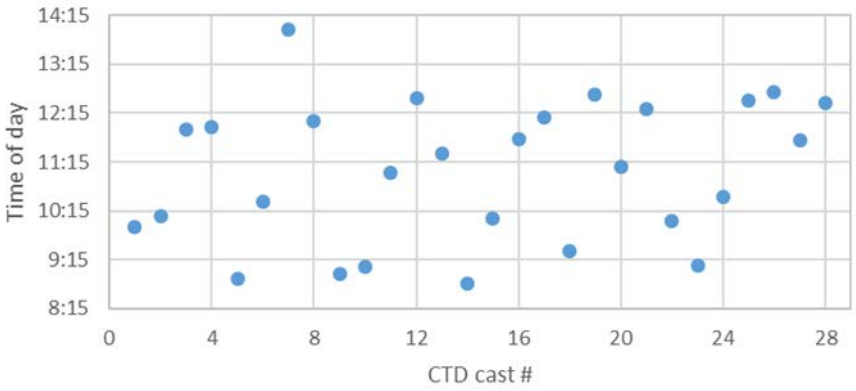

Figure 14. Time of CTD-Casts

After analysis of the CTD-cast data, and in order to use the best possible SSP for the appropriate measurement, the SSPs were averaged and grouped per area. Figure 15 shows where the different CTD casts were taken and how these were grouped into one of the seven different areas. Initially, the assigned areas for the SSPs were North, East, South, West, and Center. When further analysis showed separation of SSPs could lead to an improvement, an additional two areas (3 and 7) were added.

Figure 16 and Figure 17 show all 28 observed SSPs. Note that although there is variance within each individual observed SSP, when the observed SSPs are averaged, we conclude the SSP in each area to be linear. This linearization allowed for the extrapolation of the observed data to the bottom. From this linearization, the sound speed gradient can be determined. Together with the averaged sound speed at the surface, this will provide a sound speed at each depth. Table 2 shows the outcome of this linearization. These values were used in follow-on calculations.

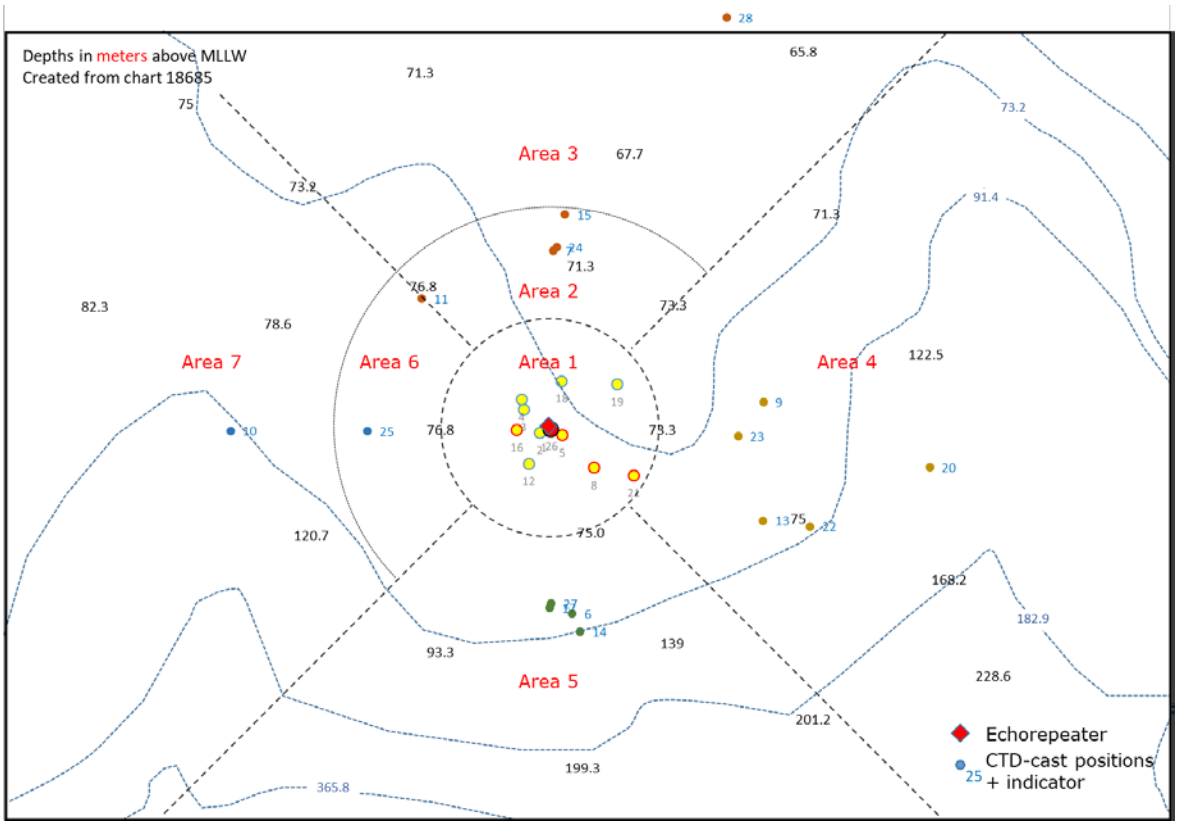

Figure 15. Locations of CTD-Casts and Their Areas

Table 2. Linearized Gradient, and Sound Speed at the Surface per Area

Area	Gradient s-1]	c_0 m/s]
1	-0.3051	1512.66
2	-0.3073	1513.08
3	-0.3910	1512.08
4	-0.2552	1513.02
5	-0.2787	1512.99
6	-0.2946	1513.71
7	-0.3050	1511.86

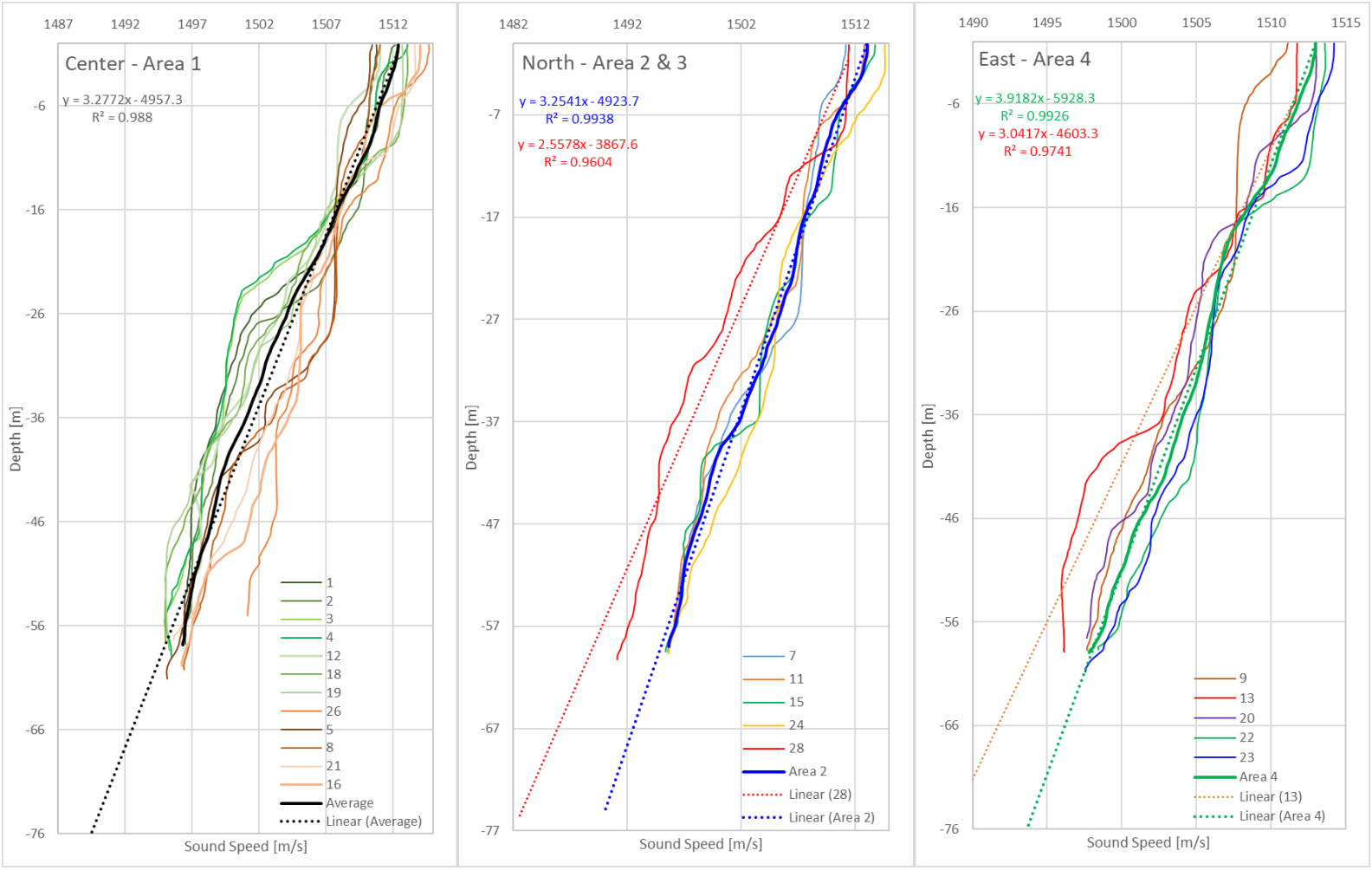

Figure 16. Observed SSP for the Center, North and East Areas

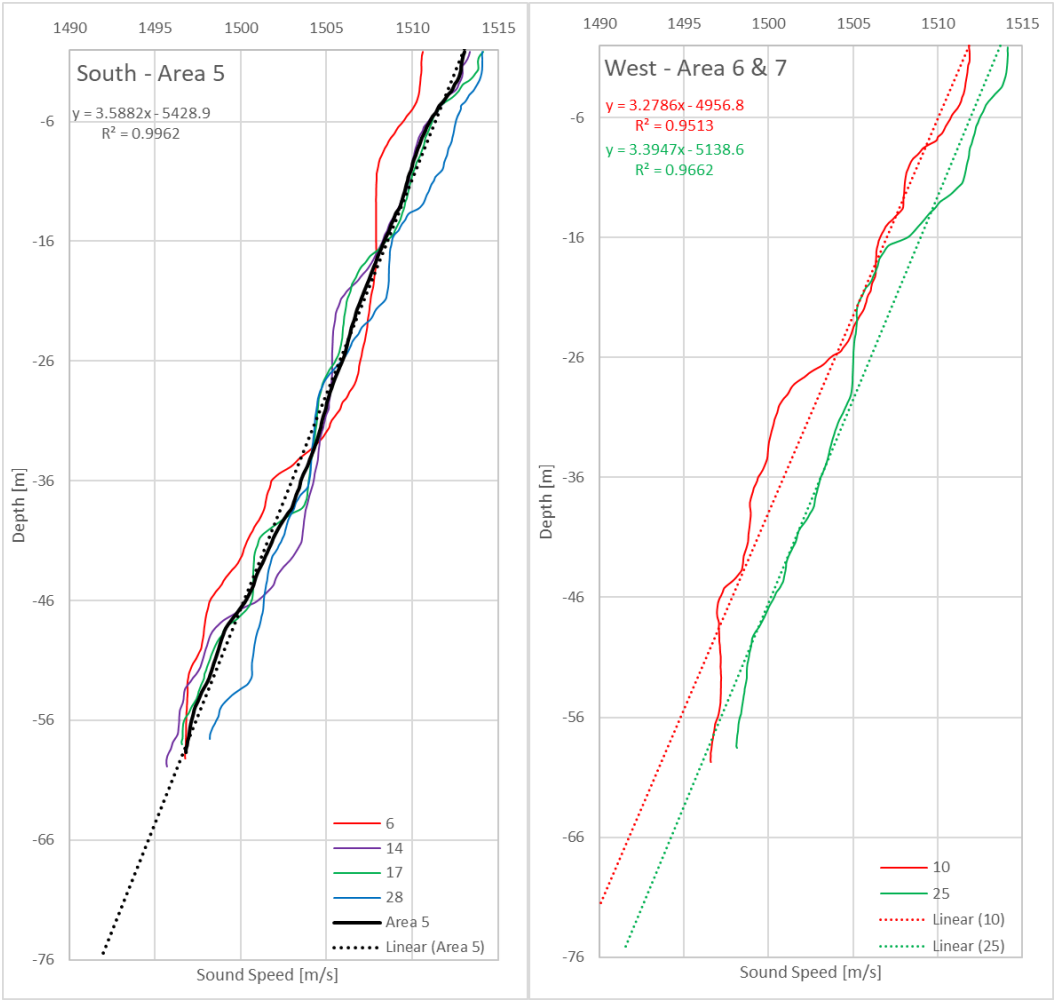

Figure 17. Observed SSPs for the South and West Areas

IV. PRE-ANALYSIS PROCESSING

A. INTRODUCTION

Before analyzing and interpreting the results of the sea trials, an understanding of the applicable geometry and its associated errors is required. Furthermore, the Wave Gilder positional data needs to be interpolated in order to reproduce accurate results. This chapter will describe both these topics.

B. GEOMETRY AND ERRORS

The Wave Glider uses GPS-positioning and the position of the echo repeater had been accurately determined using a Remus UUV. Therefore, it is, in principle, possible to compare the modem-determined range and bearing with the actual position-based range and bearing. Although this seems straightforward at first glance, a better look at the geometry, as presented in Figure 18, will quickly show there are many (small) variations involved due to the dynamics of the environment and platforms, which introduce errors. Note that this figure is not to scale.

As can be seen in Figure 18, in order to accurately compare the modem-measured range (or one-way travel time) between tow body and the echo repeater, variations in the Wave Glider position, tow body position relative to the position of the Wave Glider and variations in environment and echo repeater position should be taken into account. To provide a percentage figure on the applicable error, the estimated errors are compared to the minimum and maximum observed ranges, which are 113 m and 1120 m, respectively.

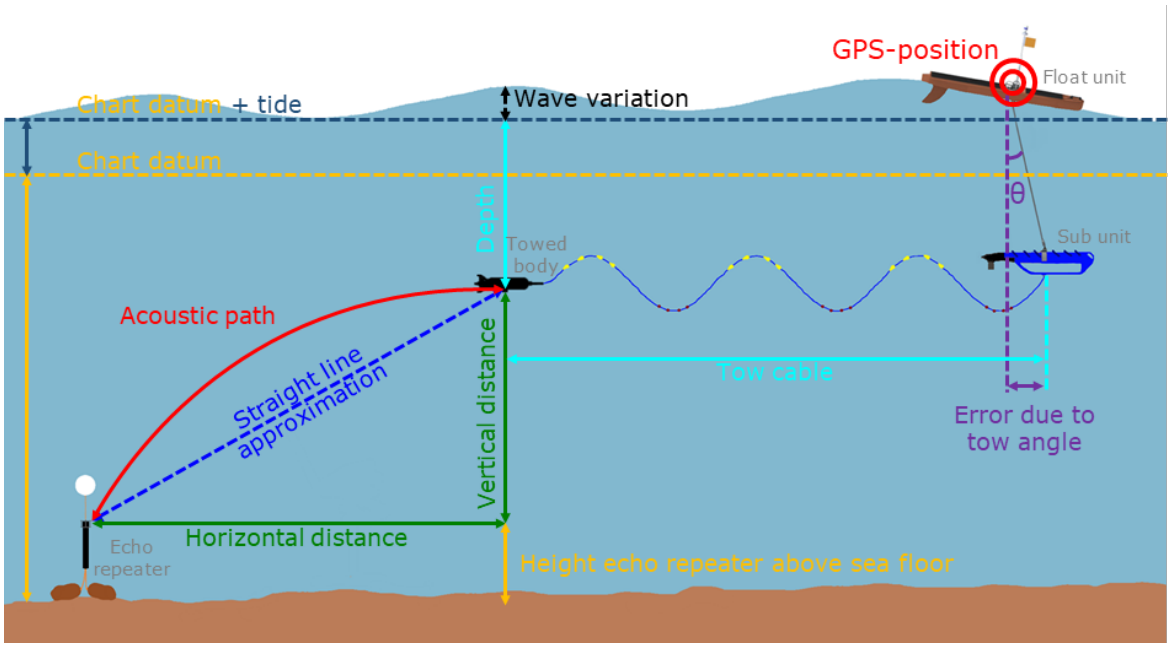

Figure 18. Overview of Geometry

1. Acoustic Path and Measured Travel Time

In order to determine the range between tow body and echo repeater, the acoustic modems determine a two-way travel time between both assets. During this travel time the sound follows the acoustic path. This path is never exactly known and can slightly vary, even between the outbound and inbound leg. This path can, however, be approximated by several methods, such as ray tracing. [It is important to understand that, at short ranges the difference between the actual acoustic path and the straight line approximation is the smallest]. In this thesis, one-way travel time over the curved path will be estimated by using a recursive approach as discussed in Section D.

The error in the measured one-way travel time is relatively small, since the modem can measure up to a tenth of a millisecond (about 15 cm). Even when assessing the error to be half a millisecond and using the maximum observed sound speed, this leads to an error of 75 cm. This corresponds to a percentage error between 0.067% and 0.66%.

2. Position of the Wave Glider

Although the Wave Glider uses accurate GPS satellite navigation, it only logs its position in the telemetry file about every five minutes. The timing resolution of each logged position is five seconds. In order to obtain the position of the Wave Glider at a specific time, linear interpolation was used. This introduced an error in the position of the Wave Glider and, as a direct result, an error in the position of the tow body. The error in the calculated position of the Wave Glider is the biggest error contributor. The error is a combination of several errors, including:

- The GPS-error itself: The Liquid Robotics SV2 Wave Glider uses a WAAS-capable GPS-receiver [10]. Therefore, the CEP50-error[2] is about 3 m, which leads to a percentage error between 0.27% to 2.65% for long and short ranges respectively;
- The error due to the five second timing accuracy: Based on the maximum observed ground speed of two knots (+/- 1 m/s), the error due to this should be less than 5 m. The estimate for this error is 0.45% to 4.42%. Note that this error is speed dependent. At the average speed over ground (0.81 kts = 0.42m/s) the error is about 2.1m, which means an error of 0.19% and 1.86%, respectively. For further computation the average speed error will be used;
- The error due to the interpolation process: This error consists of several factors. The most important one is the fact that the instantaneous speed of the Wave Glider deviates from the average speed over ground, especially when the average is calculated near a turning point or course change. Another issue is the actual path the Wave Glider is following between the five minute position intervals. We assume the Wave Glider travelled in a straight line, where in practice it might have deviated from its course (due to current, waves, wind, etc.). Both the factors are sketched in Figure 19. Since these are all factors which are hard to account for and depend on the actual unknown path between

[2] Circular Error Probable; 50 indicates 50% of the positions fall within the given circular area

two points, all errors for this part are combined in a pool of error. Since this error is mainly influenced by the calculated average speed of ground between Wave Glider positions, this pool of errors is based on the median observed change in speed over ground between two successive positions. This median was determined for each Wave Glider and then averaged. This works out to an error of about 5.5%, which is about 60 m at long range and 6 m at short range. Moreover, since course changes are executed at long ranges and the Wave Glider is on straight legs near the echo repeater, this makes sense.

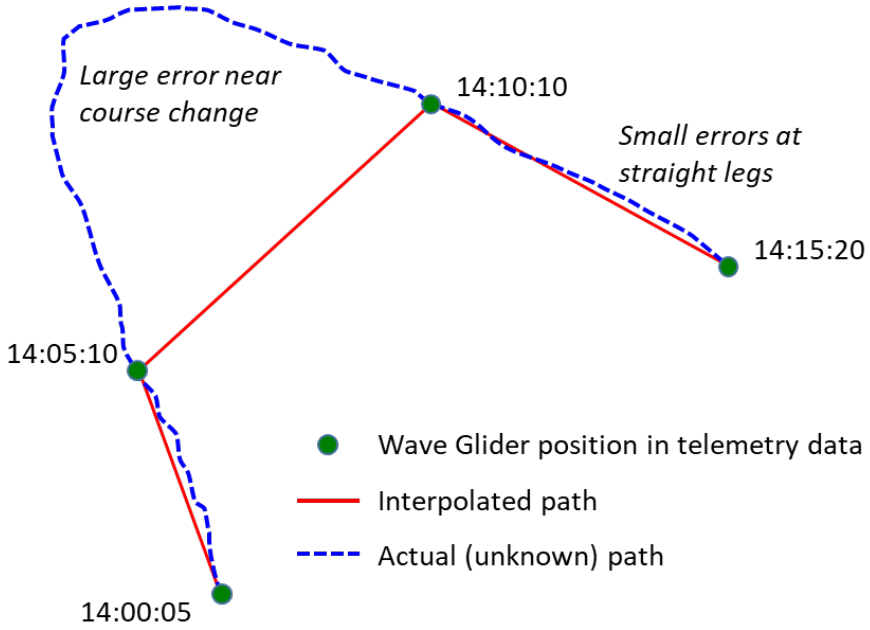

Figure 19. Difference between Actual and Interpolated Paths

Using error propagation as defined by [13], a total combined error can be calculated. With respect to the position of the Wave Glider, this error is, based on the average speed over ground, 6.38% at short range and about 5.5% at long range.

3. Distance between Tow Body and Wave Glider

Accurate knowledge of the three dimensional position of the tow body is required to make a good comparison between the modem and position-determined range (i.e., travel

time) and bearing. The first thing to consider is the distance between the sub unit and the tow body. The sub unit tows the tow body using a 12-meter long tow cable. As explained earlier this cable maintains a sinusoidal shape in order to decouple the impulsive motion of the sub unit from the tow body. The actual effective length of the tow cable is unknown, but has been assessed (by video) to be about 9.4 m on average with a speed-dependent error of +/- 1.3 m. Figure 18 also shows an error due to the tow angle. This error is assessed to be small (again based on video and photos) and incorporated in the error due to the tow cable shape. In this thesis, the tow body is considered to always be straight behind the Wave Glider. This is obviously not completely correct, especially when the Wave Glider is turning. This will cause position-determined ranges during maneuvers to be unreliable. This error in the horizontal distance between tow body and Wave Glider accounts for a range error of 0.12% at long ranges to 1.44% at short ranges.

4. Depth

The next main position parameter of the tow body is its depth. The depth of the tow body is equal or deeper than the depth of the tow point, which is at the bottom of the sub unit, situated 6.4 m below the float unit. During the April trial, a depth sensor was attached to the tow body. This sensor showed the tow body was flying at an average depth of 8.1 m (+/-40 cm). Due to changes in the tow body (additional spacer and weight), this depth cannot be assumed to be equal for the September trial. However, it is the best estimate which can be made at this point. Therefore, these inputs will be used in range calculations. As stated the depth error in April was measured to be about 40 cm, which will have a negligible effect on the calculated range at long ranges. At short range, however, this can attribute to an error of about 0.53%. Furthermore the depth of the tow body does play a role in the maximum achievable direct path range. When the tow body is deeper, it can ‘launch’ or receive rays with a bigger negative grazing angle and therefore increase the range.

5. Pitch and Roll

The pitch and roll of the tow body was unknown during the September trial. Although the system is designed to maintain a neutral (zero angle) pitch and roll, it was

unclear whether or not this was true. Again, the April trial data fills our knowledge gap. The data of the sensor in the tow body and the one attached to the tow body both show that the tow body actually flies almost level through the water most of the time. During the April trial an average pitch of about half a degree upwards and an average roll of about 1.5 degree port was observed. As before, this data cannot be immediately transferred to the September data, but does provide a good indication

As with the depth, the pitch and roll of the tow body doesn't directly influence the measured range or bearing. The error in range is therefore negligible. However, pitching (or rolling) the tow body does have some effect. First, it will change the relative beam toward the echo repeater. This might mean a sound wave is received in a weaker beam and therefore has a smaller chance to be detected (or vice versa). Secondly, a downward pitch might slightly increase the maximum achievable direct path range. The April data does show that extreme (i.e., more than 10 degree) pitches or rolls do not occur.

6. Vertical Distance

Although the depth of the tow body and the height of the echo repeater above the sea floor are approximated to be fairly stable, the vertical distance between the tow body and the echo repeater is not. This is mainly due to the (relatively slowly changing) tidal height, and the (faster) varying height of swell and waves. The instantaneous effect of the latter is not taken into consideration, whereas the tidal height is. The data obtained from the depth sensor attached to the DAT during the April trial clearly shows these slower and faster changing components of the water column above the echo repeater. The instantaneous variations in the tidal height are considered small and will average over time. Therefore, this will have a negligible effect on range and bearing

7. Sound Speed

As discussed earlier, several sound speed profiles have been determined and averaged over time for several (relatively small) areas. In practice, however, there will still be slight local variations on the linearized approximation used in this thesis. From the different measured sound speed profiles, the maximum observed deviation from the linear approximation is 0.36%

8. Position of the Echo Repeater

The modem's transducer orientation might have fluctuated by a few degrees during the trial, however this effect is assessed to be negligible. The position of the echo repeater was determined within one meter. This introduced an error of 0.089% at long range, and up to about 0.88% at close range.

9. Other Errors

Besides the above considerations, there are other errors which were not taken into account. In addition, the beam patterns of both transducers can have an impact on the results. This will be evaluated in a later section. Furthermore, just like in the horizontal case, there is a slight depth error due to the tow angle. Another error source might have been the orientation of the echo repeater. In this thesis, its orientation is considered straight up, whereas in practice it might have been slightly moving. Other very small systematical errors include the actual position of the GPS-antenna on the Wave Glider and the actual position of the acoustic center of the transducer on the tow body. There is also about a 2.4 s latency in the echo repeater between the moment it receives the range requests and sends out its response. It is assessed, that all these other error have an effect on the range of less than 0.5%.

10. Total Error

As can be seem from the above descriptions, the most dominant error is due to the positioning of the Wave Glider. The combined error of all of the above described uncertainties, again using [13], is about 6.7% at close range and about 5.5% at long range.

Making a good assessment on the total bearing error is harder. Not all of the above errors influence the calculated bearing as much as the calculated range. Again, the biggest error is the positional error.

C. CALCULATING THE TOW BODY POSITION

As mentioned above, the Wave Gliders recorded their GPS-locations with intervals of about five minutes and to an accuracy of five seconds. In order to determine the position

of the tow body as accurately as possible, linear interpolation between the recorded positions is used. Therefore, a method is required to determine distances and bearings between two geographical positions. The method adopted by the Federal Communication Commission (FCC) [14], was utilized in this thesis. Their method for measuring distances is a 'flat-earth' model, therefore it is easy to use. The method calculates the meters per degree of latitude (K_{lat}) or longitude (K_{long}) change, based on the mean latitude (LAT_{mean}). Most importantly, the FCC-method is very accurate over short distances. According to the National Association of Broadcasters (NAB) Engineering Handbook [15], this method is more accurate than using a spherical model for ranges up to 475 kilometers. The coefficients used in Equations 2 and 3 below are derived from the Clarke 1866 reference ellipsoid. $LAT_{beforeTX}$ and $LAT_{afterTX}$ in Equation 4 are the known Wave Glider GPS-latitudes right before and after the range request of the tow body. Note that these latitudes need to be in radians.

$$K_{lat} = \frac{111.13209 - 0.56605\cos(2 \cdot LAT_{mean}) + 0.00120\cos(4 \cdot LAT_{mean})}{1000} \tag{2}$$

$$K_{Long} = \frac{111.41513\cos\left(LAT_{mean}\right) - 0.09455\cos\left(3 \cdot LAT_{mean}\right) + 0.00012\cos\left(5 \cdot LAT_{mean}\right)}{1000} \tag{3}$$

$$where\, LAT_{mean} = \frac{LAT_{beforeTX} + LAT_{afterTX}}{2} \tag{4}$$

Using the calculated K-constants and the difference in latitude (ΔLAT) and longitude (ΔLONG) between the before and after position, the distance and bearing between those positions can be calculated as follows:

$$Distance_{horizontal} = \sqrt{\left(K_{lat}\Delta LAT\right)^2 + \left(K_{long}\Delta LONG\right)^2} \tag{5}$$

$$Direction = \operatorname{atan}\left(\frac{K_{lat}\Delta LAT}{K_{long}\Delta LONG}\right) \tag{6}$$

Next, the average speed over ground ($SOG_{average}$) is determined, based on the calculated distance using Equation 7 and the known time between the GPS-positions before ($Time_{beforeTX}$) and after the range request ($Time_{afterTX}$).

$$SOG_{average} = \frac{Distance_{horizontal}}{Time_{afterTX} - Time_{beforeTX}} \tag{7}$$

This average speed is then multiplied by the time difference between the time of the range request ($Time_{TX}$) and the GPS-position right before the request. That will provide the distance the Wave Glider and tow body travelled since the last known GPS-position ($Distance_{travel}$).

$$Distance_{travel} = SOG_{average} \cdot \left(Time_{TX} - Time_{beforeTX} \right) \tag{8}$$

Next, the tow body and Wave Glider are assumed to both move in the direction calculated using Equation 6. The tow body has then moved from the last known GPS-position ($Distance_{travelTB}$), the calculated travel distance minus the 'fixed' distance between Wave Glider and tow body ($Distance_{WG\text{-}TB}$).

$$Distance_{travelTB} = Distance_{travel} - Distance_{WG-TB} \tag{9}$$

The inverse method can now be used to find the change in latitude and longitude since the last known GPS-position. This results in the best estimate of the tow body position at the time of the range request. Figure 20 shows the actual Wave Glider track during the trial in blue. The green dots indicate calculated tow body positions at the time of a successful range request, while unsuccessful range request are not indicated.

After the best estimated position of the tow body has been calculated, the horizontal distance between the tow body and echo repeater can be calculated using Equations 2 to5, where now $LAT_{beforeTX}$ and $LAT_{afterTX}$ are the latitudes of the echo repeater and the tow body, respectively. ΔLAT and ΔLONG are now the differences in latitude and longitude of the echo repeater and the tow body. The direction (and therefore bearing) between the echo repeater and the tow body can then be calculated using Equation 6.

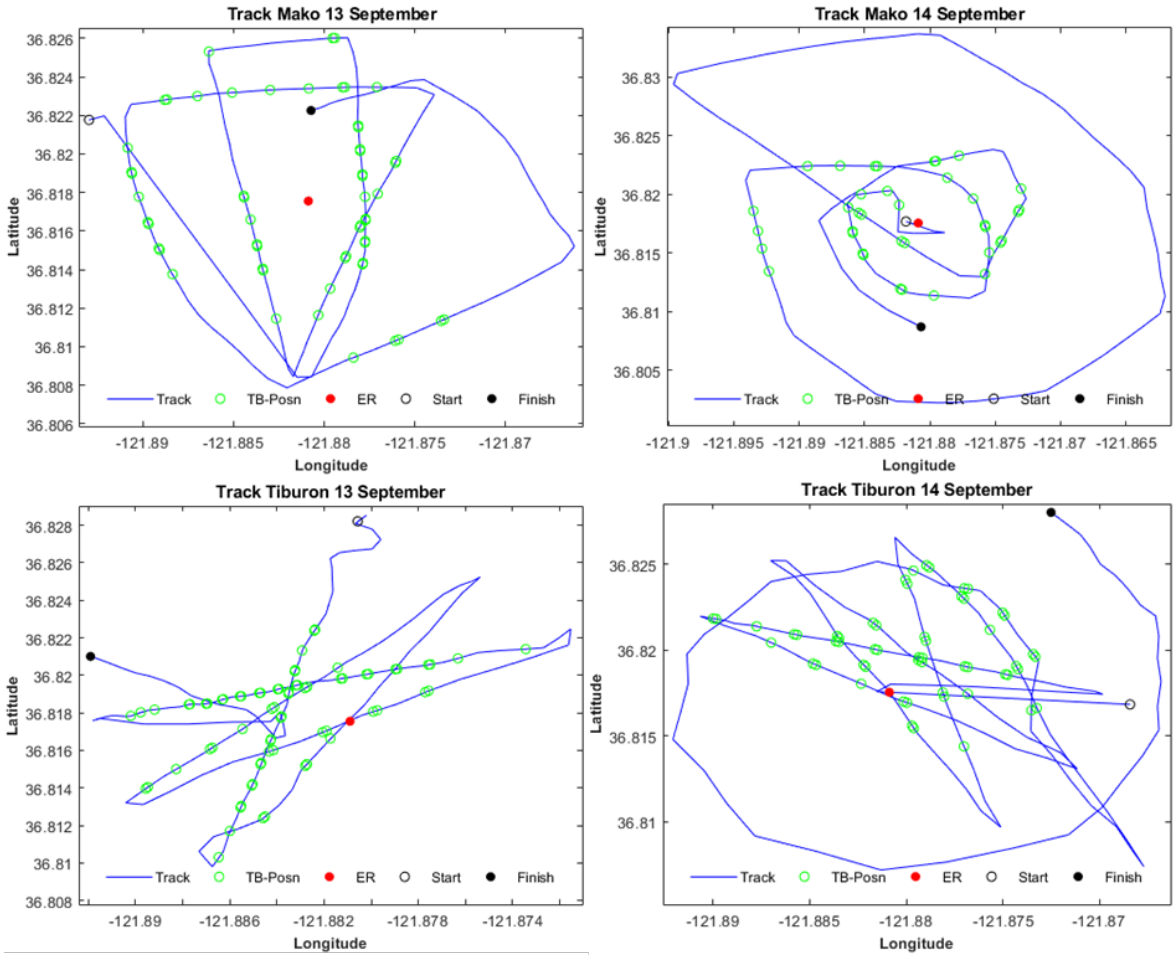

Figure 20. Wave Glider Tracks and Calculated Tow Body Positions

From Figure 18, it becomes apparent that the vertical distance between the tow body and the echo repeater can be calculated as follows:

$$Distance_{vertical} = Waterdepth\,at\,ER + Tidal\,height - TB\,depth - ER\,height \qquad (10)$$

Combined with the horizontal distance, the straight-line approximation (or slant range) can simply be calculated using the Pythagorean Theorem.

D. CALCULATING THE ONE-WAY TRAVEL TIME

In order to compare the calculated range results with the measured range or one way travel time, the length of the acoustic path needs to be calculated. Using just the calculated vertical and horizontal distances between the estimated tow body position and the echo repeater, one cannot calculate the arc length of the acoustic path. However, this arc length can be estimated. This was done using an iterative process. For this (looped) process, the initial grazing angle was estimated to be the grazing angle of the straight-line approximation (angle α in Figure 21). Next, the radius of curvature (R) of a circular ray path leaving the tow body with this launch angle within the appropriate sound speed profile can be calculated using Equation 11 below [16]. Here c_{TB} is the sound speed at the depth of the tow body, g is the gradient of the linearized sound speed profile, and χ_{TB} is the grazing (launch) angle from the tow body (which is initially equal to α).

$$R = \frac{c_{TB}}{|g| \cdot \cos(\chi_{TB})} \tag{11}$$

Using Snell's law, the grazing angle at the echo repeater's depth can be calculated. With both grazing angles known, one can now calculate the horizontal range (r) from the tow body at which the estimated acoustic ray hits the depth of the echo repeater (i.e., the vertical distance) using Equation 12.

$$r = R \cdot (\sin(\chi_{ER}) - \sin(\chi_{TB}) \tag{12}$$

Here χ_{ER} is the (estimated) grazing angle at the echo repeater. The range r can be compared with the previously calculated horizontal distance using Equation 5. The next step is to decrease the grazing launch angle by a small increment and repeat the above calculation and comparison. This loop continues until the difference between range r and the horizontal distance is less than a threshold value (in this case 10 cm). While range r gets closer to the calculated horizontal distance, the estimated grazing angles get closer to the actual angles χ_{TB} and χ_{ER}. Besides the grazing angles, this process also provides a best estimate of the arc length and the radius of curvature, as given by Equation 13.

$$Arc = R \cdot \theta, where\, \theta = \chi_{ER} - \chi_{TB}\,(in\, radians) \tag{13}$$

Figure 21 illustrates the variables used in the above described loop process.

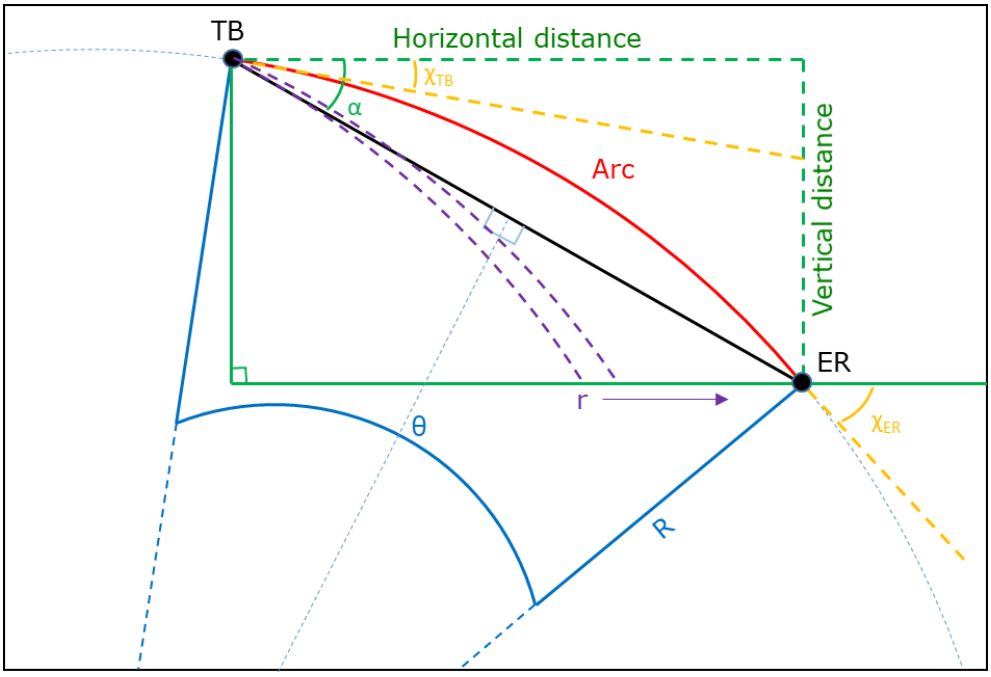

Figure 21. Iterative Process to Find Grazing Angles and Arc Length

Once a good estimation of the grazing angles is established, the one way travel time can be calculated. For this, a Riemann sum method was used, where the vertical distance was divided in small increments. For each increment, the sound speed at the average depth of the increment was determined. Using Equation 13, the arc length of each increment was calculated and divided by the determined sound speed to get the one way travel time for the increment. Finally, all the one way travel times of all increments were summed, which provided the total one way travel time.

$$Travel_{oneway} = \sum_{n}^{\frac{Distance_{vertical}}{100000}} \frac{Arc_n}{c_{n,avg}} \tag{14}$$

V. RESULTS

After pre-processing the data and understanding the errors to be expected, the results can now be accurately compared and interpreted.

A. COMPARING RANGE RESULTS

The calculated one-way travel time, as discussed in the previous chapter, can be accurately compared to the one way travel time determined by the modem. Figure 22 to Figure 25 show the results of this comparison. The left graphs shows the calculated range between the tow body and the echo repeater as a blue line. The red dots are the ranges determined by the modem. The right graphs shows, indicated by a blue circle, the difference between the calculated one-way travel time and the one-way travel time determined by the modem. Since the one-way travel time is proportional to the range, the calculated percentage differences are also applicable to the determined ranges. As can be seen the one-way travel times determined by the modem are very close to the calculated one-way travel time. The maximum observed difference is about 10% for Mako and about 13% for Tiburon. However, the main percentage difference is in all cases below five percent and as such within the error rang estimated in Section IV.B.10 to be between 5.5% and 6.7%

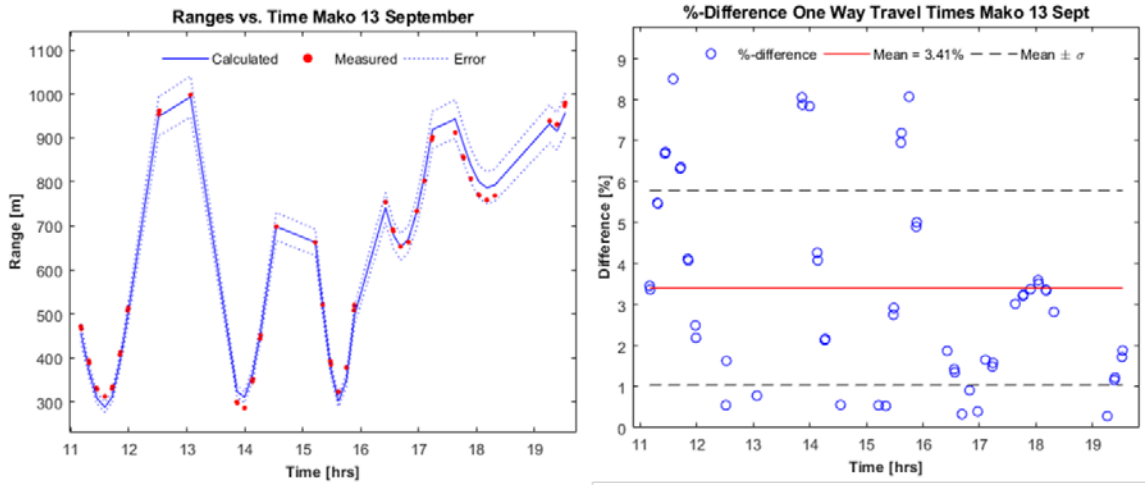

Figure 22. Range Comparison Results Mako 13 September

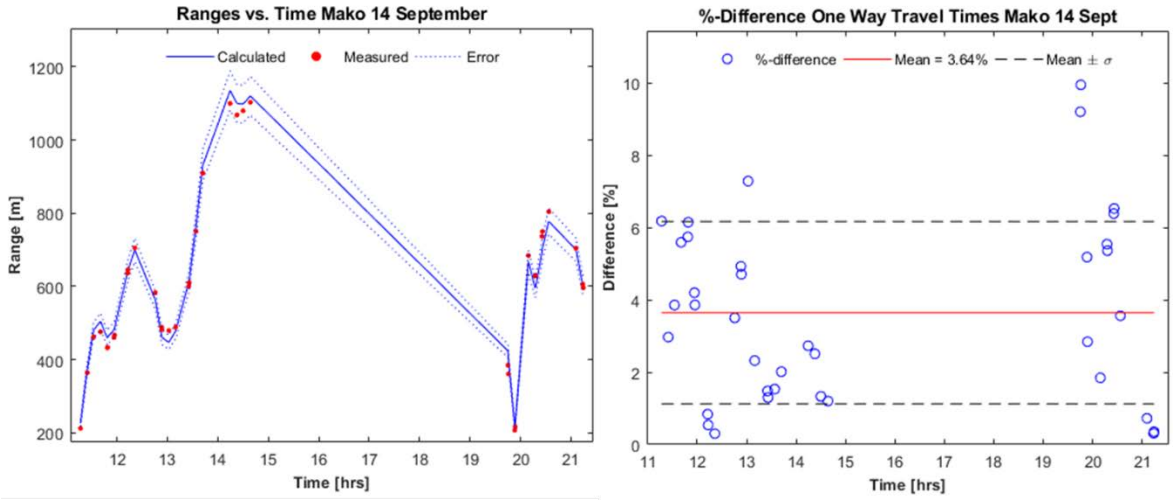

Figure 23. Range Comparison Results Mako 14 September

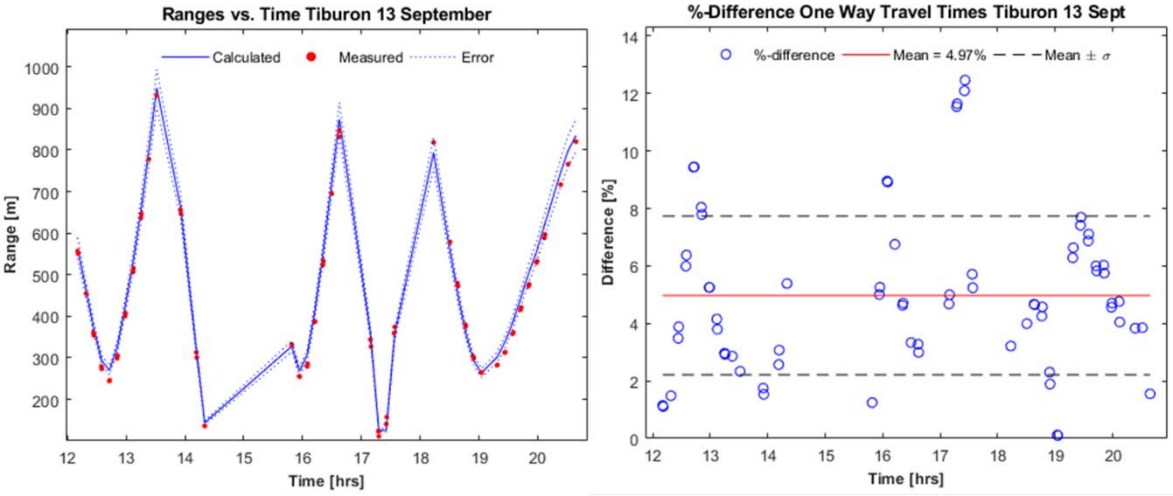

Figure 24. Range Comparison Results Tiburon 13 September

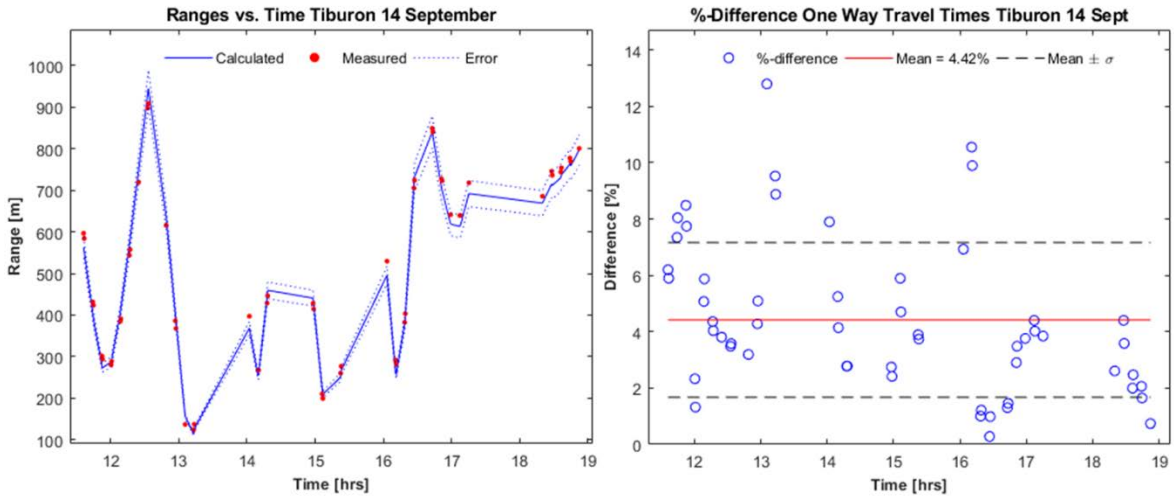

Figure 25. Range Comparison Results Tiburon 14 September

B. COMPARING BEARING RESULTS

As previously noted, the modems onboard the Wave Gliders incorperate a directional transducer. The DAT transducer actually consists of two parts. One omni-directional transmit ceramic ring and a four element tetrahedral shape array, which is purely used to determine the bearing and inclination of the received signal.

The DAT-transducer uses a broadband component of a message to form an estimate of the arrival angle. Both an estimate of the vertical angle (inclination) and the horizontal angle (bearing) are made. During the September trial, no pitch data of the tow body was recorded. Therefore, it is not possible to compare the modem-determined inclination angle with the calculated vertical receive angle. It is, however, possible to compare the calculated and the modem-estimated bearings.

Figure 26 and Figure 27 show the comparison between measured and calculated bearings between Mako's tow body and the echo repeater. As with the range comparison, the left graph shows the calculated bearing as a blue line and the measured bearings as red dots. At an initial glance at just the left graphs, it seems the measured bearings are tracking the calculated bearing. The more detailed graph on the right, however, shows the errors observed. Individual bearings are observed to be as far off as 60 degrees. On average, the difference between the calculated and measured bearing was about 19 degrees.

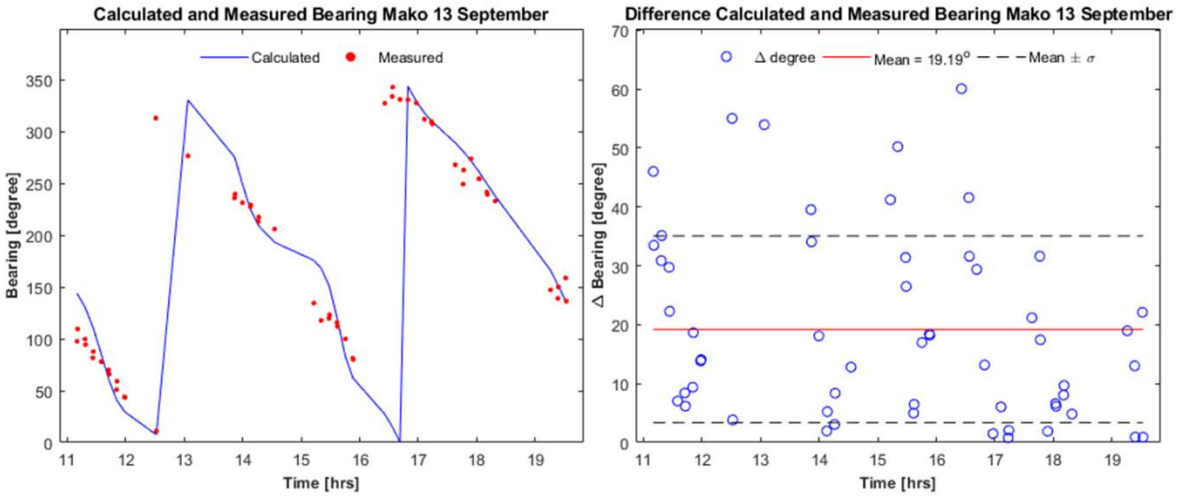

Figure 26. Calculated and Measured Bearings for Mako 13 September

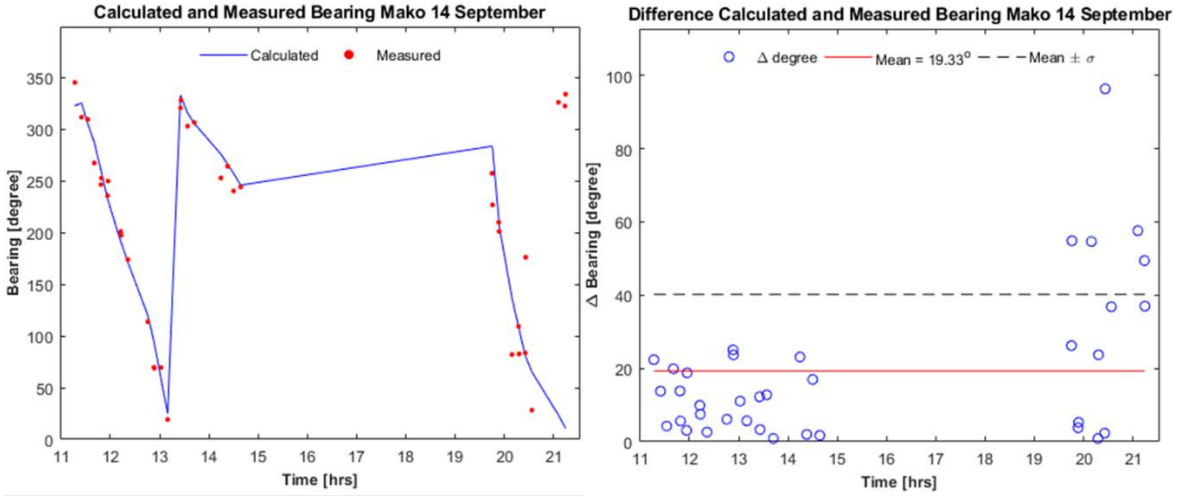

Figure 27. Calculated and Measured Bearings for Mako 14 September

One possible cause for the offset between calculated and measure bearing is the influence of the tow body. During the September trial, the DAT-transducer was not fully exposed outside the tow body. Therefore, a decision was made to introduce an additional spacer, which would lower the transducer significantly and fully expose the tetrahedral receive portion of the DAT.

. Another remarkable observation, in Mako's data, is that on 14 September the measured bearings of Mako seemed to be better before the Wave Glider went out of range.

After range was regained, around 20:00 hours, the bearing grouping was more disperse than before. The reason for this artifact is unknown.

The bearing measurements by Tiburon show a very different result. Although the exact same method was used to calculate the bearings, they initially seem to be way off. Note, in the left graphs, there seems to be a systematical error in the bearing measurements, since the measured bearings do follow the bearing trend. A possible explanation for this could be an uncalibrated or incorrectly configured compass. If a 90 degree offset would be implemented this would improve the left graph of Figure 28 greatly. However, it would not improve the left graph of Figure 29.

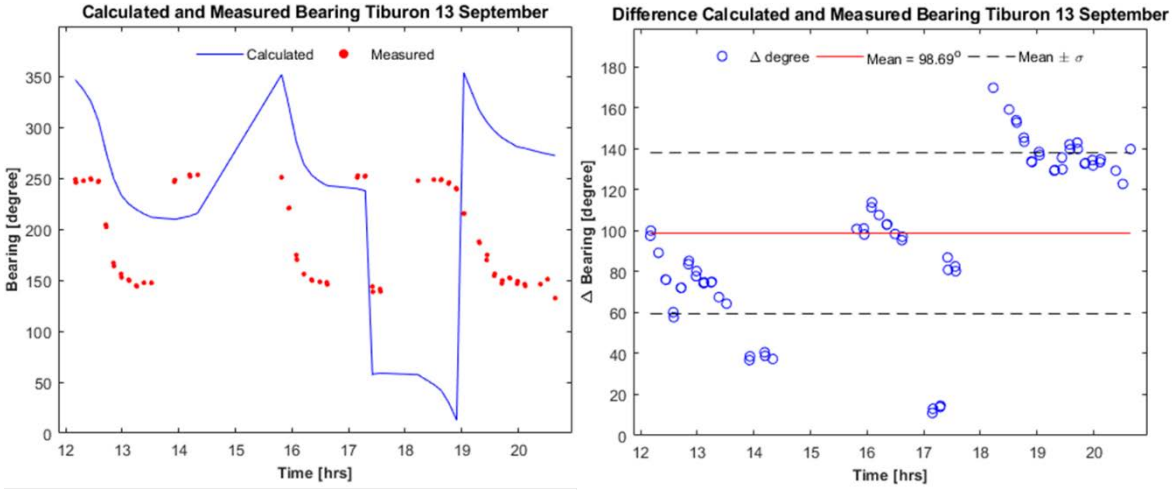

Figure 28. Calculated and Measured Bearings for Tiburon 13 September

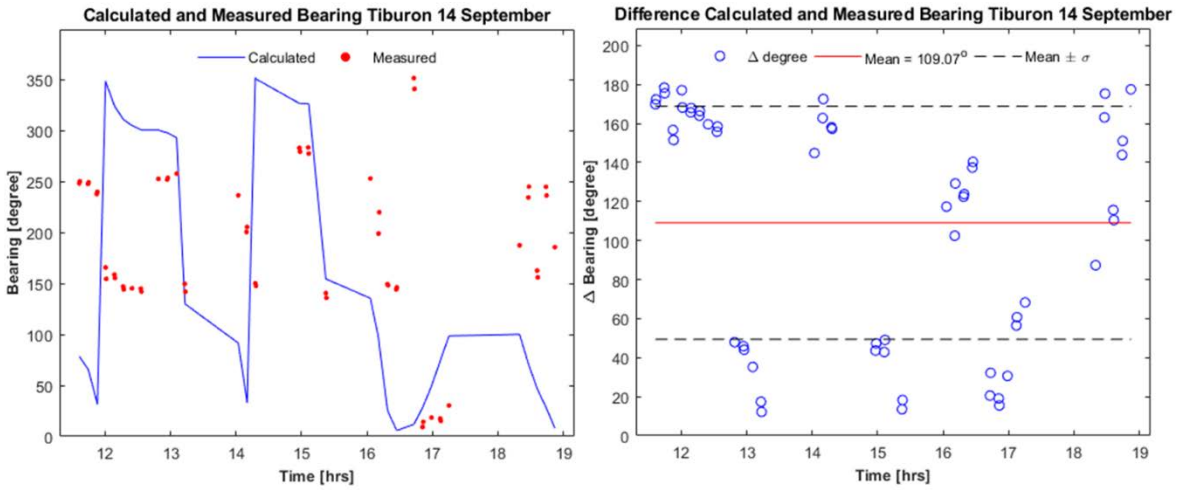

Figure 29. Calculated and Measured Bearings for Tiburon 14 September

After the September trial, the measured bearings seem capable, if configured correctly, of providing a rough estimate of the true bearing. However, the 20 degree average error might not deem it suitable for applications with more accurate needs. Presently the bearing information is provided on a single request basis. Adding a Kalman filter could potentially improve the provided bearing information, which could make the bearing output more suitable for navigation purposes.

C. RAY TRACING RESULTS

Using the Bellhop beam tracing model, a very good estimate can be made of the actual acoustic path in the specific scenario. During the sea trial of September 2017, 592 range requests were sent from the tow bodies to the echo repeater. Nearly 40 percent (218) of those range requests were successful (i.e., the echo repeater generated a response and sent this to the tow bodies). The ranging routine inside the acoustic modem (see Section II.A.2) then estimated the range between tow body and echo repeater and stored the probe signal's matched filter output. Since there are many successful range requests and matched filter outputs, a lot of time would be required to investigate the predicted ray trace path for each of those. Therefore, a selection has been made of several range requests. The ray tracing arrival output was then compared to the actual recorded matched filter data, which included the probe signal match filter response. This comparison was done mainly to better

understand and interpret the recorded data. It helped to identify direct and multi-path arrivals and assess their impact. Due to the trial set up (with the echo repeater very near to the bottom, and not in the water column), it was expected that the strongest arrival should always be the direct path. The ray trace data was also used to check the launch and receiving grazing angles, which were calculated to compare the range results between the modem-determined and calculated range (see Section IV.D).

1. Selected Examples and Approach

The following paragraph shows the outcome of the ray tracing analysis for a couple of selected examples. For each of the selected examples, the appropriate averaged sound speed profile and bottom profile were used as discussed in Section III.C.4 and Section III.C.1, respectively. The calculated horizontal and vertical distances described previously were used as input. Using the latter makes sure the effect of the tide is taken into account. Bellhop calculated eigenrays for grazing angle between -30 and 30 degrees. For most cases, larger grazing angles result in five boundary bounces or more and are more than 25 dB lower in amplitude than the direct path arrival. At greater angles, more surface interference is expected due to the roughness of sea surface. Since the observed noise levels were only about 20dB below the direct path arrivals, these ray paths with larger grazing angles will be lost in the noise. Furthermore, Bellhop was set to calculate 12000 beams, which means the angular resolution of the Bellhop calculation is 5/1000 of a degree. For the Bellhop calculations, a step size of 15 cm was used. As a result the Bellhop predictions are accurate up to this error.

For this section the following examples were selected:

1. Medium range by Mako on 13 September
2. Medium range by Mako on 14 September
3. Medium range by Tiburon on 13 September
4. Medium range by Tiburon on 14 September
5. Close range by Tiburon on 13 September

6. Close range by Tiburon on 14 September

7. Long range by Mako on 13 September

8. Long range by Mako on 14 September

For the set of medium range examples, it is expected that both direct path and several multi-paths will be observed. The predicted arrivals of eigenrays are roughly grouped into sets of four. The first set of four arrivals are in (general) order of arrival: direct path (DP), single-surface bounce (S), single-bottom bounce (B) and bottom-surface bounce (BS). The second set of arrivals are: surface-bottom bounce (SB), bottom-surface-bottom bounce (BSB), surface-bottom-surface bounce (SBS) and bottom-surface-bottom-surface bounce (BSBS). The third group of arrivals are: surface-bottom-surface-bottom bounce (SBSB), bottom-surface-bottom-surface-bottom bounce (BSBSB), surface-bottom-surface-bottom-surface bounce (SBSBS) and bottom-surface-bottom-surface-bottom-surface bounce (BSBSBS). Due to the multiple boundary interactions and the additional path length, the amplitude of the third group is in general expected to be low compared to the noise level.

Table 3 shows an example arrival output from Bellhop. Note the grouping of the arrivals as discussed above. The tabulated data belongs to example 7 and the path color coding is identical to the coding used in the eigenray visualizations, which are shown in the next section. Also note that the arrivals of group four are all well below the noise level, which is in this case about 20dB below the peak arrivals.

Table 3. Example of Bellhop Arrival Output

	Norm. Ampl. [dB]	Phase [°]	Arrival Time [ms]	ΔTime [ms]	ΔPath [m]	xER [°]	xTB [°]	#Surface bounces	#Bottom bounces	Path
Group 1	0.00	0.0	660.00	0.0000	0.0000	-9.7480	1.8264	0	0	DP
	-7.43	180.0	660.04	0.0348	0.0522	-10.0360	2.8577	1	0	S
	-1.87	86.6	660.38	0.3768	0.5652	9.7240	1.6274	0	1	B
	-8.89	263.9	660.43	0.4233	0.6350	10.0540	3.0931	1	1	BS
Group 2	-3.17	229.3	675.57	15.5680	23.3520	-14.5245	-10.9702	1	1	SB
	-6.16	276.7	676.13	16.1275	24.1913	14.6625	-11.1486	1	2	BSB
	-3.49	404.1	677.22	17.2185	25.8278	-15.2205	11.8809	2	1	SBS
	-6.74	446.4	677.81	17.8039	26.7059	15.3585	12.0619	2	2	BSBS
Group 3	-14.67	387.8	705.04	45.0354	67.5531	-21.8872	-19.7715	2	2	SBSB
	-21.95	401.1	705.87	45.8647	68.7970	22.0372	-19.9377	2	3	BSBSB
	-15.34	565.8	707.94	47.9347	71.9020	-22.5293	20.4850	3	2	SBSBS
	-22.91	578.1	708.79	48.7869	73.1803	22.6793	20.6530	3	3	BSBSBS
Group 4	-29.18	562.2	747.38	87.3757	131.0635	-28.9019	-27.3993	3	3	SBSBSB
	-38.69	569.3	748.45	88.4493	132.6740	29.0459	-27.5494	3	4	BSBSBSB
	-29.59	741.3	751.31	91.3021	136.9532	-29.4719	28.0005	4	3	SBSBSBS
	-39.21	748.2	752.40	92.3950	138.5925	29.6160	28.1573	4	4	BSBSBSBS

The next paragraph will describe the eight different examples mentioned above. Each example will be formatted in a table. The first row indicates the appropriate Wave Gliders track and highlights the position of the discussed example. It also shows the actual raw logged range message, which logs:

- Executed command (send ATR20)
- Time of transmission of range request (Tx time) and time of receipt of probe signal (Rx Time) at the tow body.
- Measured bearing from echo repeater to tow body and measured inclination from the tow body (negative is upward).
- Measured range, based on half the round-trip (or two-way travel) time multiplied by 1500 m/s.
- Measured Doppler speed (negative is opening)
- File name of the matched filter output.

The next line provides the appropriate area (and as such the appropriate SSP-data) and the tidal height as predicted by [11]. The lines following are outputs of the calculation based on the interpolated positions as described in Section IV.C and Section IV.D. Additionally, to the previously described calculations, an inverse sound speed (SS) has been determined by dividing the calculated curved range by half of the measured round-trip time. This value provides an indication of the average experienced sound speed.

$$SS_{inverse} = \frac{Range_{curved}}{TravelTime_{one-way,measured}} \tag{15}$$

The next set of lines show the output of the Bellhop algorithm. More specifically it provides the grazing angle at the echo repeater and the tow body. These angles are based on the direct path arrival, as is also shown in the Table 3 example. The curved range calculated in this section is based on the launch and arrival angles calculated by Bellhop. Then Equations 11 and 13 are used to calculate the arclength of the curved path between tow body and echo repeater. Equation 15 then provides the inverse average sound speed over this path. Using this inverse average sound speed a 'best range' based on the measured one-way travel time multiplied by the inverse sound speed is calculated.

After these parameters, three different figures are shown. First the visualization of the eigenrays, then the combined matched-filter-Bellhop output for the first 150 ms followed by an appropriately zoomed version of the same output. These figures are described and explained in Section II.B.2.

2. Selected Examples

Table 4. Example 1: Medium Range, Mako, 13 September

Range message			
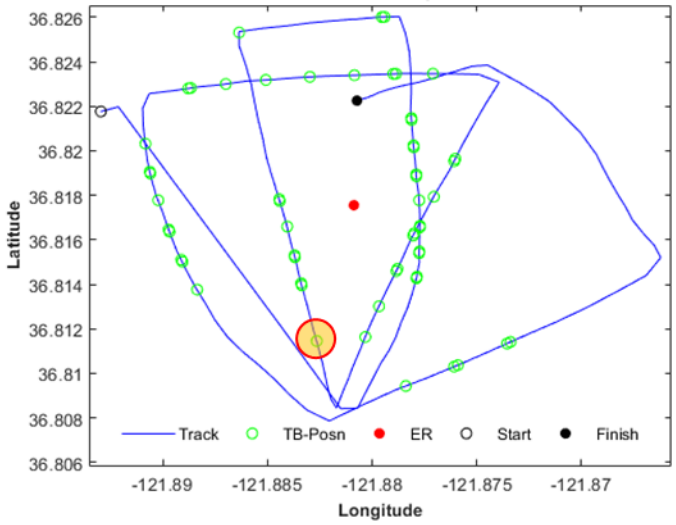	send ATR20 Tx time:14:32:40.9939 Rx Time:14:32:44.3282 Bearing 205.9, -12.3 (Local) Range 11 to 20 : 697.5 m (Round-trip 930.0 ms) speed -0.2 m/s Probe filename is 2017913_1432_2.wav		
Relevant environment parameters			
Tidal height (m)	1.37	Area:	5
Estimated (based on interpolated positions and recursive ray model)			
Latitude TB at TX-time:	36,81145646	Vertical distance (m):	68.92
Longitude TB at TX-time:	-121,8826505	Horizontal distance (m):	694.57
Bearing (°)	193.1	Slant range (m):	697.98
Angle from ER (°):	-9.3794	Curved range (m)	698.43
Angle at TB (°):	-1.9548	$\text{TravelTime}_{\text{1-way}} \cdot \text{SS}_{\text{inverse}}$ (m)	694.56
One-way travel time (ms)	467.59	$\text{SS}_{\text{inverse}}$ i.a.w. eq. 15 (m/s)	1493.7
Bellhop			
Angle from ER:	-9.3534	Curved range (m)	693.81
Angle at TB:	-1.9781	Inverse average SS (m/s)	1492.1

(continued)

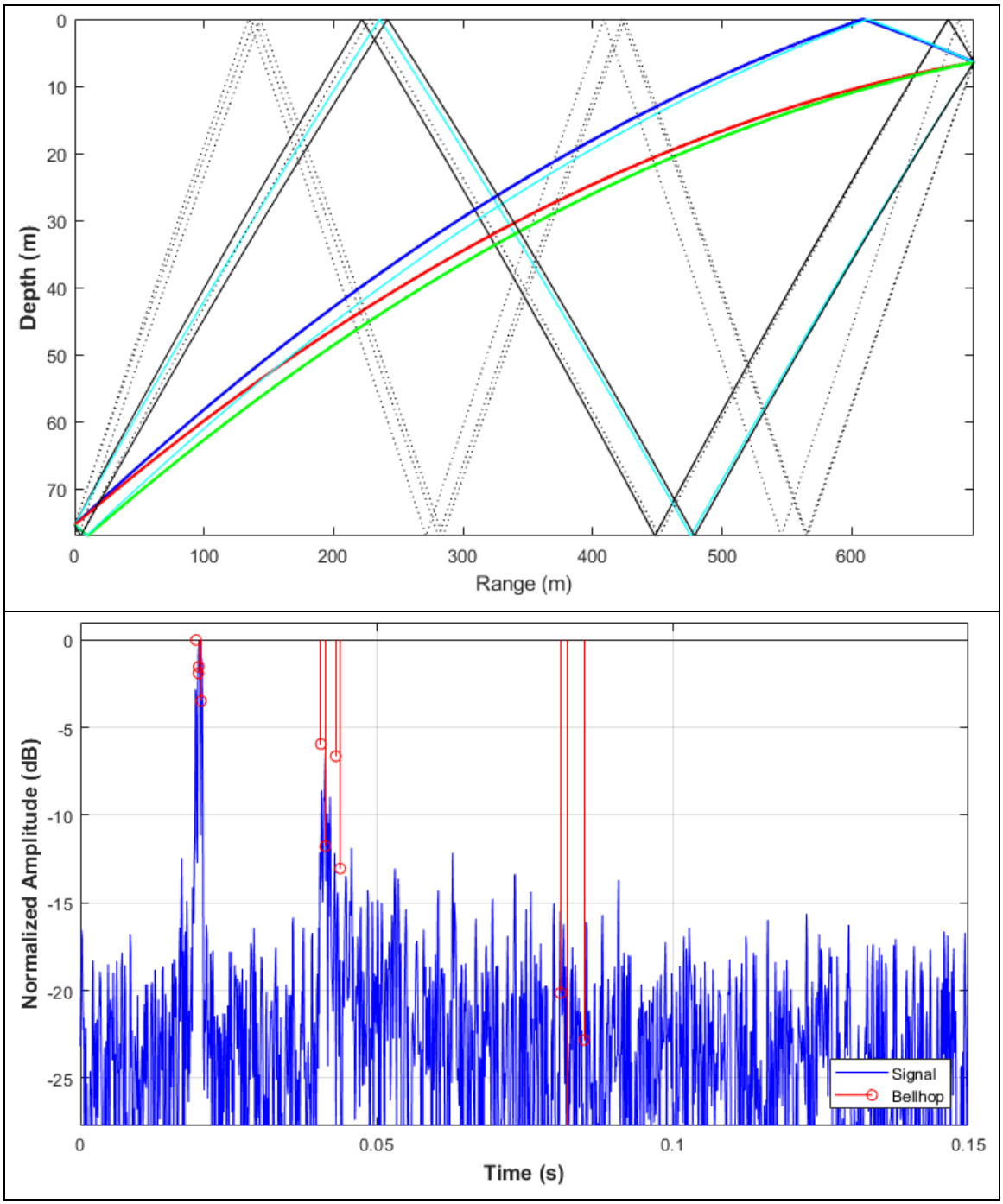
Depth (m)
Range (m)
Normalized Amplitude (dB)
Time (s)
Signal
Bellhop

(continued)

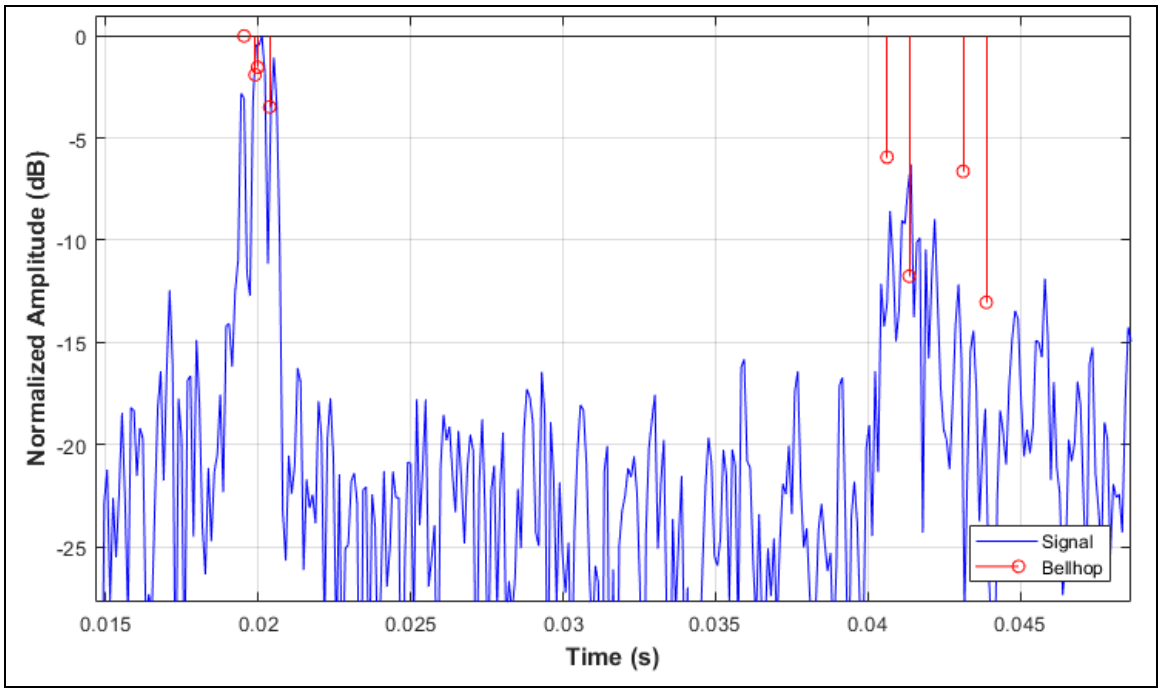

As expected, this example clearly shows direct path and several other multi-path arrivals in the matched filter output. Both the first and the second group of arrivals are clearly visible above the noise level. The third group is not visible in this case. Zooming in on the first group, it appears possible, in this example, to identify arrivals of the DP, S-bounce, B-bounce, and BS-bounce. The match filter output shows about a 3 dB reduction in amplitude for the DP versus the S-bounce and B-bounce paths, where the latter provides the strongest response. This would result in 0.4 ms difference in the one-way travel time, which corresponds to a path length difference of about 60 cm. As shown in the third section of Table 4 all calculated ranges are within five meters or 1% of each other. The main reason these ranges are so close can also be seen in the combined matched filter/Bellhop graph. Since the predicted arrivals agree fairly well with the actual arrivals, the SSP used appears to be a reasonable representation in this case. Within the second group, the SB-bounce and BSB-bounce seem to be visible. Both the SBS-bounce and BSBS-bounce cannot be unambiguously identified.

Table 5. Example 2: Medium Range, Mako, 14 September

Range message			
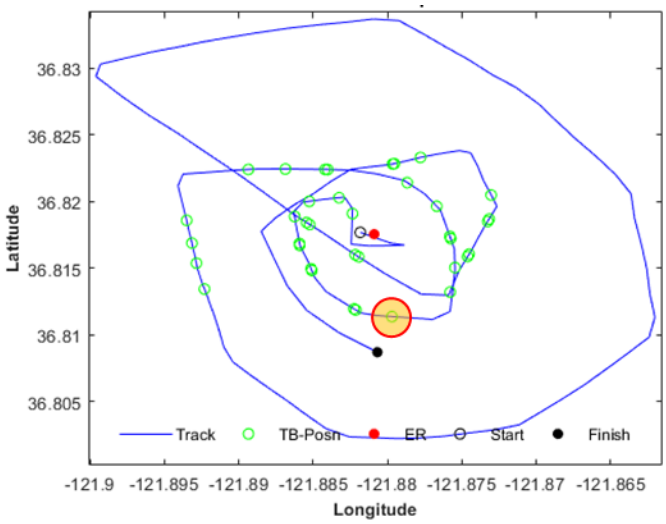	send ATR20 Tx time:12:21:16.5195 Rx Time:12:21:19.8628 Bearing 173.8, 3.2 (Local) Range 11 to 20 : 704.4 m (Round-trip 939.2 ms) speed -0.3 m/s Probe filename is 2017914_1220_2.wav		
Relevant environment parameters			
Tidal height (m)	0.82	Area:	5
Estimated (based on interpolated positions and recursive ray model)			
Latitude TB at TX-time:	36.811358448	Vertical distance (m):	68.37
Longitude TB at TX-time:	-121.8796930	Horizontal distance (m):	695.55
Bearing (°)	171.2	Slant range (m):	698.91
Angle from ER (°):	-9.3316	Curved range (m)	699.35
Angle at TB (°):	-1.8969	$\text{TravelTime}_{\text{1-way}} \cdot \text{SS}_{\text{inverse}}$ (m)	701.47
One-way travel time (ms)	468.19	$\text{SS}_{\text{inverse}}$ i.a.w. eq. 15 (m/s)	1493.8
Bellhop			
Angle from ER (°):	-9.3033	Curved range (m)	700.29
Angle at TB (°):	-1.9167	Inverse average SS (m/s)	1491.3

(continued)

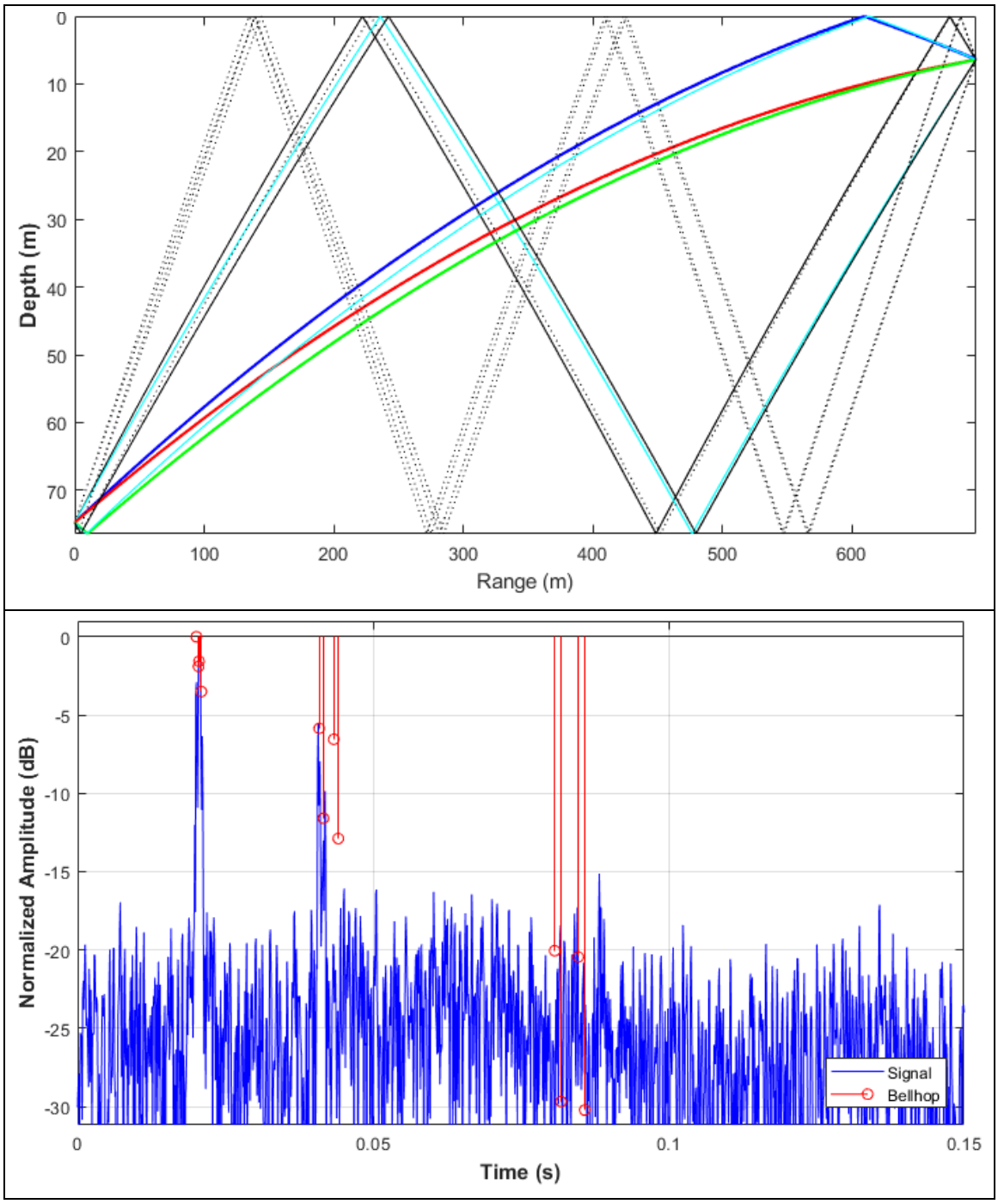
Depth (m)
Range (m)
Normalized Amplitude (dB)
Time (s)
Signal
Bellhop

(continued)

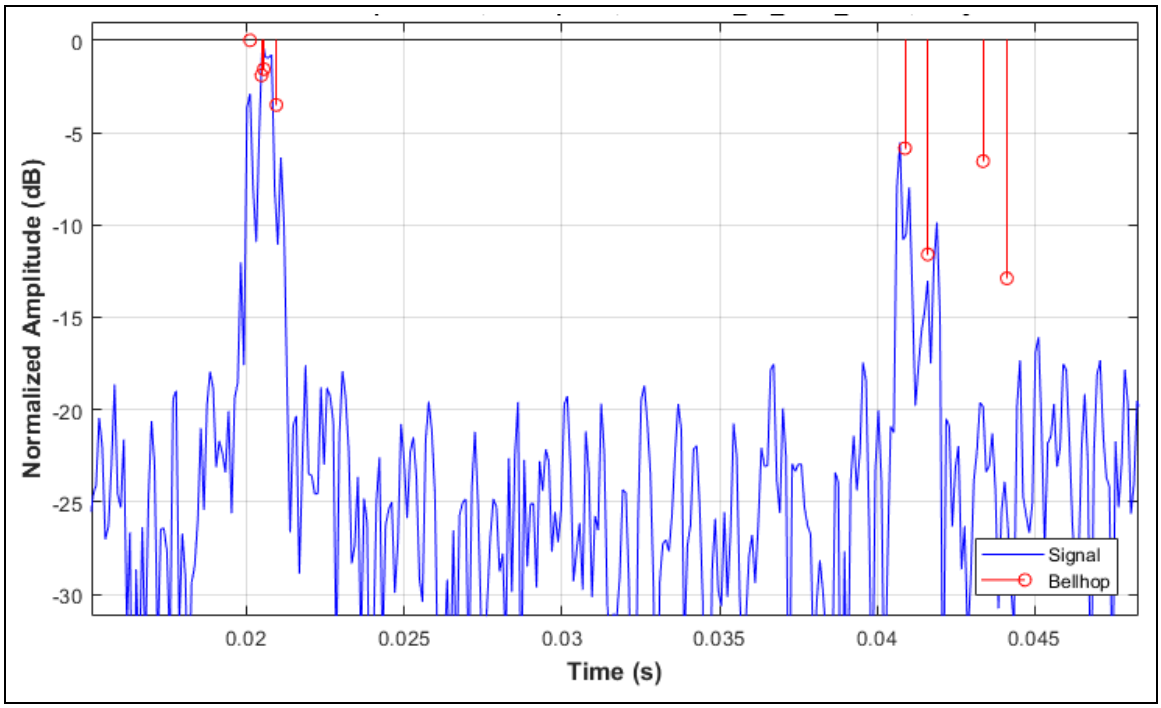

As in the previous example, arrivals of the first and second group are clearly visible. The predicted Bellhop output suggests there might be a response visible from the third group, although it would be just on the edge of the noise level. The matched filter results are consistent with this prediction, since these arrivals cannot be identified. As in the previous example, all different ranges are within five meters and one percent. Note that the inverse sound speeds are also very close (<0.2%). Again, the first two arrivals of the second group are visible, but the last two of this group appear to have vanished in the noise. As before, the direct path arrival does not appear to be the strongest arrival. It appears that the simultaneously arriving S-bounce and B-bounce path constructively interfere which explains the 3 dB amplitude level increase.

Table 6. Example 3: Medium Range, Tiburon, 13 September

Range message			
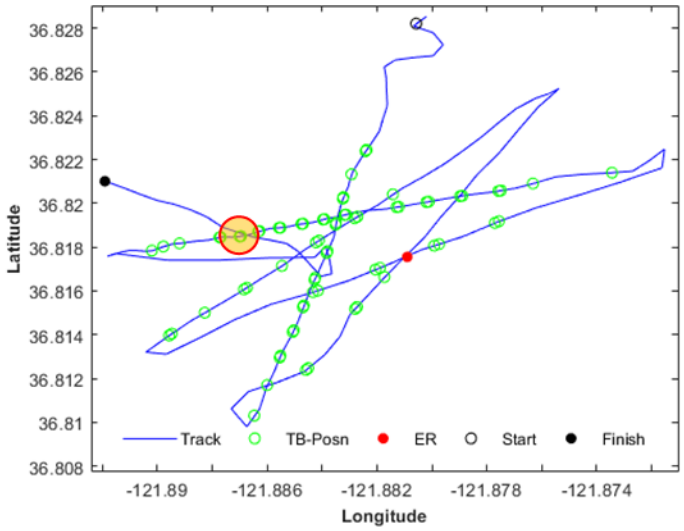	send ATR20 Tx time:19:59:14.2967 Rx Time:19:59:17.4097 Bearing 149.0, 7.1 (Local) Range 10 to 20 : 531.6 m (Round-trip 708.8 ms) speed -0.2 m/s Probe filename is 2017913_1958_2.wav		
Relevant environment parameters			
Tidal height (m)	1.09	Area:	6
Estimated (based on interpolated positions and recursive ray model)			
Latitude TB at TX-time:	36.818488016	Vertical distance (m):	68.64
Longitude TB at TX-time:	-121.8869919	Horizontal distance (m):	554.61
Bearing (°)	280.8	Slant range (m):	558.84
Angle from ER (°):	-10.1695	Curved range (m)	559.03
Angle at TB (°):	-3.9432	$\text{TravelTime}_{\text{1-way}} \cdot \text{SS}_{\text{inverse}}$ (m)	532.72
One-way travel time (ms)	371.90	$\text{SS}_{\text{inverse}}$ i.a.w. eq. 15 (m/s)	1503.2
Bellhop			
Angle from ER (°):	-10.1654	Curved range (m)	559.10
Angle at TB (°):	-3.9384	Inverse average SS (m/s)	1577.6

(continued)

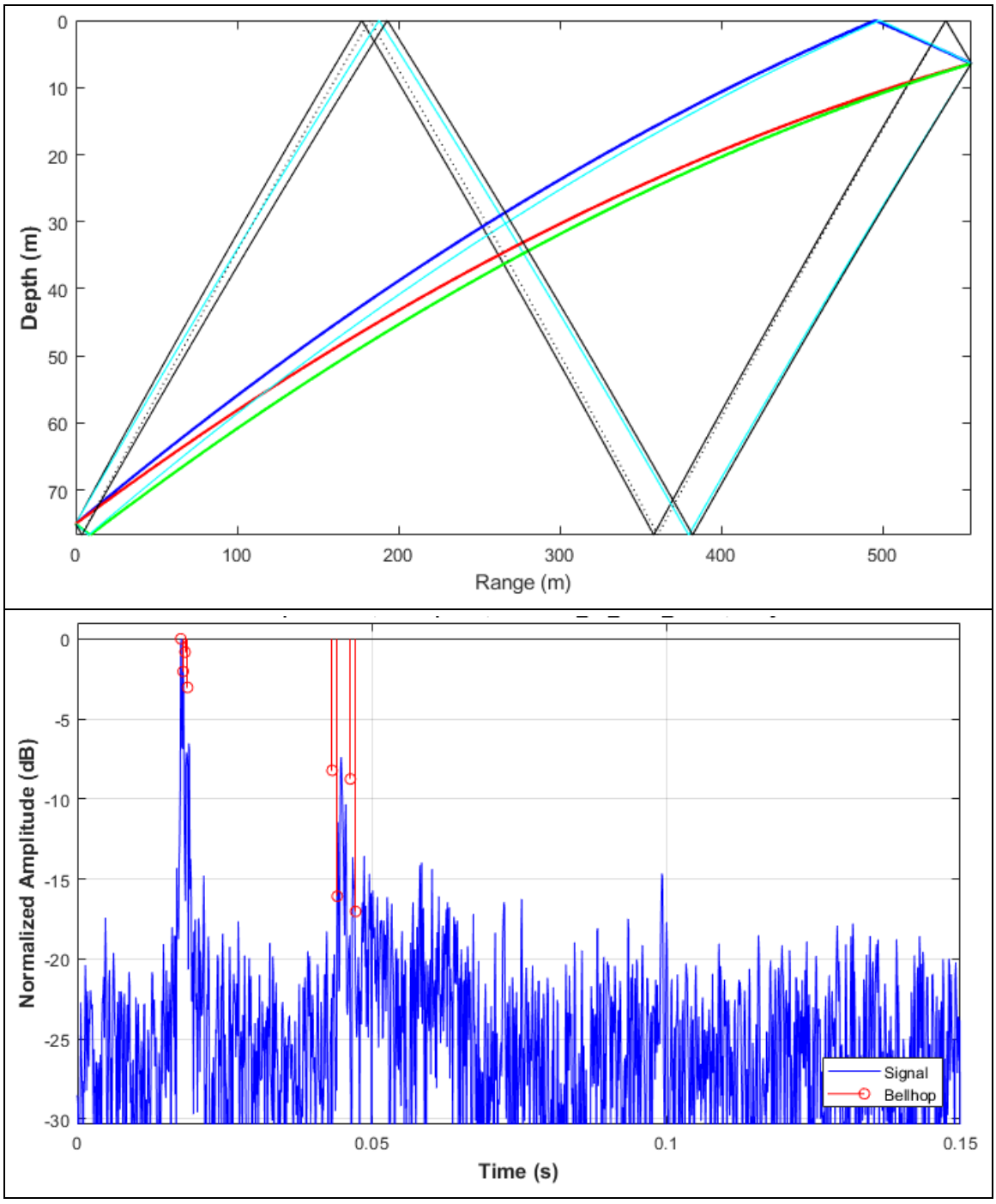
Depth (m)
Range (m)
Normalized Amplitude (dB)
Time (s)
Signal
Bellhop

(continued)

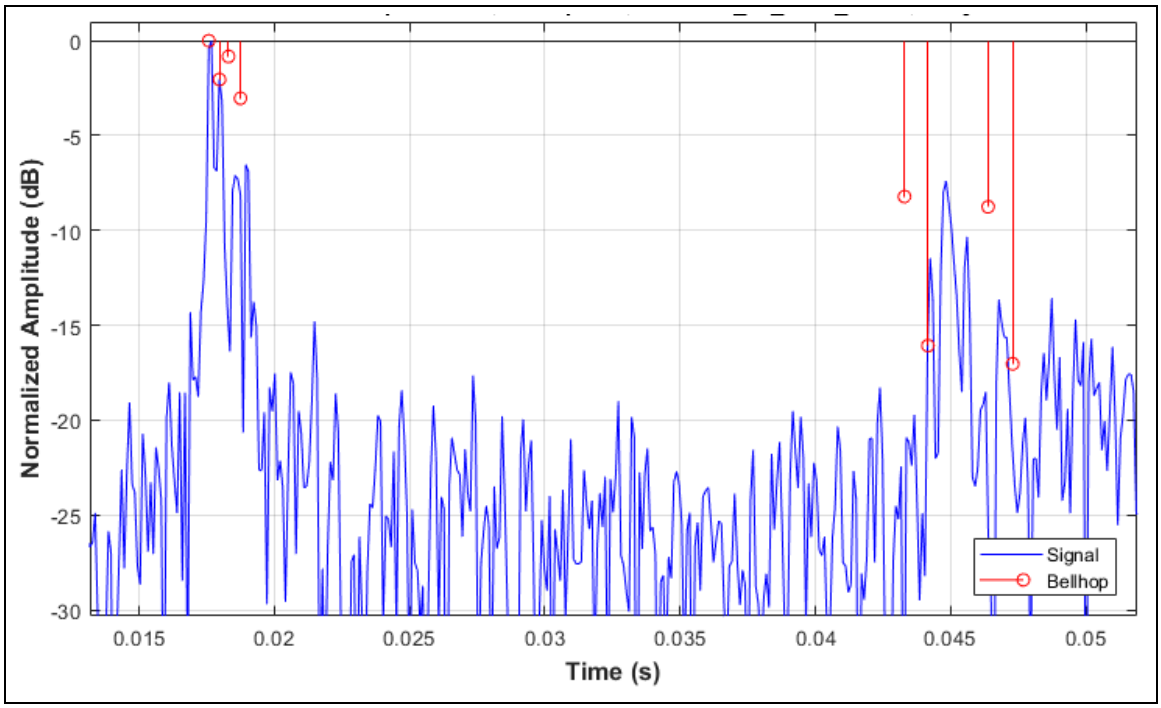

The range of this medium range example is a little closer than the previously two discussed examples. In this case, the third group is no longer predicted to arrive at the tow body, because the required 'launch' angles from the ER are about 33 degrees. As previously discussed these larger launch angles were filtered out of the Bellhop results, since they result in amplitude levels below the noise level (due to the multiple bottom and surface losses) and are therefore difficult to detect. In this example, the direct path does produce the strongest arrival, but there is also a bigger difference (about 4.7%) between the measured and estimated range. The measured round-trip travel time seems to be about 20 ms (equivalent to about 30 meters) shorter than expected. Note that the difference is still within the expected error range and therefore can be considered a good range. Also note that this slight range difference does result in an unphysically high inverse sound speed using the Bellhop data.

Table 7. Example 4: Medium Range, Tiburon, 14 September

Range message			
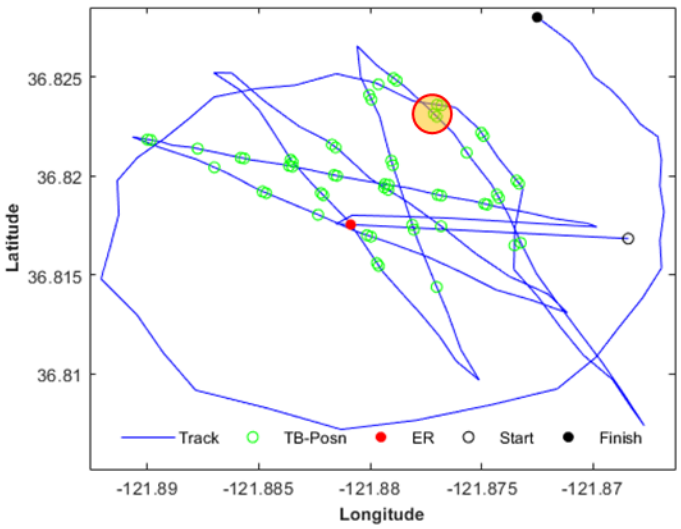	send ATR20 Tx time:16:51:04.1298 Rx Time:16:51:07.5032 Bearing 9.2, -39.5 (Local) Range 10 to 20 : 726.8 m (Round-trip 969.1 ms) speed -0.1 m/s Probe filename is 2017914_1650_1.wav		
Relevant environment parameters			
Tidal height (m)	1.59	Area:	2
Estimated (based on interpolated positions and recursive ray model)			
Latitude TB at TX-time:	36.823139404	Vertical distance (m):	69.14
Longitude TB at TX-time:	-121.8771516	Horizontal distance (m):	703.84
Bearing (°)	28.3	Slant range (m):	707.23
Angle from ER (°):	-9.7327	Curved range (m)	707.82
Angle at TB (°):	-1.488	$\text{TravelTime}_{\text{1-way}} \cdot \text{SS}_{\text{inverse}}$ (m)	728.31
One-way travel time (ms)	470.92	$\text{SS}_{\text{inverse}}$ i.a.w. eq. 15 (m/s)	1503.1
Bellhop			
Angle from ER (°):	-9.7283	Curved range (m)	707.77
Angle at TB (°):	-1.4844	Inverse average SS (m/s)	1460.7

(continued)

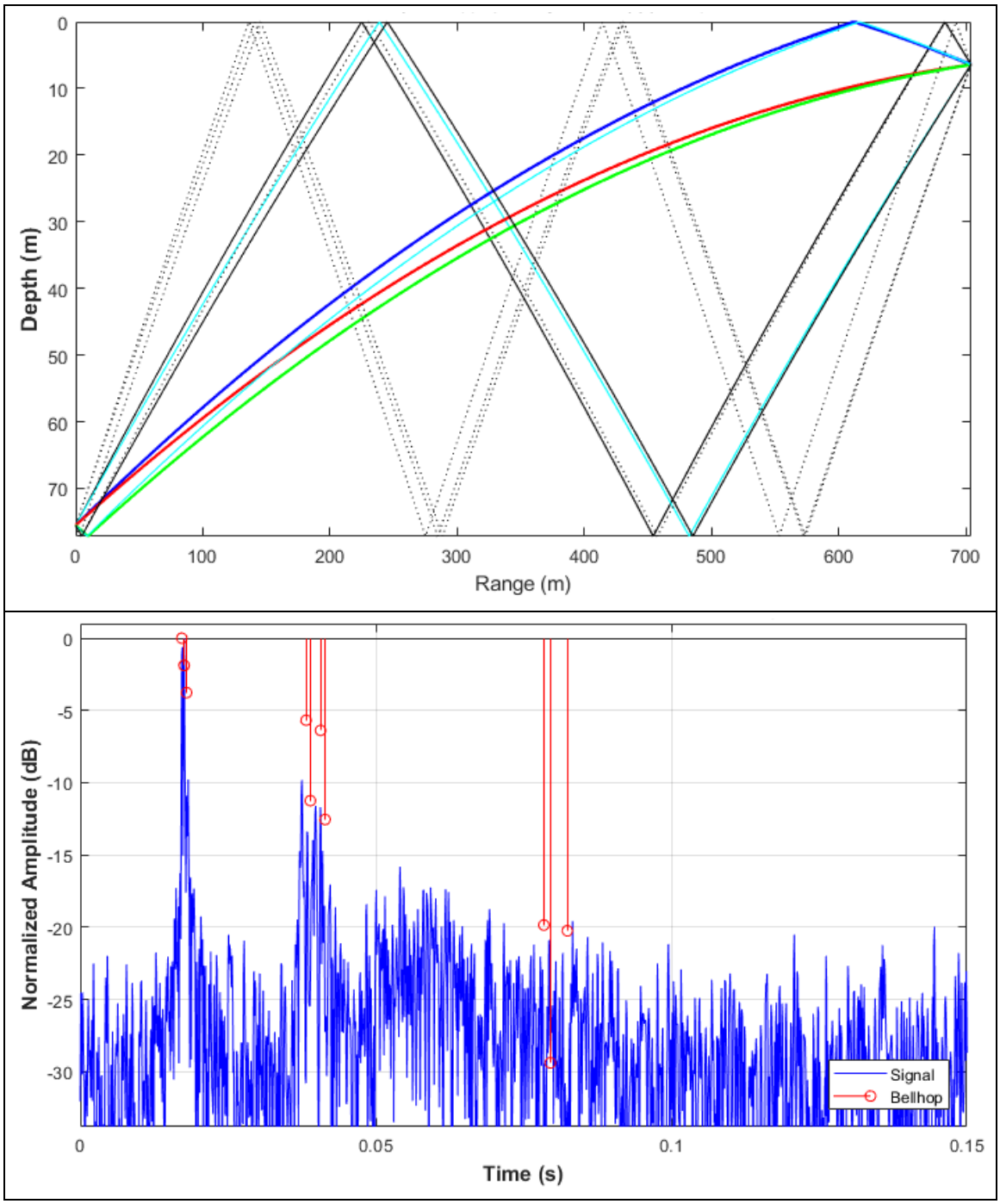
Depth (m)
Range (m)
Normalized Amplitude (dB)
Time (s)
Signal
Bellhop

(continued)

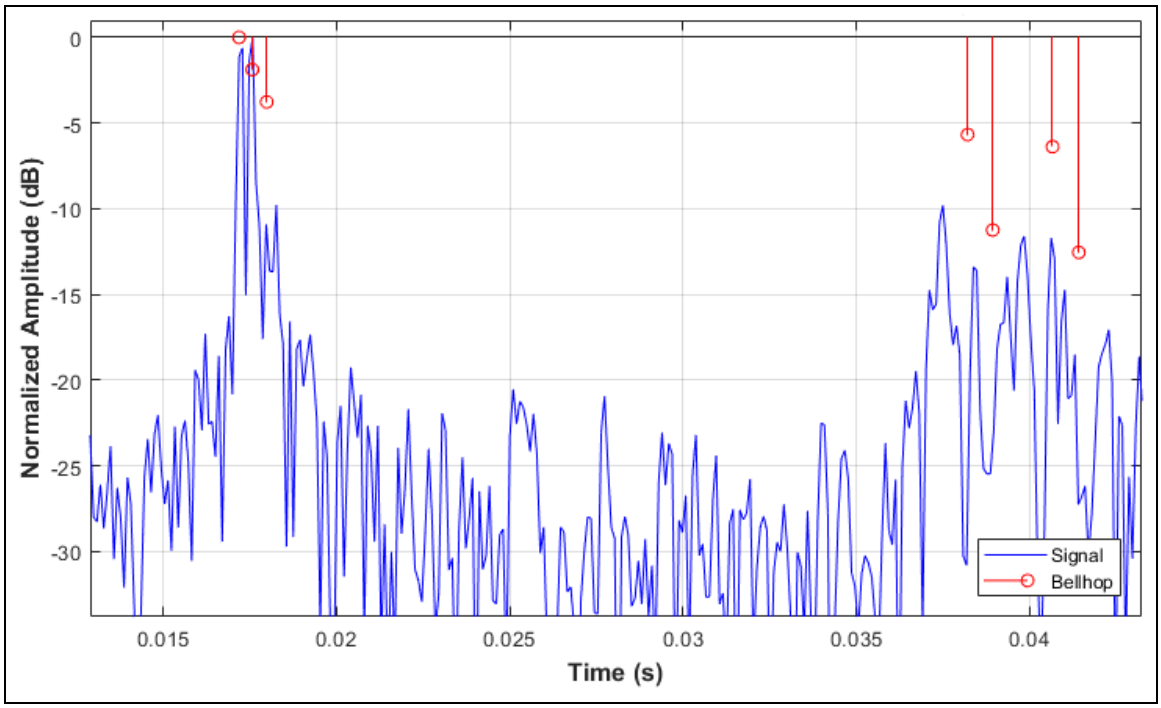

The ranges for this example are, like example one and two, again around 700 m. The difference between measured and calculated ranges is about 3%. Although this is still within error, comparing the matched filter output with the Bellhop prediction suggests the actual sound speed may be higher than used for the prediction. Note that the actual arrivals from the second group lead the predicted arrivals. This difference is about 3.5% and is consistent with the difference between measured and calculated ranges.

Table 8. Example 5: Close Range, Tiburon, 13 September

Range message			
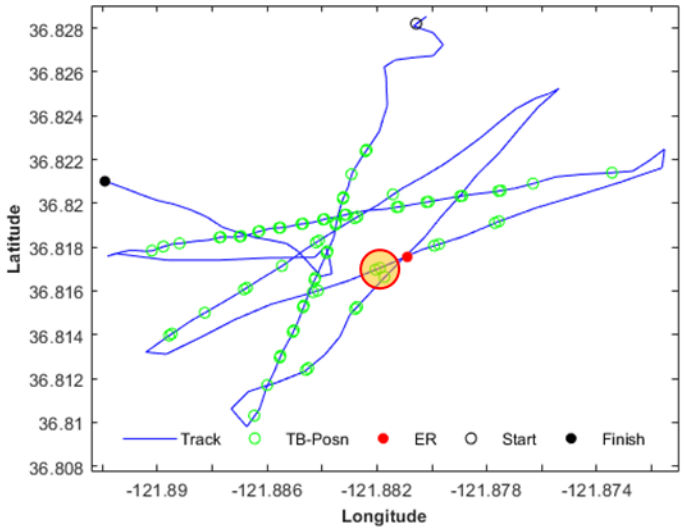	send ATR20 Tx time:17:17:46.6617 Rx Time:17:17:49.2139 Bearing 252.3, 11.3 (Local) Range 10 to 20 : 111.0 m (Round-trip 148.1 ms) speed 0.2 m/s Probe filename is 2017913_1717_2.wav		
Relevant environment parameters			
Tidal height (m)	1.64	Area:	1
Estimated (based on interpolated positions and recursive ray model)			
Latitude TB at TX-time:	36.817048924	Vertical distance (m):	69.19
Longitude TB at TX-time:	-121.8818805	Horizontal distance (m):	104.88
Bearing (°)	237.8	Slant range (m):	125.64
Angle from ER (°):	34.049	Curved range (m)	125.56
Angle at TB (°):	32.828	$\text{TravelTime}_{\text{1-way}} \cdot \text{SS}_{\text{inverse}}$ (m)	111.09
One-way travel time (ms)	83.70	$\text{SS}_{\text{inverse}}$ i.a.w. eq. 15 (m/s)	1500.2
Bellhop			
Angle from ER (°):	-34.0236	Curved range (m)	125.63
Angle at TB (°):	-32.8015	Inverse average SS (m/s)	1696.6

(continued)

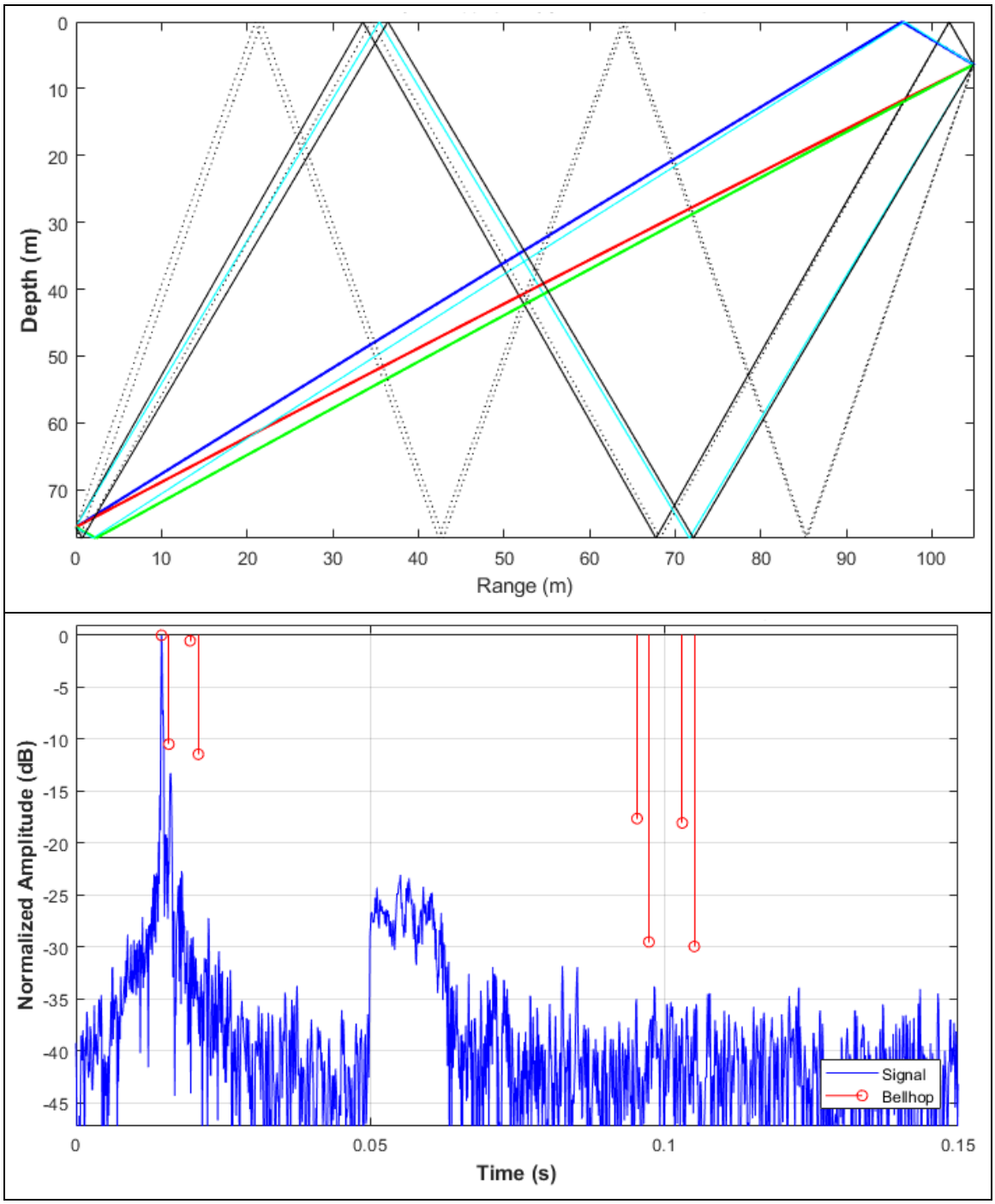
Depth (m)
Range (m)
Normalized Amplitude (dB)
Time (s)
Signal
Bellhop

(continued)

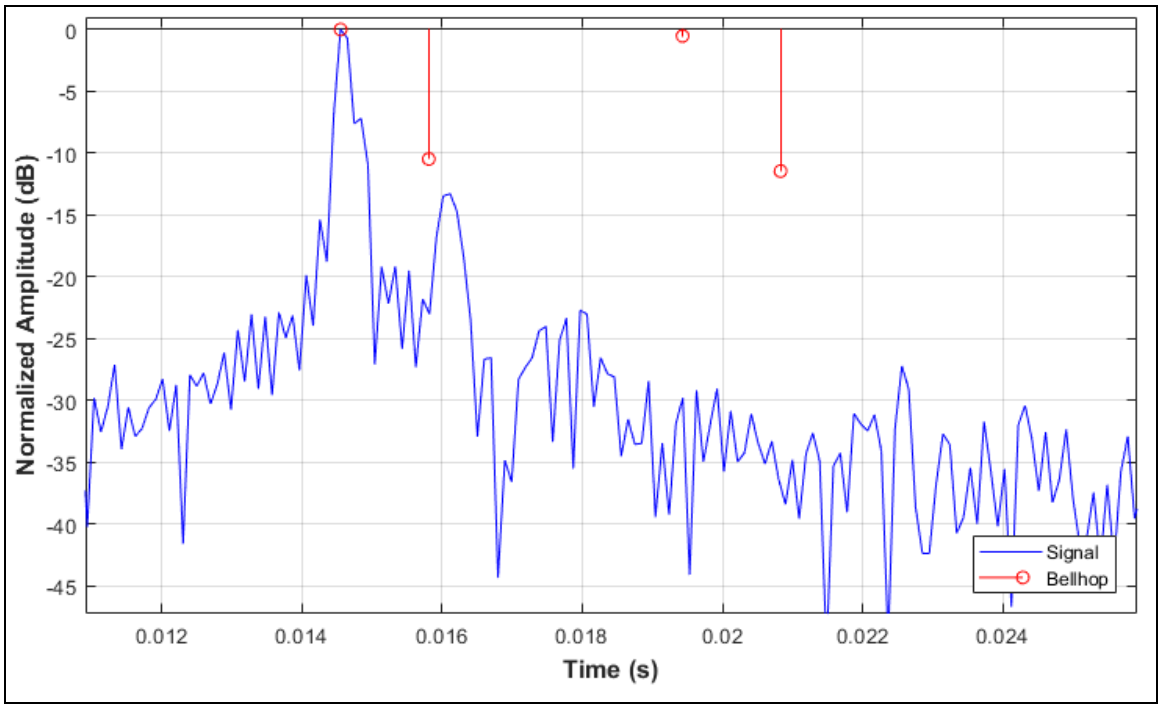

This example shows one of the smallest observed ranges. The direct path has a grazing angle of more than 30 degrees. Therefore, the Bellhop model is run with a bigger spread in launch angles (-75 to 75 degrees). The matched filter output shows a very strong direct arrival, about 35 dB above the noise. No arrivals from the second group are visible in the matched filter, although these are predicted by Bellhop to be above the noise level.. This might be caused by stronger boundary losses at these greater angles (more than 70 degrees) than are accounted for in the Bellhop model. Also note that the inverse sound speed based on the Bellhop curve and the roundtrip time is unphysically high. This might be due to the fact that at short ranges the error in range is larger than at long ranges. In this case the error is about 11% which is bigger that the predicted error. Another thing to notice is the artifact in the matched filter output at exactly 50 ms. This (15–20 ms long) artifact is visible in almost all matched filter output with ranges less than 450 m. This artifact is discussed in more detail in Section V.C.3.

Table 9. Example 6: Close Range, Tiburon, 14 September

Range message			
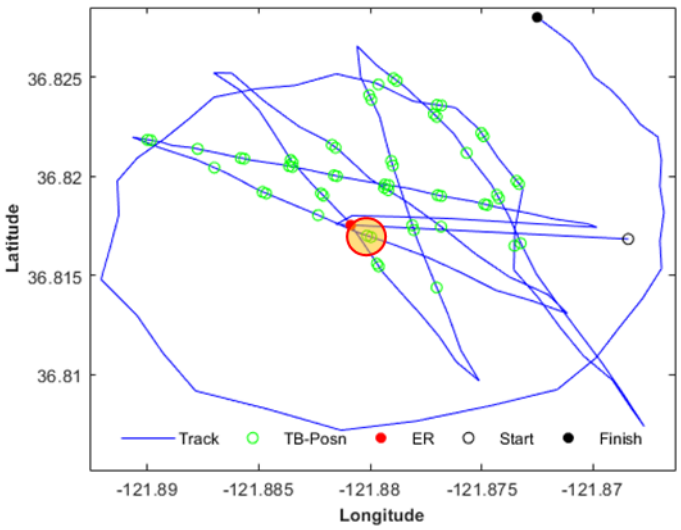		send ATR20 Tx time:13:13:04.1339 Rx Time:13:13:06.7032 Bearing 149.6, -13.4 (Local) Range 10 to 20 : 123.8 m (Round-trip 165.1 ms) speed -0.3 m/s Probe filename is 2017914_1313_1.wav	
Relevant environment parameters			
Tidal height (m)	0.90	Area:	1
Estimated (based on interpolated positions and recursive ray model)			
Latitude TB at TX-time:	36.817008015	Vertical distance (m):	68.45
Longitude TB at TX-time:	-121.8801402	Horizontal distance (m):	89.88
Bearing (°)	132.2	Slant range (m):	112.97
Angle from ER (°):	-37.8462	Curved range (m)	112.90
Angle at TB (°):	-36.8000	$\text{TravelTime}_{\text{1-way}} \cdot \text{SS}_{\text{inverse}}$ (m)	123.85
One-way travel time (ms)	75.25	$\text{SS}_{\text{inverse}}$ i.a.w. eq. 15 (m/s)	1500.3
Bellhop			
Angle from ER (°):	-37.8138	Curved range (m)	112.93
Angle at TB (°):	-36.7668	Inverse average SS (m/s)	1368.1

(continued)

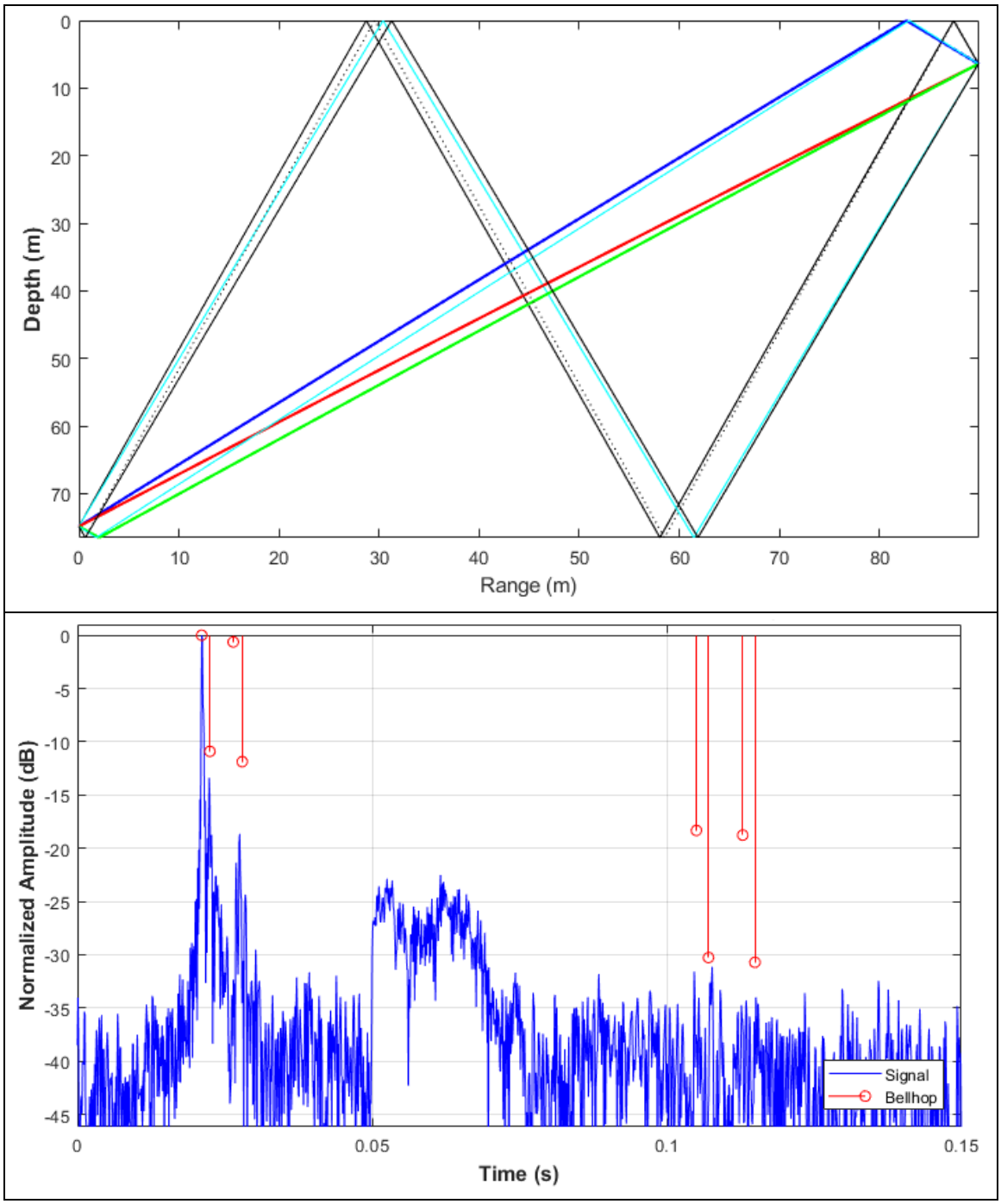
Depth (m)
Range (m)
Normalized Amplitude (dB)
Time (s)
Signal
Bellhop

(continued)

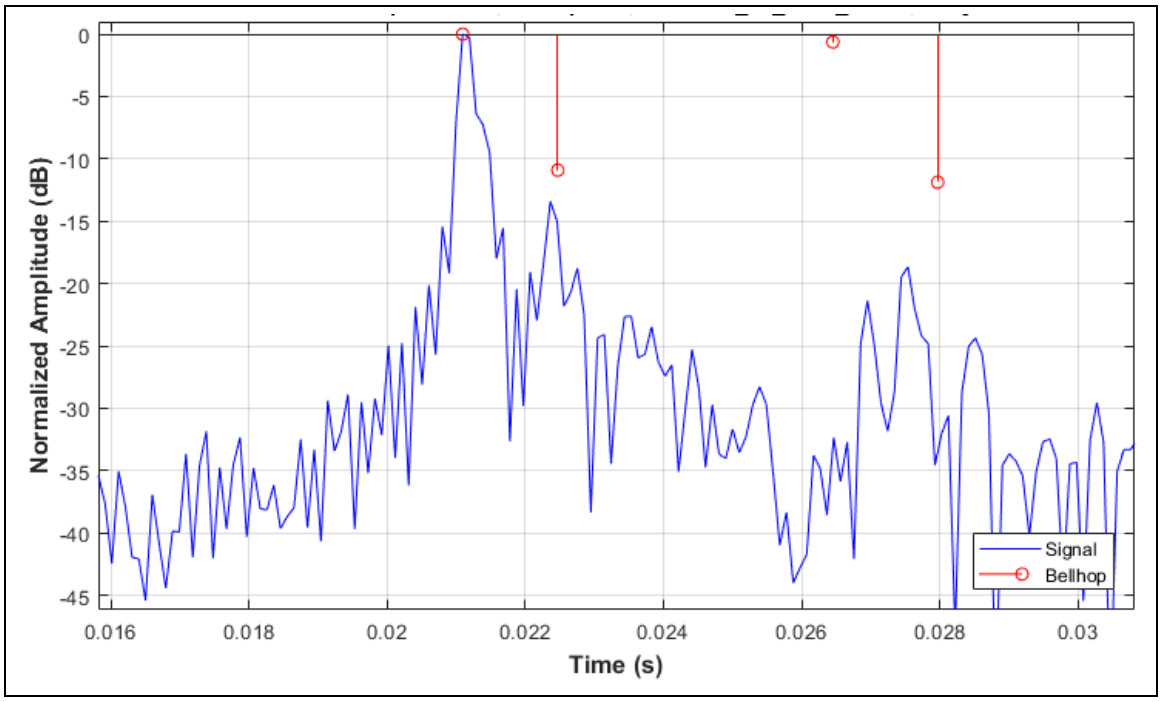

The matched filter output of this second short range example again shows a very strong direct arrival, about 35 dB above the noise. As before, no arrivals from the second group are visible in the matched filter output. Also note in this example the inverse sound speed based on the Bellhop curve and the roundtrip time is unphysically low. Furthermore, the artifact at 50 ms is again clearly visible.

Table 10. Example 7: Long Range, Mako, 13 September

Range message			
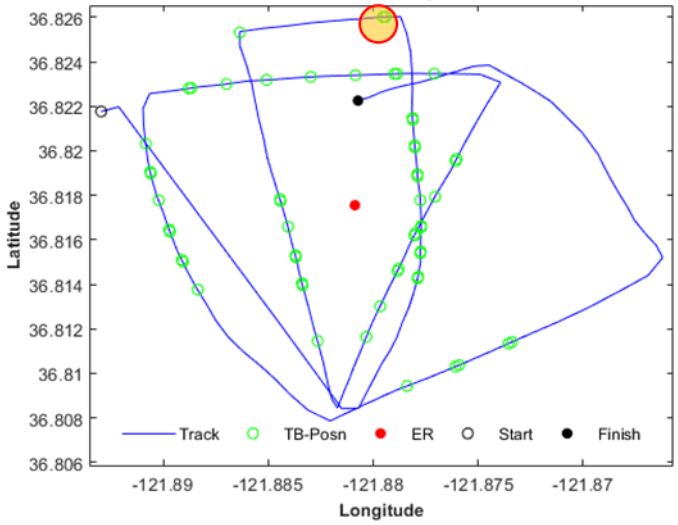	send ATR20 Tx time:13:03:53.7000 Rx Time:13:03:57.4347 Bearing 276.5, 16.0 (Local) Range 11 to 20 : 997.8 m (Round-trip 1330.4 ms) speed 0.2 m/s Probe filename is 2017913_1303_2.wav		
Relevant environment parameters			
Tidal height (m)	1.06	Area:	2
Estimated (based on interpolated positions and recursive ray model)			
Latitude TB at TX-time:	36.825309454	Vertical distance (m):	68.61
Longitude TB at TX-time:	-121.8795443	Horizontal distance (m):	989.68
Bearing (°)	330.4	Slant range (m):	992.06
Angle from ER (°):	9.7521	Curved range (m)	993.70
Angle at TB (°):	-1.8203	$\text{TravelTime}_{\text{1-way}} \cdot \text{SS}_{\text{inverse}}$ (m)	1001.46
One-way travel time (ms)	660.04	$\text{SS}_{\text{inverse}}$ i.a.w. eq. 15 (m/s)	1505.5
Bellhop			
Angle from ER (°):	-9.7480	Curved range (m)	993.87
Angle at TB (°):	1.8264	Inverse average SS (m/s)	1494.1

(continued)

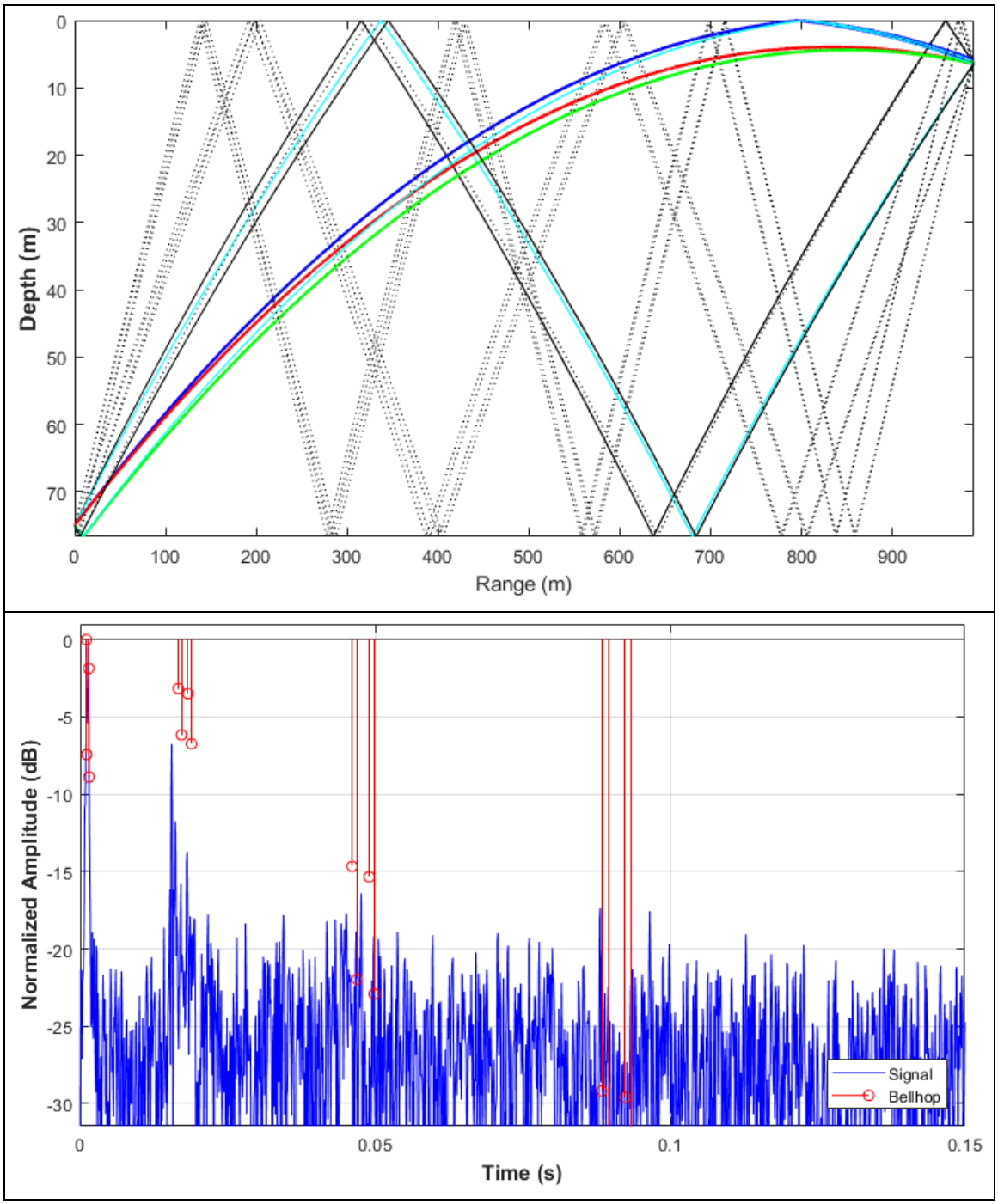
Depth (m)
Range (m)
Normalized Amplitude (dB)
Time (s)
Signal
Bellhop

(continued)

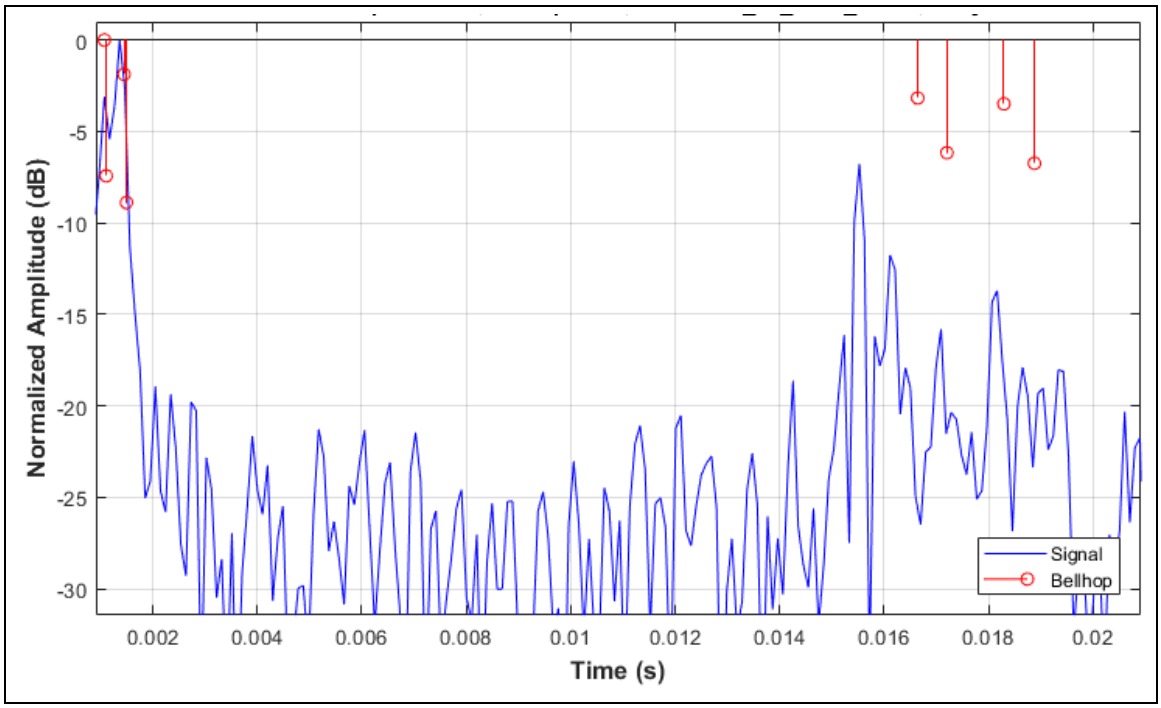

This example shows the maximum range acquired by the modem employed by Mako. It is very similar to the medium range examples which were discussed before. According to Bellhop predictions, the DP and S-bounce paths arrive nearly simultaneously, as do the B-bounce and BS-bounce. The matched filter output shows that the combination of the latter appears to have a stronger response than the DP and S-bounce arrival. Note that the second group arrives earlier than expected by Bellhop. Therefore, the actual sound speed was greater than implemented in the model. Note that, at this maximum range, the response of the second group of arrivals is still significantly above the noise level.

Table 11. Example 8: Long Range, Mako, 14 September

Range message			
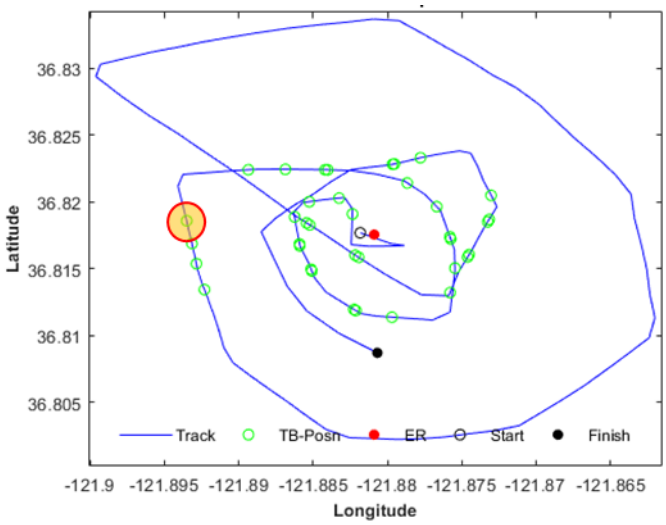	send ATR20 Tx time:14:14:37.9246 Rx Time:14:14:41.7945 Bearing 252.7, 17.6 (Local) Range 11 to 20 : 1099.2 m (Round-trip 1465.7 ms) speed -0.3 m/s Probe filename is 2017914_1413_2.wav		
Relevant environment parameters			
Tidal height (m)	1.07	Area:	6
Estimated (based on interpolated positions and recursive ray model)			
Latitude TB at TX-time:	36.818586186	Vertical distance (m):	68.62
Longitude TB at TX-time:	-121.8934934	Horizontal distance (m):	1130.75
Bearing (°)	275.8	Slant range (m):	1132.83
Angle from ER (°):	- 9.8011	Curved range (m)	1135.07
Angle at TB (°):	2.8552	$\text{TravelTime}_{\text{1-way}} \cdot \text{SS}_{\text{inverse}}$ (m)	1104.07
One-way travel time (ms)	753.07	$\text{SS}_{\text{inverse}}$ i.a.w. eq. 15 (m/s)	1507.3
Bellhop			
Angle from ER (°):	-9.7983	Curved range (m)	1135.37
Angle at TB (°):	2.8613	Inverse average SS (m/s)	1549.3

(continued)

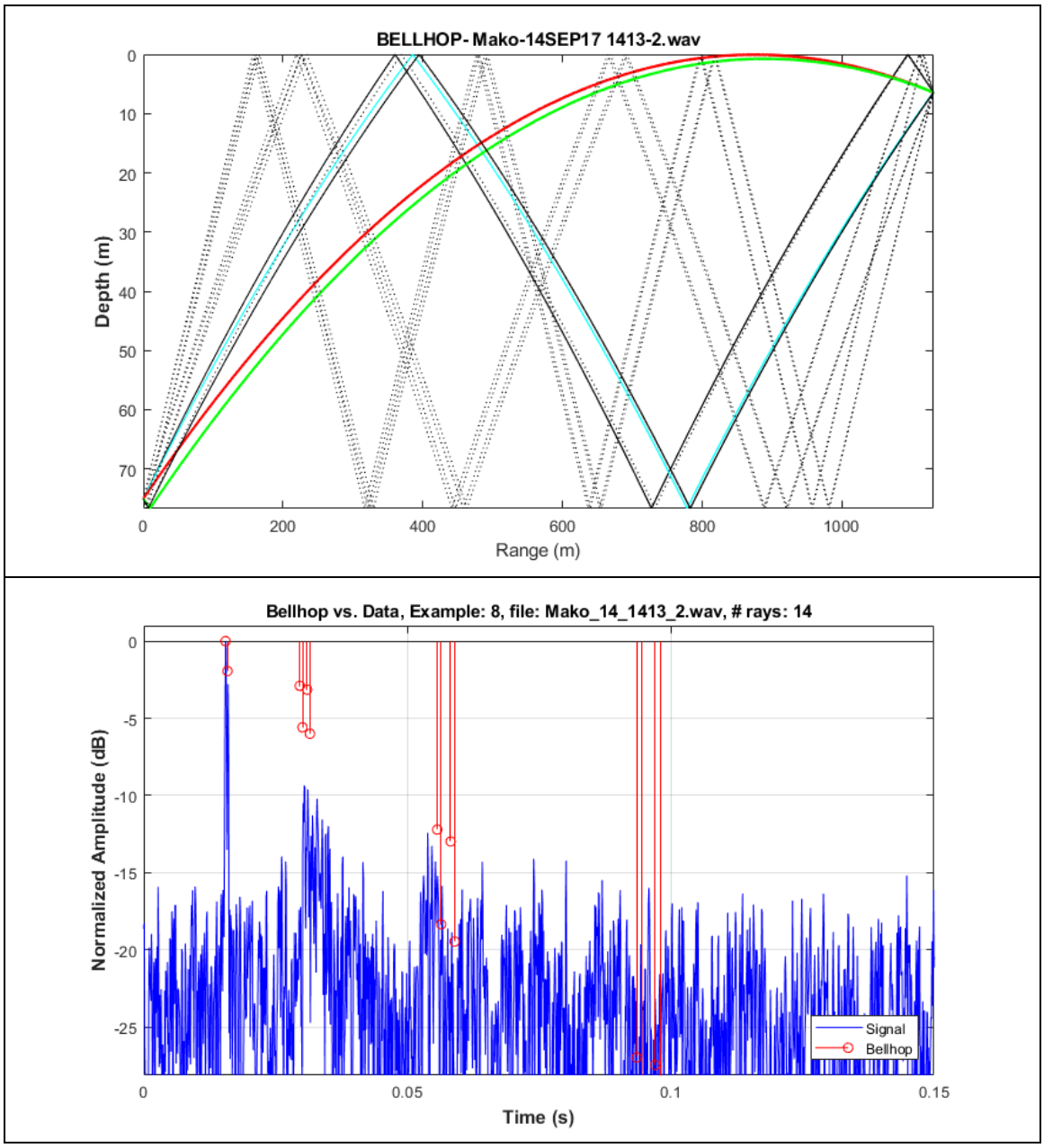
BELLHOP- Mako-14SEP17 1413-2.wav
Depth (m)
Range (m)
0
10
20
30
40
50
60
70
0
200
400
600
800
1000
Bellhop vs. Data, Example: 8, file: Mako_14_1413_2.wav, # rays: 14
Normalized Amplitude (dB)
Time (s)
0
-5
-10
-15
-20
-25
0
0.05
0.1
0.15
Signal
Bellhop

(continued)

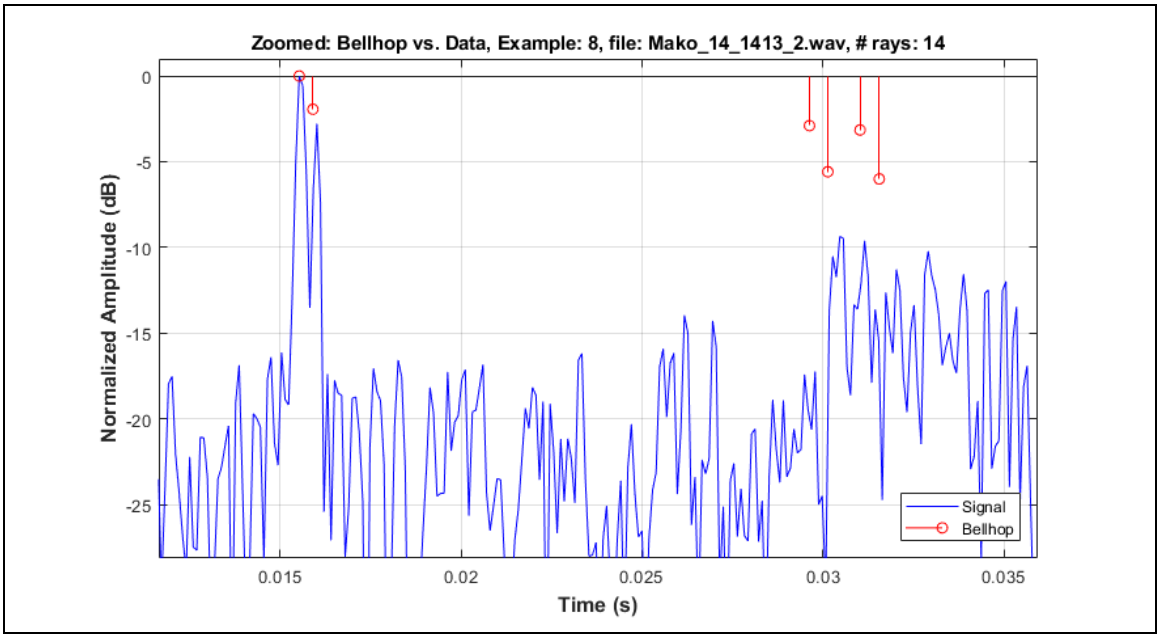

This last example is the maximum range observed during the entire trial. Notice that Bellhop does not predict an S-bounce or BS-bounce arrival. This is probably because the DP-arrival is (according to Bellhop), for all practical purposes, the same as the S-bounce since it has a grazing angle of zero degrees at the surface. The BS-bounce likely has a path very similar to the B-bounce path. The matched filter output shows two distinct peaks in the first group of arrivals, which seems to agree with the previous statement. The second group of arrivals is still well above the noise floor (about 5 dB). Even the third group of arrivals appears to be identifiable in this example.

3. Unknown Arrival

At all close-range range requests a remarkable artifact was observed. This artifact is probably something within the Teledyne-Bethos system, but is at present not understood. Figure 30 shows the artifact within the red ellipse. The direct path arrival is clearly visible. At this short range, no multi-path were observed (note there is no response visible near the second group of predicted arrivals).

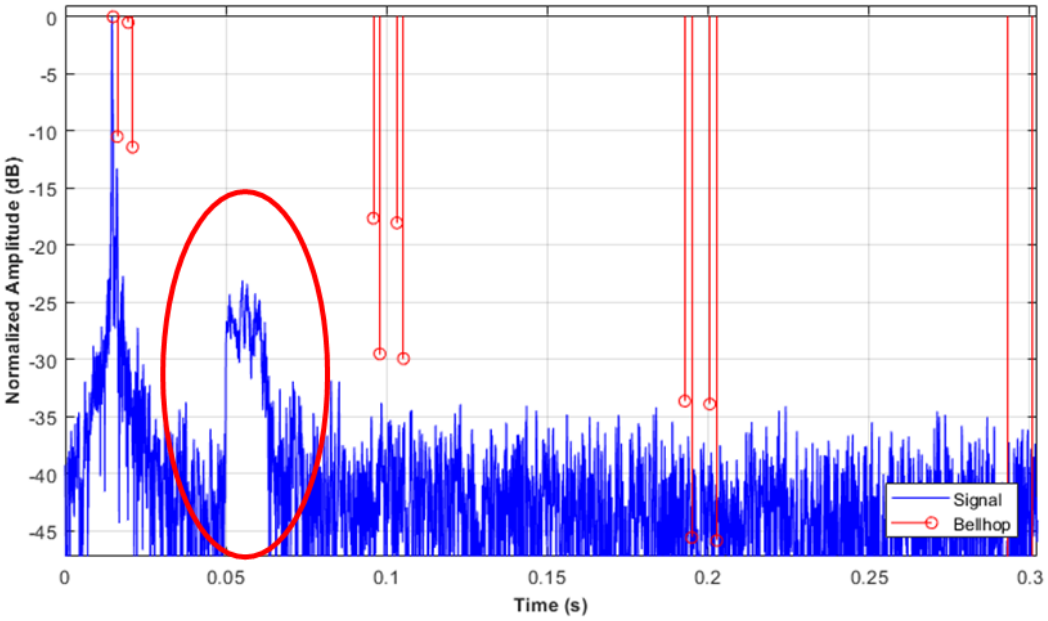

Figure 30. Unknown Artifact in Match Filter Output

Investigating several short range matched filter outputs, it appears the artifact always arrives 50 ms after the matched filter range gate opens. Although it is significantly weaker than the direct path response, it is far wider, about 15–20 ms. Figure 31 shows several outputs, each time showing the artifact starts at 50 ms and lasts about 15–20 ms. Note that the artifact appears in both opening and closing scenarios, where the range (between the tow body and echo repeater) is increasing and decreasing, respectively.

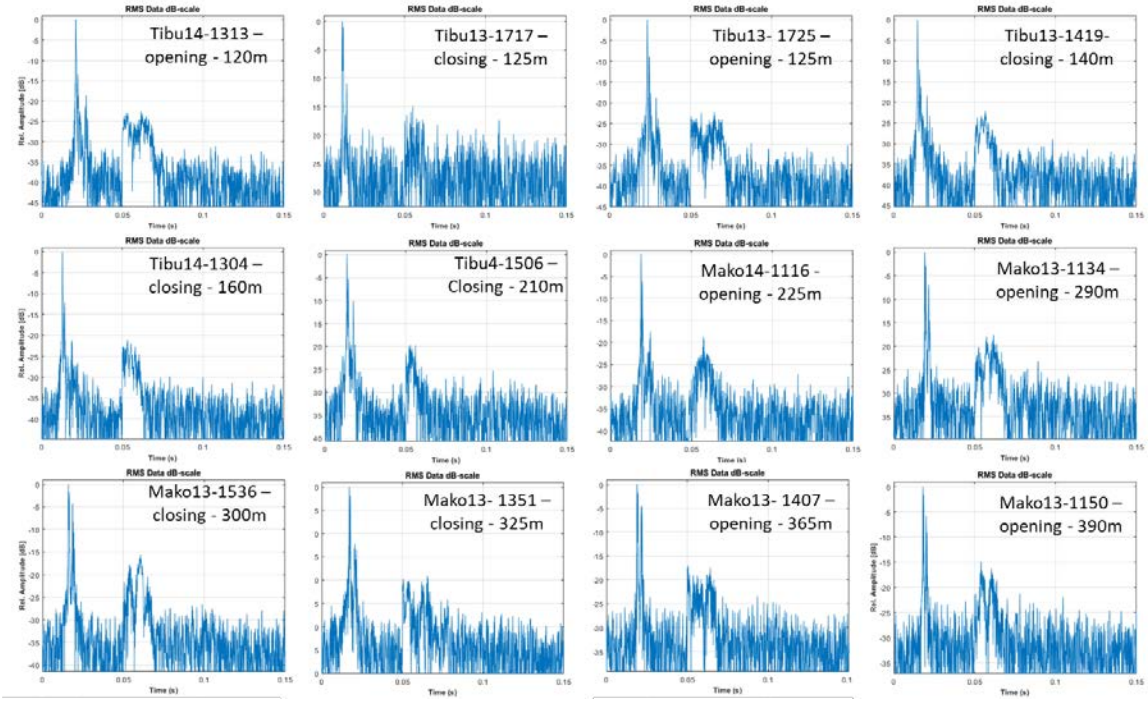

Figure 31. Several Close Range Matched Filter Outputs

D. CONCLUSIONS

Based on multiple examples, of which just a selection is discussed above, the following conclusions were drawn:

Bellhop is, in general, very capable of predicting the matched filter outcome. With the Bellhop prediction plotted within the matched filter data, it seems possible to identify individual arrivals, especially within the first arrival group. Within the second arrival group, this appears to be more difficult. The third group of arrivals is sometimes visible, but sits most often at the noise level and is therefore difficult to distinguish.

The recorded data shows that the strongest arrival in these geometries always belongs to the first arrival group. Data also shows that, within this group, it is not always the DP arrival which produces the highest matched filter output. In several matched filter outputs the strongest arrival was due to constructive interference by the simultaneously arriving S-bounce and B-bounce path.

The second group of four rays is, in all cases, easily observable above the noise level. The individual arrivals within this group are often more ‘smeared’ out than is predicted by Bellhop. If the second group of arrivals lines up with the Bellhop predictions, this suggests the sound speed model used was sufficiently accurate.

An unknown set of ‘arrivals’ were observed in the data that were not part of the propagation predicted by Bellhop. These arrivals however never seem to have interfered with the execution of a range request. It would be advisable to investigate the origin of these artifacts, to confirm they do not interfere with the ranging routine.

The maximum observed range seems to correlate with the longest possible direct path between the echo repeater and the tow body. Beyond this theoretical maximum range, no successful range requests were made, although there is still significant amplitude in the matched filter output from group two arrivals.

THIS PAGE INTENTIONALLY LEFT BLANK

VI. THE APRIL SEA TRIAL

A. IMPLEMENTED CHANGES TO THE SEPTEMBER TRIAL

From 16 to 20 April, a second sea trial was executed in Monterey Bay. During the April sea trial, the same assets were used in the same area as the September sea trial. Several lessons learned from the September sea trial were implemented. One of the main differences was the use of an additional spacer, as shown in Figure 32. This spacer allowed a far bigger part of the transducer to be exposed outside the tow body, as can be seen in the same figure. As described in Section V.B, only the part of the transducer below the yellow tape was exposed during the September sea trial. Using the additional spacer, we were able to expose the entire operational part of the transducer. Another change was the (intended) use of the "fast mailbox" option in the Wave Glider management system. With this option, the Wave Glider should have saved its GPS-position every minute instead of once every five minutes. A third change was the fact that two echo repeaters were deployed. Besides the same omni-directional ATM-925 module, another ATM-925 module with a DAT transducer was deployed. A fourth change was the use of a Loggerhead OpenTag[3] sensor on the tow bodies to log depth, heading, roll and pitch. Additionally, the tow bodies were requested to report their heading, roll and pitch data separately. Furthermore, an RBRduet[4] sensor was attached to both echo repeaters to monitor the depth of the echo repeater. These last changes greatly improved the understanding of the estimated position and behavior of the tow body and echo repeater.

In addition, some other small changes were implemented, like the use of the AML Smart X sound speed profiler instead of the SonTek Cast-Away CTD-profiler. This sound speed sensor provides a more accurate sound speed profile, since the sound speed is directly measured instead of calculated based on measured conductivity and temperature. The specified sound speed accuracy of the SonTek CastAway is ± 0.15m/s, whereas the accuracy of the AML sound velocity sensor is ± 0.025m/s. Furthermore, a longer

[3] See http://www.loggerhead.com/opentag-motion-datalogger.

[4] See https://rbr-global.com/products/compact-loggers/rbrduet-td.

deployment cable was used, so the sensor could be dropped just above the sea floor, which gave us the SSP of the entire water column instead of only about 57 m, as was done during the September trial.

Figure 32. DAT-Transducer Including Spacer (left), Mounted in the Tow Body (right)

B. EXECUTION PROBLEMS

Although the weather during the sea trial was favorable for Wave Glider operations, the April trial experienced a couple of unfortunate mishaps, which did not occur in September. First of all Wave Glider Thresher (formally known as Mako) was found flooded after arriving back in the area of operation on the second trial day. Thresher was beyond short term repair. This meant that for this trial, only Tiburon was going to be able to provide data. During the trial, Tiburon was often observed to move at speeds far slower, and less consistent, than observed in September. Furthermore, there were problems communicating with Tiburon. Tiburon did not log its positional data with one minute intervals as it was ordered several times. Tiburon also did not log any speed through water data as it did in September, indicating a possible problem with the Airmar water speed sensor on board of the Wave Glider. Additionally, the telemetry data seemed to produce

ambiguous data, especially regarding the measured ground speed. During the second half of the trial, when Tiburon successfully logged GPS-positions with two minute intervals, these telemetry problems were solved.

Regarding the ranging, there were also problems with the gathered data set. During the trial there were two echo repeaters moored at the bottom. One had an omni-directional transducer and was also used during the September sea trial. The second had a DAT-transducer and was not used during the September trial. After the trial, it became apparent that none of the ranges between the tow body and the omni-directional echo repeater were successful. Fortunately, the ranges to the DAT-echo repeater were. This provided a total of 65 successful range requests, during which both range and bearing information was logged. These successful range requests happened between 18:30 UTC on April 17 until 07:30 UTC on April 18. Outside this time frame no useful range data or probe files were recorded.

C. OBSERVATIONS AND RESULTS

This section will discuss the observations and results of the April trial. It will mainly focus on observed differences between both sea trials. Before discussing the range and bearing results, the observed weather and SSPs will briefly be discussed. The results of the sensors attached to the tow body and echo repeater will then be examined.

1. Weather, SSP and Environment

The days before the April sea trial were quite windy, which results in significant swell. During the sea trial, the wind and with it the wind wave height died down. The swell during the sea trial was still significant. In general the weather was, just like in September, favorable for operations with Wave Gliders. Table 12 provides the main weather statistics for both test days.

Table 12. Weather Conditions During the April Sea Trial

Weather	17 April	18 April
Wind	West, 1 m/s to 7 m/s	West 7 m/s decreasing to 1 m/s
Wind Waves	Decreasing 0.6 m to 1.8 m. Periods from 4.5 s to 7 s	Decreasing 0.5 m to 1.2 m. Periods from 4.5 s to 7 s
Swell	Northwest –2.5 m, Period decreasing 11.5 to 13.5 s	Northwest –2.5 m. Period decreasing 10 s to 12.5 s
Temperature	8-11 °C	9-12 °C

During the sea trial, three complete SSP-runs were executed, during which the SSPs were measured at the echo repeater position and 1 km north, east, south and west of this position. In general, the water was much colder than in September and showed a very different profile. Furthermore, the differences in sound speed between the different locations was less. Figure 33 shows all 15 SSPs taken on 17 April. The time of the measurement is indicated in the legend. Figure 33 also shows the averaged SSP and a linear approximation, as it was used for the September data. Notice that the linearized SSP is far off from the averaged profile.

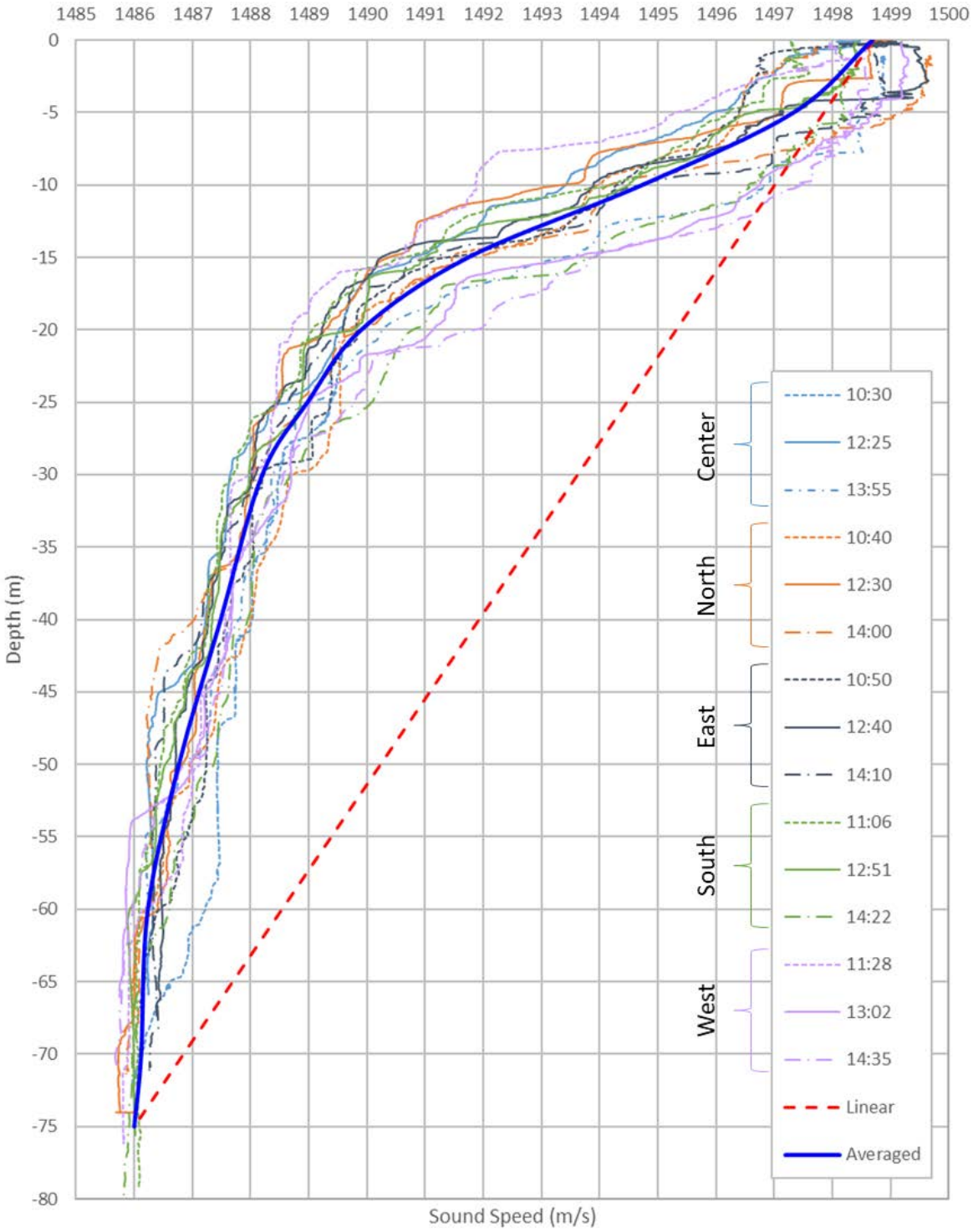

Figure 33. SSPs Taken During the April Trial

2. Depth, Roll and Pitch of the Tow Body

In order to better understand the range data, a good understanding of the behavior of the tow body is required. As explained in Section IV.B, error in depth, pitch and roll can influence the actual range measurement. Figure 34 shows the output of the Loggerhead OpenTag depth sensor over time. The first thing to notice is that the tow body does not appear to be at the same depth as the attachment point at the sub unit, as was initially assumed. Secondly, as can be seen there is quite some variation in the observed depth. When correlated to speed data it became apparent that the tow body 'flies' shallower with higher speeds. As explained in Section IV.B.4, the average observed depth of the tow body (8.1 m) was used to improve range calculations.

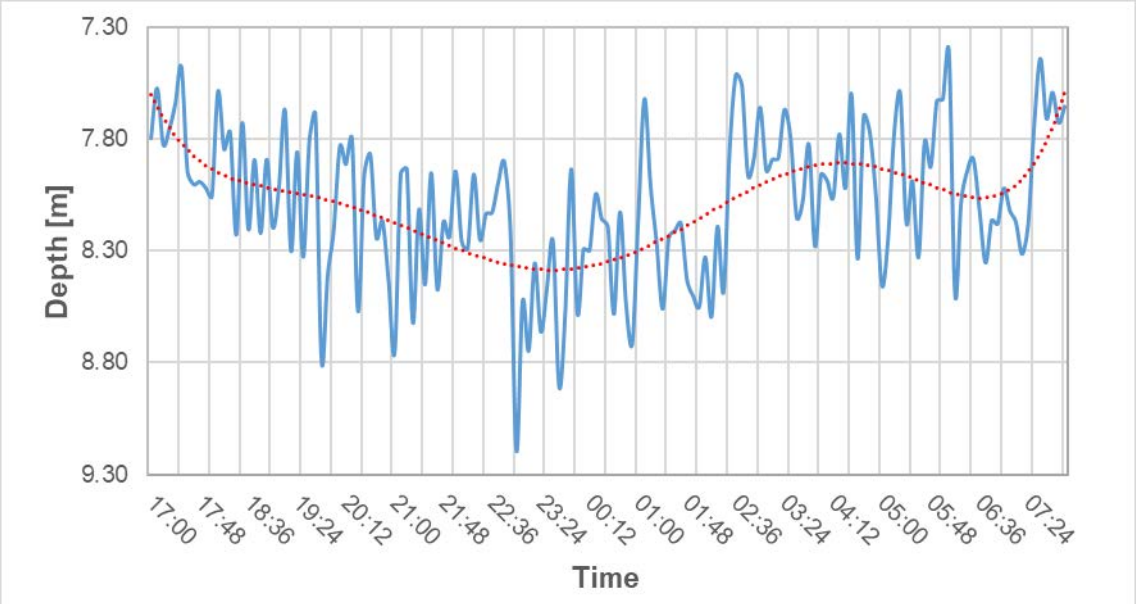

Figure 34. Observed Depth Tow Body Tiburon

After examining the depth of the tow body, the next thing to better understand the behavior of the tow body is to investigate the changes in pitch and roll over time. Figure 35 and Figure 36 show both the observed pitch and roll. Notice that although there are fluctuations, these fluctuations are in general quite small. Deviations in pitch and roll never exceed 10 degrees, which could influence the range measurements. The average observed

deviation in pitch was -0.85 degrees and the average observed roll deviation was 2.34 degrees. The observed data confirms that the tow body flew fairly stable through the water.

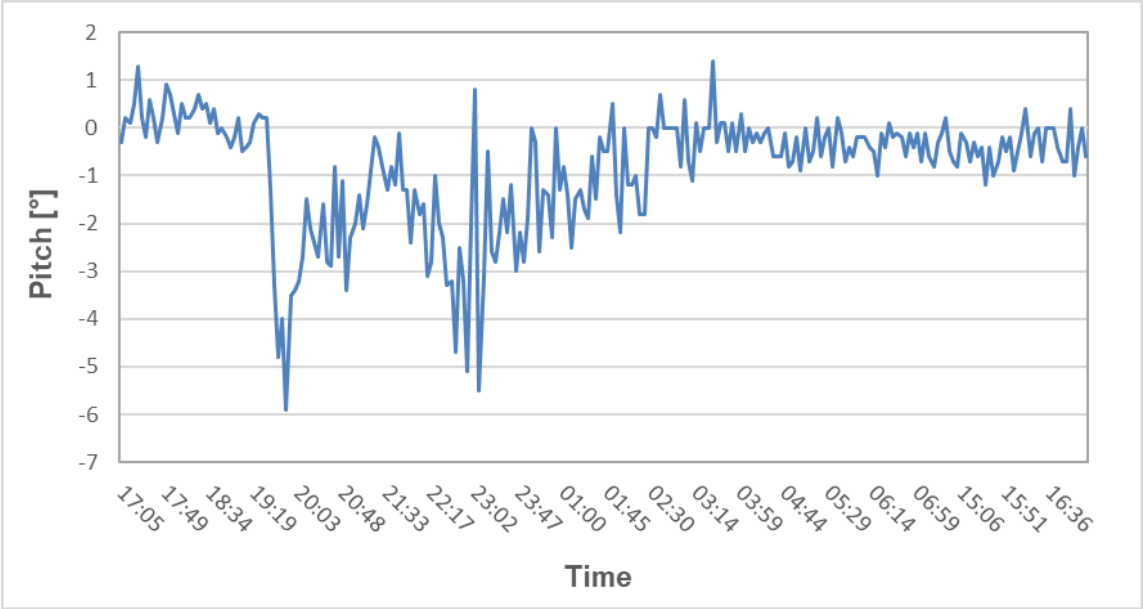

Figure 35. Observed Pitch Data from Tow Body Tiburon

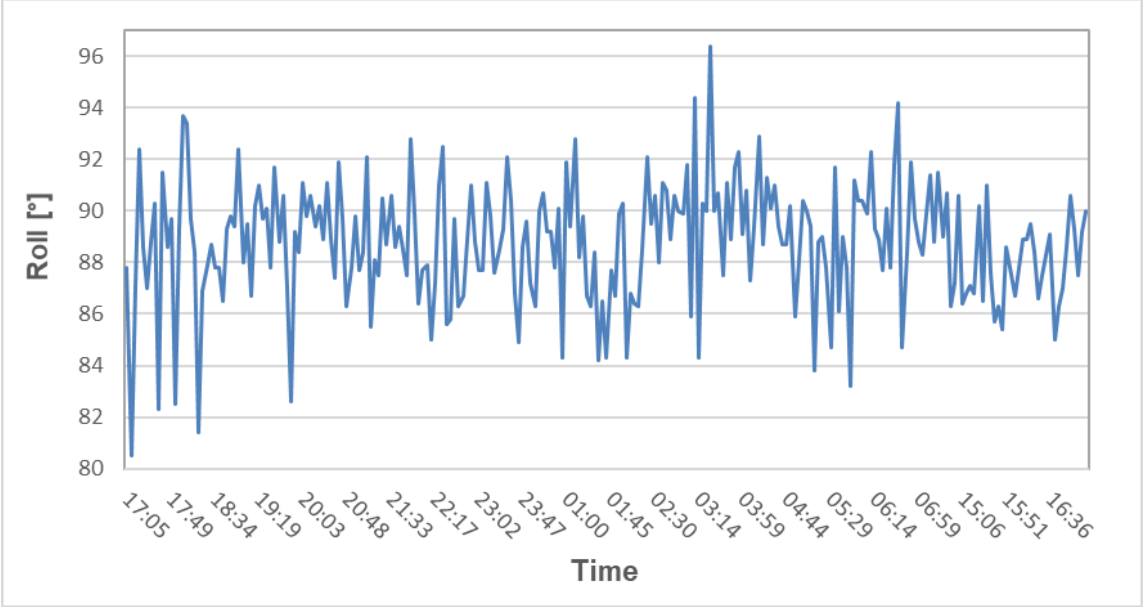

Figure 36. Observed Roll Data from Tow Body Tiburon

3. Compass Data of the Tow Body

During the April sea trial, the modem was also directed to record heading. In addition, the Loggerhead OpenTag logged the magnetic field data (in x, y and z components). Comparing the resulting heading of the tow body, there did not appear to be any consistency. When both measurements were compared to the recorded heading of the sub unit, there was also no apparent consistency, even when taking into account currents and magnetic declination. On the other end of the system, there was consistency between the heading of the sub unit, the recorded heading of the Wave Glider and the calculated courses over ground.

The modem also logged both the measured true and relative bearing between the tow body and the DAT echo repeater. Using heading information, it should be possible to convert the relative bearing to a true bearing. Again this conversion did not show any consistency.

Based on the above two observations, it is concluded that the output of the compass on board the tow body of Tiburon was faulty. As a result, the bearing information is also not trustworthy.

4. Depth of the Echo Repeater

As previously mentioned, an RBRduet sensor was attached to both echo repeaters during the trial (as shown in Figure 37). The main objective was to monitor the measured depth (i.e., pressure), which would be a good indicator of the stability of the echo repeater.

Figure 37. RBRduet Sensor Attached to the DAT Echo Repeater

Figure 38 provides insight into how the raw pressure data of the sensor was manipulated in order to draw conclusions from its measurements. First notice (top left) that the trend of raw measured pressure data seems to follow the tide observed during the trial. In the top right graph, both the pressure changes due to tidal variation and the observed air pressure were subtracted from the data. Furthermore, the pressure data in bar was converted to depth in meters using the average observed density of the water (1024.3 kg/m^3) in the area of operations. Notice the depth now seems to fluctuate around an average of 73.119 m. Also note that the amplitude of oscillations is decreasing over time, which is consistent with the observed decrease in wave height and swell. The bottom left spectrogram shows that the majority of the energy was below 150 mHz. It also shows a decrease over time, consistent with wave height observations. Next, all the frequencies below 150 mHz (equivalent to wave with periods above 6.67 s) were filtered out of the data. The result is shown on the bottom right of Figure 38.

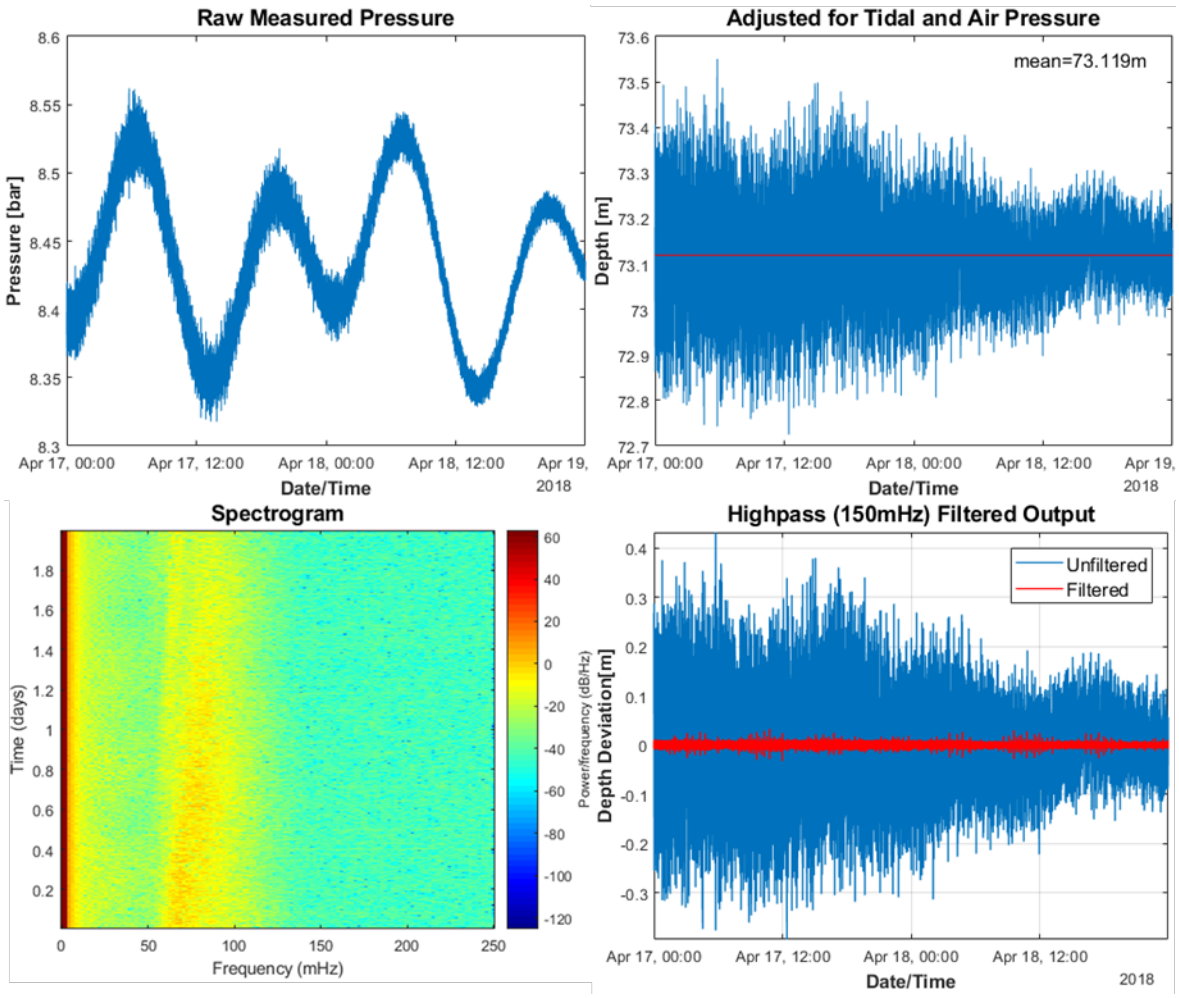

Figure 38. Manipulation of the RBRduet Pressure Data

After the above described process, only the oscillations in depth at the echo repeater remain. Figure 39 shows the final result. Notice that the majority of the fluctuations are within one centimeter. As a result, this indicates the echo repeater's depth, and therefore its position and orientation, remained stable over time.

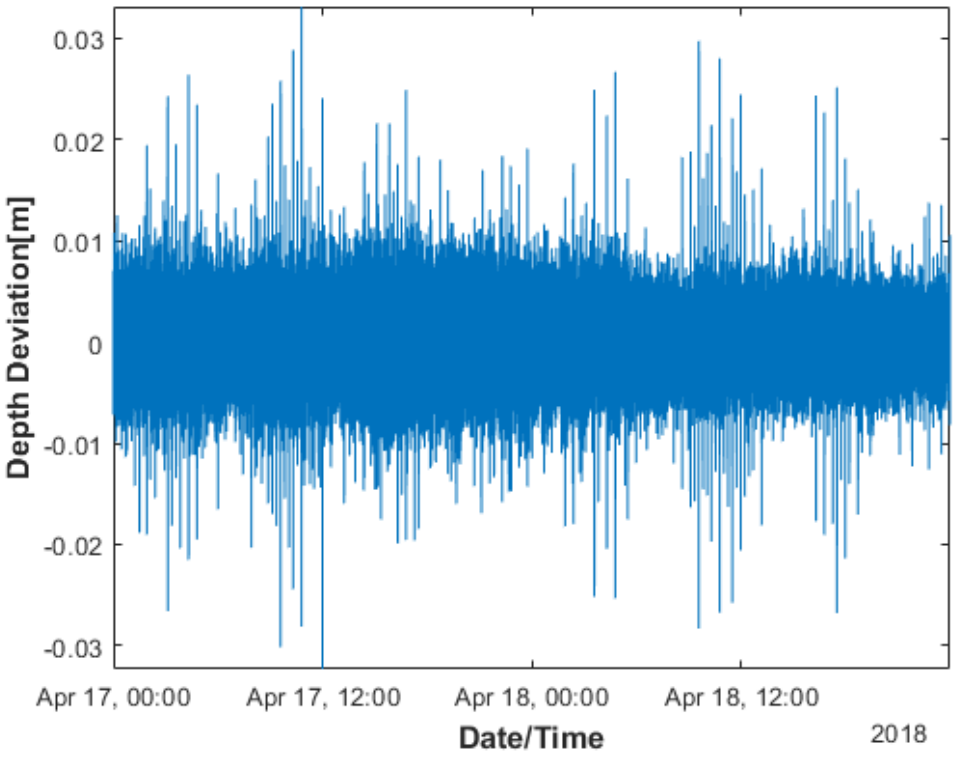

Figure 39. Depth Fluctuations of the DAT Echo Repeater

5. Position of the DAT-Echo Repeater

During the September trial, a Remus UUV was used to accurately determine the location of the echo repeater. During the April trial, a Remus was not available. Therefore, the Automated Acoustic Survey software, developed by the Space and Naval Warfare Systems Command (SPAWAR), was used to obtain an accurate location of the echo repeater. Basically this program uses a continuous GPS-input and executes several ping ranges between a separate transducer and the acoustic release attached to the echo repeater [17]. After executing several ranges at several locations (in our case about 400 m north, south, east and west of the echo repeater) the software estimates the most probable location of the echo repeater. Due to an unknown offset of the GPS-receiver and the transducer in the water, there were systematic errors in this measurement. During the April sea trial, two geolocation runs were executed resulting in the following positions: 36.817898667, -121.881936333 and 36.817934167, -121.881826167. These positions are calculated to be 10.59 m apart, which is an error consistent with the expected error due to the discussed

offset. For further calculation, the best estimate of the DAT echo repeater's location was considered to be the average of both these measurements. Therefore, the following position was used to calculate the range between tow body and echo repeater: 36.817916417, -121.88188125.

6. Range and Bearing Results

Using the 65 successful ranges and the best DAT-echo repeater position, the best estimated ranges between echo repeater and tow body were calculated using the same approach as discussed in Sections IV.C and IV.D.

Figure 40 shows the track the Wave Glider followed on 17 and 18 April. As before locations corresponding to good ranges are indicated by green circles.

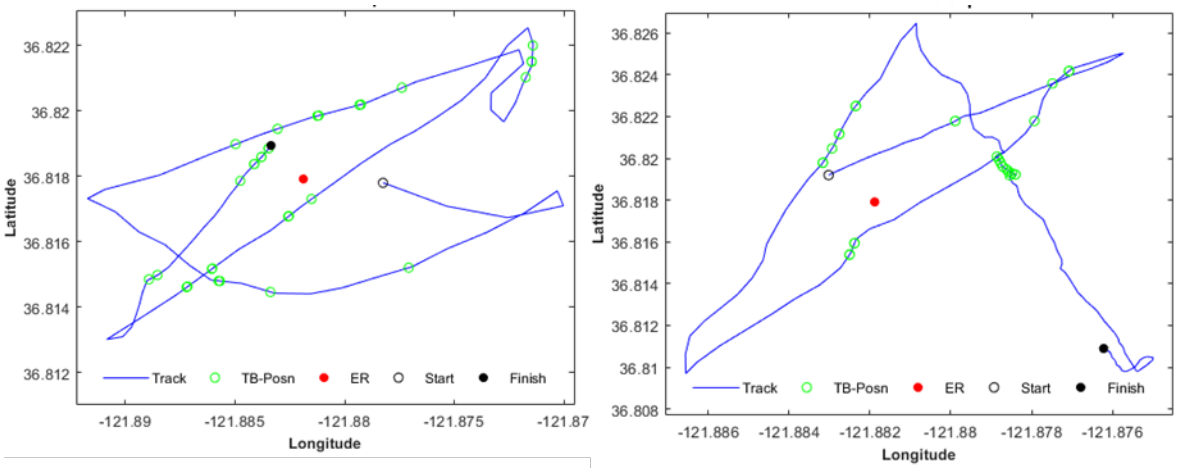

Figure 40. Tracks and Good Ranges 17 and 18 April

Figure 41 and Figure 42 show the range results from the April trial on both dates. Notice that there appears to be, in contrast to the September trial, little consistency between the calculated and measured ranges. The right graph shows the percentage difference in one-way travel time averages more than 60% and 35% on 17 and 18 April, respectively. This is much higher than observed in September, when percentages were consistently about 4%. The observed error cannot be explained following the logic in the Section IV.B, Geometry and Errors.

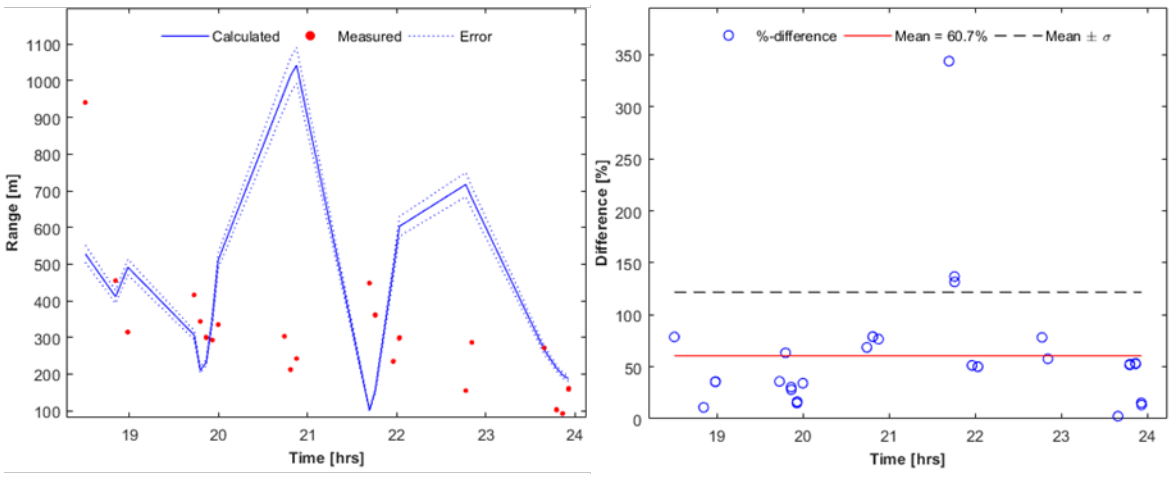

Figure 41. Range Results 17 April

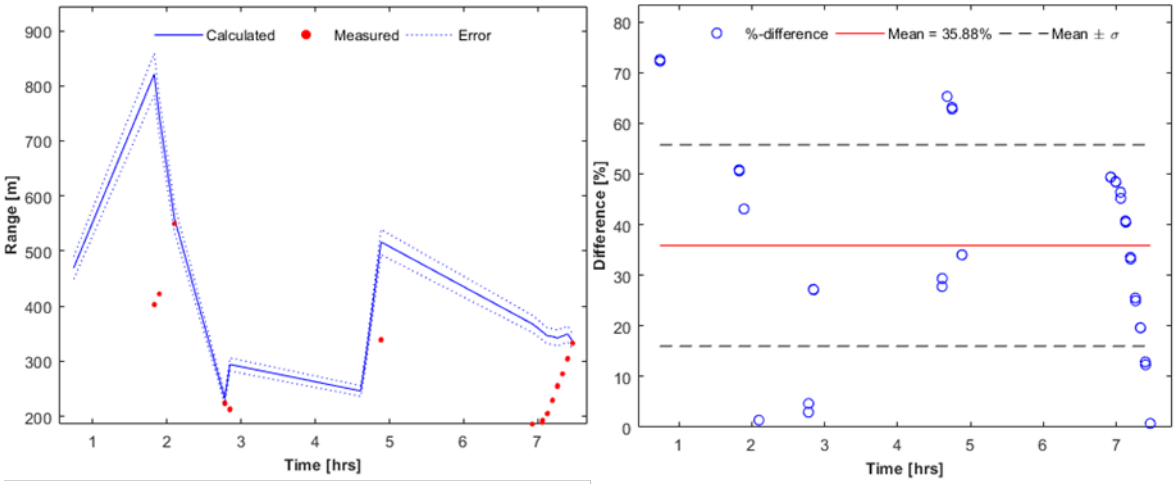

Figure 42. Range Results 18 April

As with the range results, the bearing results in Figure 43 and Figure 44 do not show any consistency. During the September trial, there was also a large error observed in the bearing data. However, the September data does show some consistency and is therefore somewhat useful. The data obtained during the April trial seems not suited for any further use. This data supports the previously made observations regarding the faulty compass data (see Section 3).

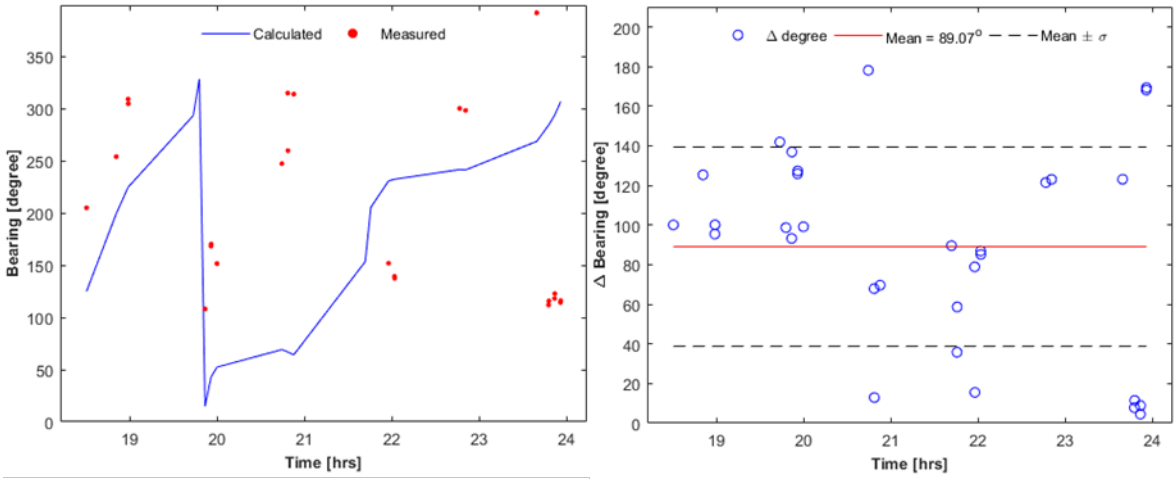

Figure 43. Bearing Results 17 April

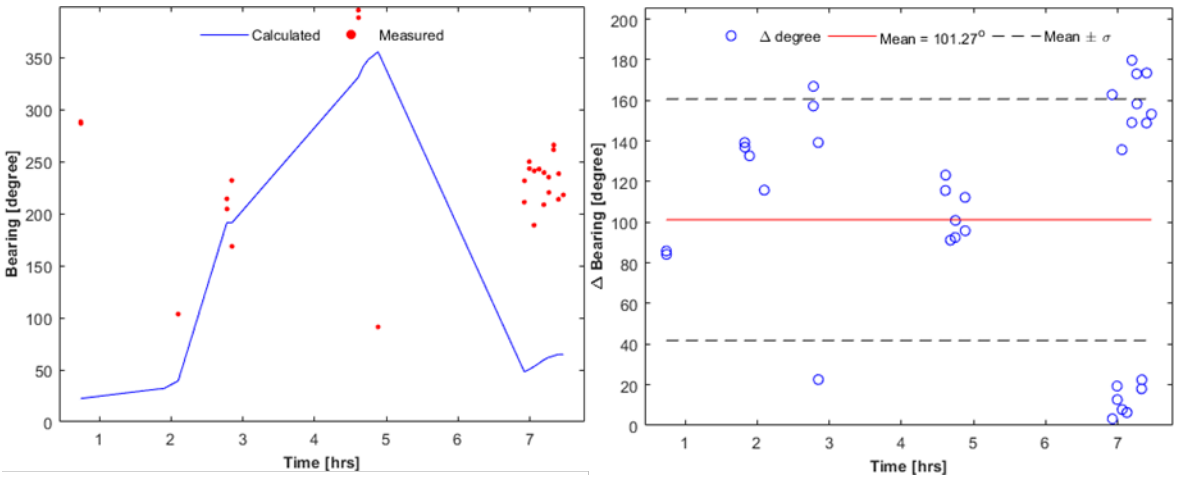

Figure 44. Bearing Results 18 April

7. Ray Tracing

As for the September trial, the matched filter output was compared with the Bellhop arrival computations. This section will briefly discuss some of the general results obtained.

Figure 45 shows a medium range example, where the calculated curved range between tow body and echo repeater is 821.13 m. The ranges determined using the one-way travel time was 403.0 m. Notice that Bellhop clearly predicts a second group arrival. In the April data set, no second group arrivals were observed.

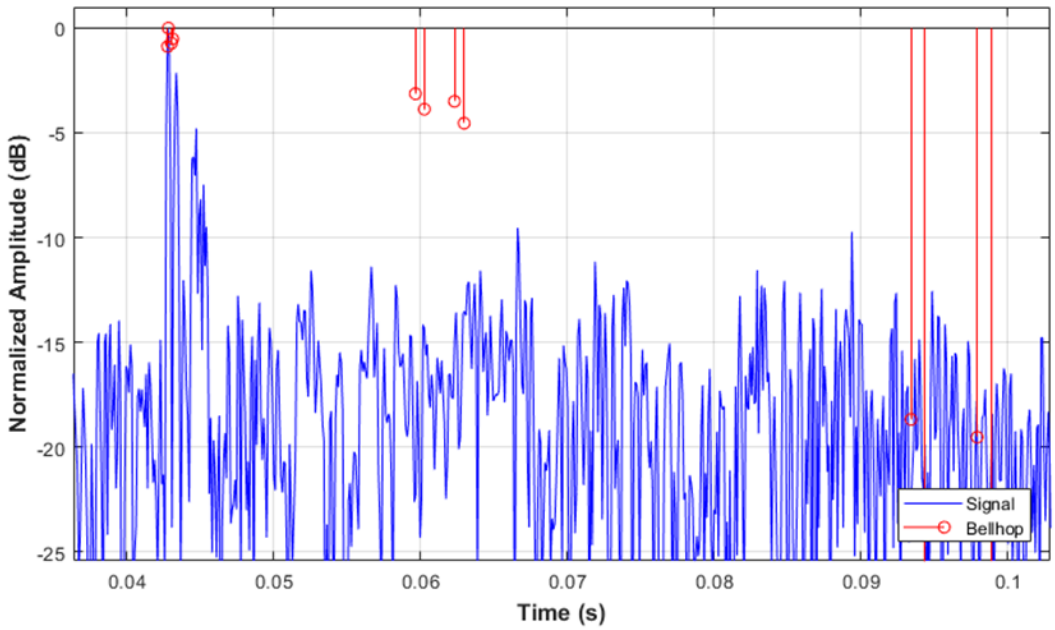

Figure 45. Long Range Example 17 April

Figure 46 shows a short range example, where the calculated curved range was 101.22 m and the measured range 449.25 m. Besides this large difference, there were several other noteworthy observations in the short range matched filter outputs. First of all, no artifacts, as discussed in Section V.C.3, were observed in the April data set. Secondly, the noise level appeared to be much higher, since the difference between the noise level and the first group arrival peaks is about 12 dB, where it was almost 35 dB during the September trial. Furthermore, the noise level appears to be about the same at close range as it is at longer ranges. The observation that the noise level was higher than observed in September can be explained by the rougher sea conditions. The observation that the matched filter peaks at medium and short range have similar relative strength, however, cannot be explained.

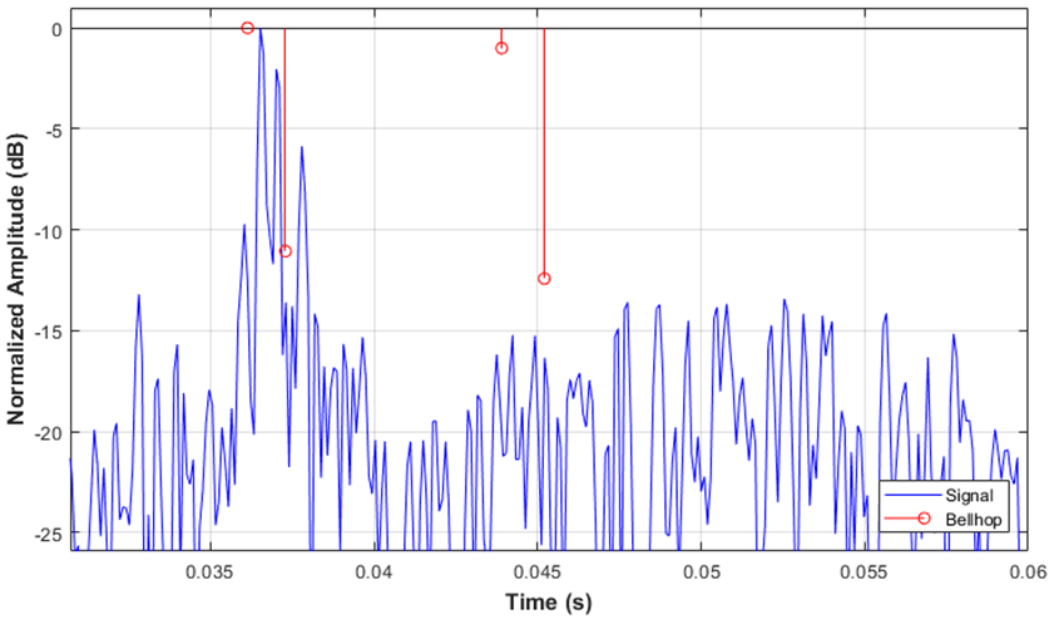

Figure 46. Short Range Example 17 April

D. CONCLUSIONS

Compared to the September trial the obtained data set of the April sea trial shows a multitude of inconsistencies. As a result, this data set is not trustworthy. Further research is required to investigate the underlying causes of these inconsistencies, so these can be prevented in the future. So far it seems at least the compass sensor in the modem was faulty. This does not, however, explain the differences between measured and calculated one-way travel time.

The additionally gathered information regarding depth, pitch and roll of the tow body and the depth sensor data of the echo repeater did prove useful. As mentioned before, the data shows both sensors were relatively stable. As a result, future research could successfully incorporate beam pattern data in Bellhop predictions to better understand the measured acoustic field of different arrivals.

VII. BEAM PATTERN

A. INTRODUCTION

The beam pattern of a transducer indicates the variation of the intensity (or sound pressure) level with angle around the transducer. Often beam patterns of transducers are normalized, meaning the angular response is compared to the angle with the maximum response. Beam patterns are often provided by manufactures to provide information about a transducer's angular sensitivity to receive, or reciprocally, its angular ability to transmit. Beam patterns can be represented in the horizontal and vertical plane. Sometimes three dimensional representations are provided. However, these provide little information since they are hard to read and are often used to create a three dimensional awareness of a beam pattern. If the beam pattern indicated a "dip" at a certain angle, this means the transducer is less sensitive at this angle. This may lead, in some cases, to operational constraints.

After the April trial, we established that the tow body flies nearly level through the water. Furthermore, the echo repeater also appears to be relatively stable. Therefore, the receiving inclination angle can directly be compared to the measured vertical beam patterns, which will provide a normalized sensitivity at that particular receive angle.

B. VERTICAL BEAM PATTERNS PROVIDED BY TELEDYNE BENTHOS

The Teledyne modems used in the sea trials make use of two types of transducers. The DAT-transducer used in the tow body is directional and uses four transducer elements in a tetrahedral configuration. Using phase differences, the modem can determine the direction (both bearing and inclination) of a received signal. The transducer used in the echo repeater is considered to be omni-directional.

Figure 47 shows the vertical radiation pattern provided by Teledyne Benthos for one of the NPS's DAT-transducers. The colors are added to indicate which part of the transducer's beam pattern is used to receive (or transmit) short, medium and long range signals. Here medium range is defined as a grazing angle at the tow body between 0 and 20 degrees downward. This corresponds to about 200 to 900 meters range. For short distances greater angles (green) are required. The grazing angle becomes negative

(upward) for long ranges (red). Notice most of the energy is transmitted towards the zero degree grazing angle and there is little variation (about 3 dB) along the most relevant beams (-5 to 30 degrees)

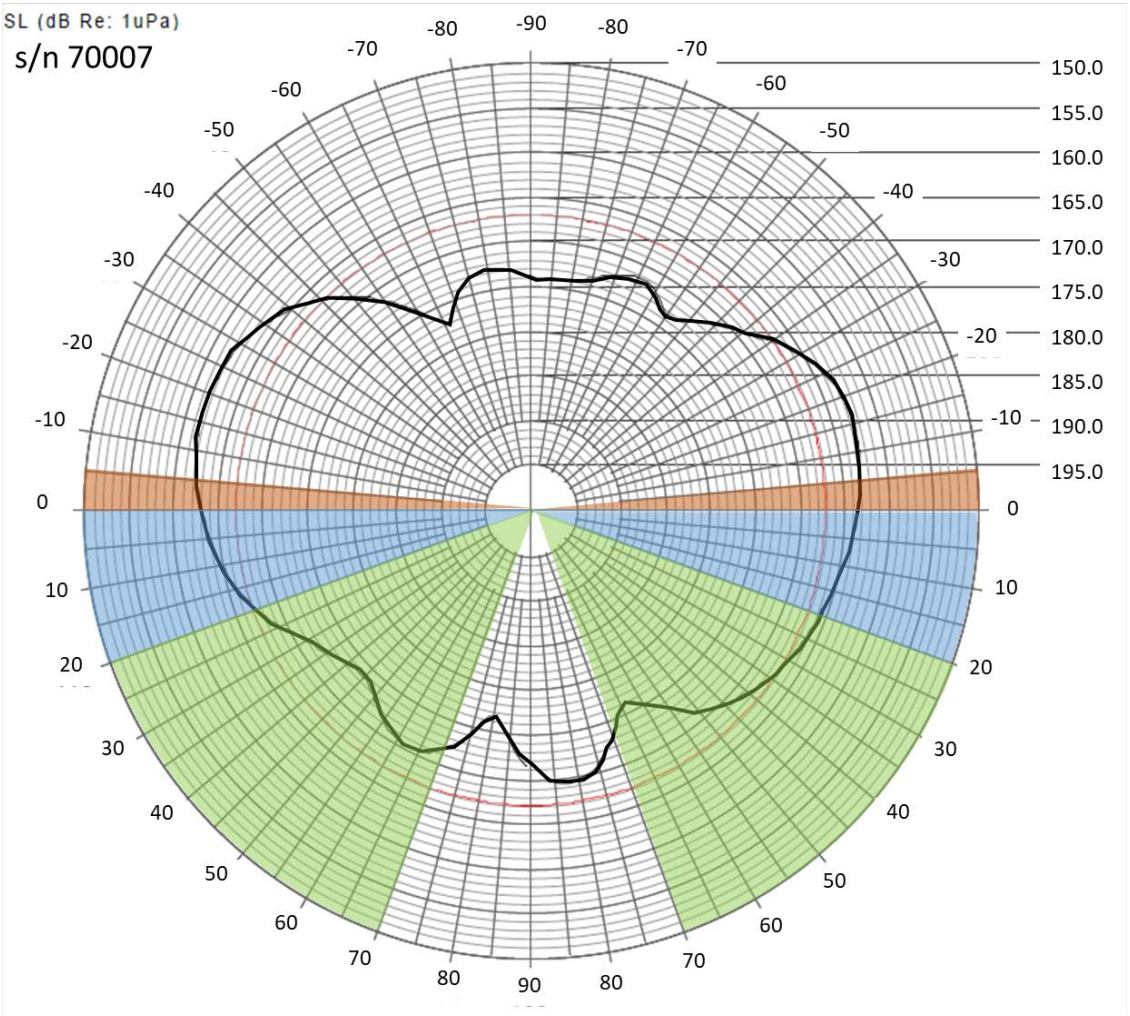

Figure 47. Teledyne Benthos Supplied Vertical Beam Patterns of the DAT-Transducer

C. EXECUTION

1. Introduction

Although these manufacturer provided beam patterns do provide a good initial guess of the actual beam pattern, it does probably not effectively represent the setup used

during the trial. The actual beam pattern during the trial was most probably influenced by the tow body, which houses the transducer and the modem. Therefore, beam pattern measurements of the transducer integrated into the tow body were executed.

2. The Measurement Set Up

The beam pattern measurements were executed in one of the anechoic water tanks of the Naval Postgraduate School (7.30 m long by 1.78 m wide and 2.16 m deep). The walls and bottom of the water tank are coated with anechoic tiles, which absorbs frequencies above 10 kHz.

The tow body was attached to a mounting, which was, via a rod, connected to an indexer. This indexer allowed accurate rotation of the tow body while submerged in the water tank. At 2.07 m away from the center of rotation, a hydrophone was lowered into the water tank via a similar rod. Figure 48 shows a picture of this set up while the tow body and the hydrophone were in the water tank.

Both the acoustic center of the DAT-transducer and the hydrophone were lowered exactly 1 m below the water surface of the tank. Figure 49 and Figure 50 provide a more detailed sketch of how the tow boy was mounted and rotated. The horizontal mounting was especially challenging, since the water tank was too small for the tow body to complete a 360 degree rotation.

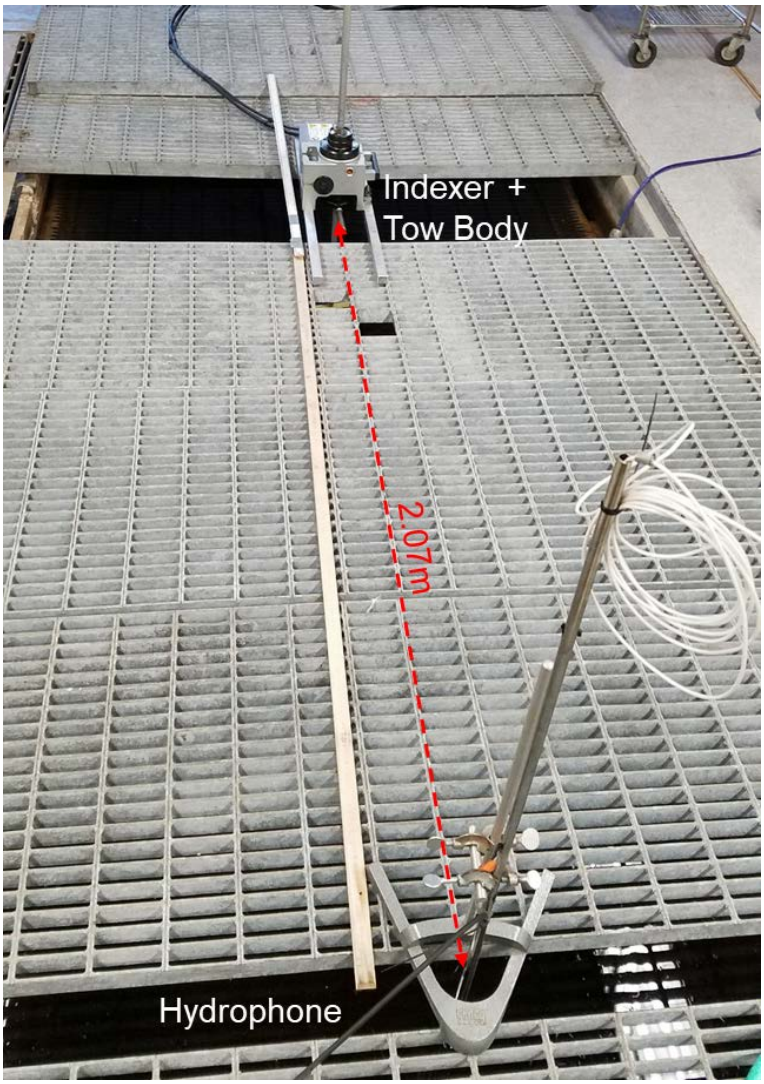

Figure 48. Measurement Set Up

Furthermore, Figure 49 and Figure 50 show the position of the acoustic center of the omni-directional part (a ceramic ring) of the DAT-transducer. Note that during the September trial the acoustic center was clearly inside the tow body, whereas in April it was far more exposed. Also note in the same figures that due to the position of the acoustic center, there was an offset with the center of rotation. As will be explained, a correction was made for this offset while processing the data.

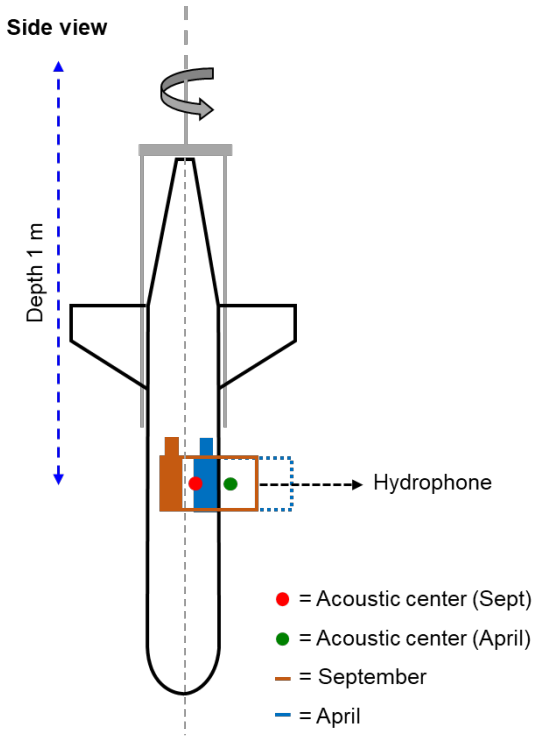

Figure 49. Sketch of X-Axis Measurement Set up

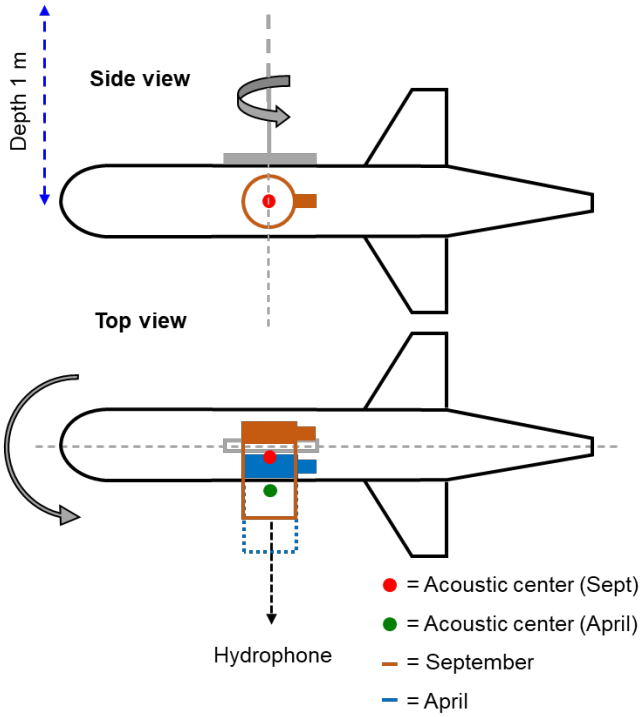

Figure 50. Sketch of Y-Axis Measurement Set up

3. Data Measurements

The ATM-900 series modem inside the tow body was set in pinger mode and executed 3.125 ms pings at 12 kHz, 800 ms apart. This means that, at this frequency, a signal consisting of (12000 Hz x 3.125 ms =) 37.5 cycles was generated. The hydrophone output was connected to an oscilloscope, which displayed the voltage measured by the hydrophone due to the receipt of this ping sent by the modem-DAT-combination. The output of the hydrophone was saved for further analysis.

For each produced beam pattern, the tow body was rotated 360 degrees in five degree increments. This rotation was first conducted counter clockwise and thereafter clockwise. As mentioned before, it was not possible to execute a full rotation around the y-axis (see Figure 51) due to the water tank size limitations. Therefore, whenever the tow body approached a limitation, the whole set up had to be moved about 32 cm. This has some small effects on the accuracy of the y-axis measurements. In total, four data sets were gathered, including rotation around the x-axis and y-axis for the September configuration and x-axis and y-axis rotation for the April configuration.

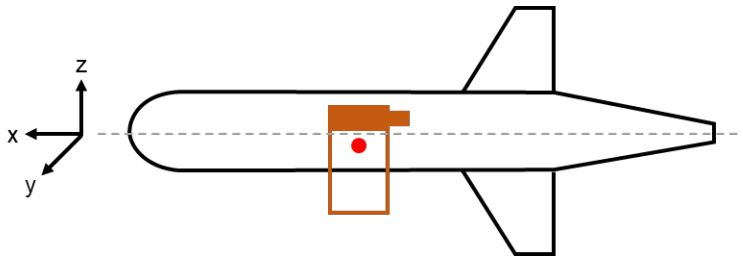

Figure 51. Axis of Rotation

Due to the size of the water tank and the limitations of the modem (i.e., fixed length of the ping signal) multi-paths were clearly visible in the recorded data. Since the walls and the bottom of the anechoic tanks are covered with absorbing material, the most noticeable multi-path was due to the surface reflection. Figure 52 shows an example of the recorded signal. Since both the hydrophone and the acoustic center of the DAT transducer were 1 m below the surface and the distance between the tow body axis of rotation and the hydrophone was 2.07 m, the difference in arrival cycles between the direct arrival and the

surface reflected arrival could be calculated using the Pythagorean theorem, the frequency and the sound speed (1481 m/s) as,

$$\frac{\left(\sqrt{2.07m^2+(2\cdot 1m^2)}-2.07m\right)\cdot 12000Hz}{1481\,{}^{m}\!/_{s}}=6.55cycles \qquad (16)$$

This means that after 6.55 cycles, the receive voltage due to the surface reflection is expected to add to the receive voltage due to the direct path. When, on the other edge of the signal, the direct arrived signal vanishes (after 37.5 cycles) the surface reflection remains for another 6.55 cycles. As can be seen in Figure 52, this was exactly what was observed. Due to this (and other less visible) multi-path(s), only the (averaged) measured amplitude of the first six cycles was taken in to account. The very first cycle however, was also disregarded, since this cycle did not show a consistent amplitude.

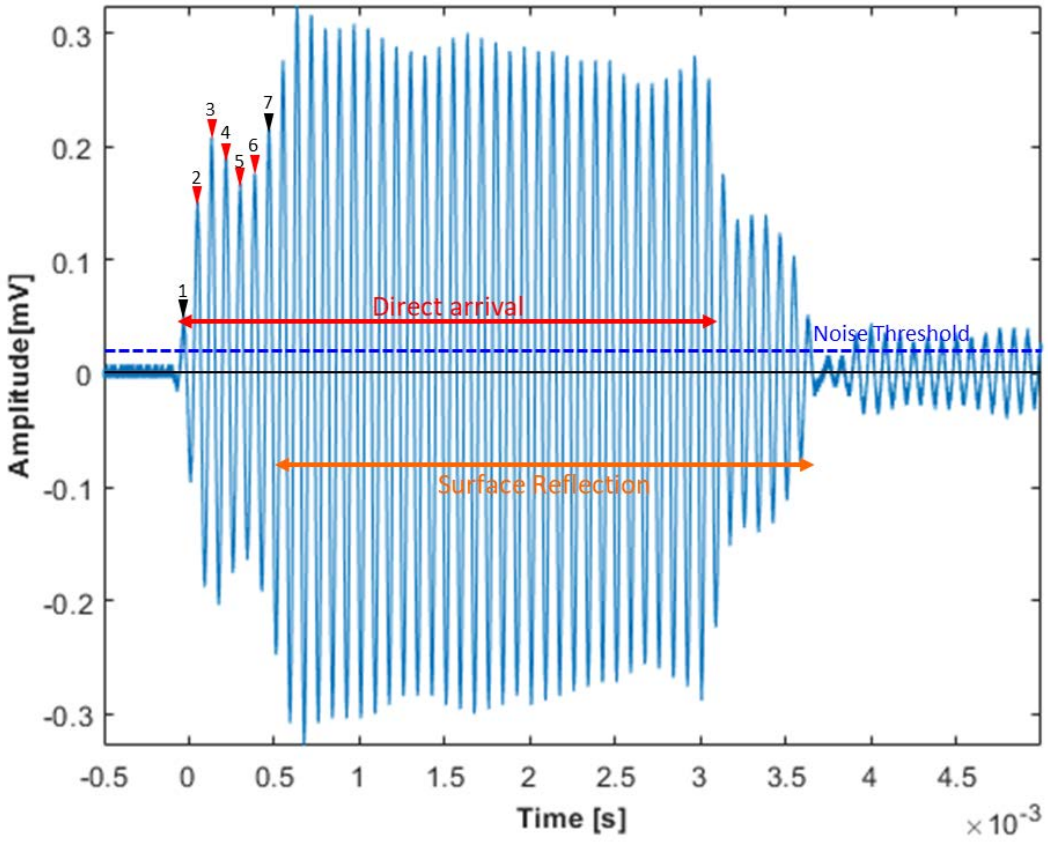

Figure 52. Example of Recorded Signal

As has been explained, during these measurements the DAT-transducer was pinging and therefore the resulting beam patterns are actually showing radiation patterns, rather than relative receive sensitivity patterns, which was the pattern of interest. Due to system restrictions, no experiment could be generated to measure receive patterns. However, we can assume reciprocity, and therefore assume that the receive patterns are very similar to the beam patterns measured.

4. Corrections

As mentioned in Section 2, the way the tow body was mounted created an offset between the axis of rotation and the acoustic center of the ceramic ring in the DAT-transducer. Figure 53 shows in detail which corrections were needed. First of all, notice the range correction. When the tow body orientation was zero, facing the hydrophone, the acoustic center was actually closer to the hydrophone than the constant distance between the axis of rotation and the hydrophone. As the figure indicates, the corrected range varies by increment angle between $R_{axis} \pm r$. Spherical spreading was used to calculate the transmission loss correction, as

$$TL_{corrected} = 20 \cdot \log_{10}\left(\frac{R_{corrected}}{R_{axis}}\right). \tag{17}$$

Secondly, an angle correction was needed. Figure 53 shows this correction was between zero and α degrees. The actual angle the averaged receive voltage corresponds to is not β, but β+α, where the angle α can be calculated as

$$\alpha = \arcsin\left(\frac{r \cdot \sin(\beta)}{R_{corrected}}\right). \tag{18}$$

The measured offsets (r) for the September and April configurations were 1.3 cm and 9.6 cm, respectively.

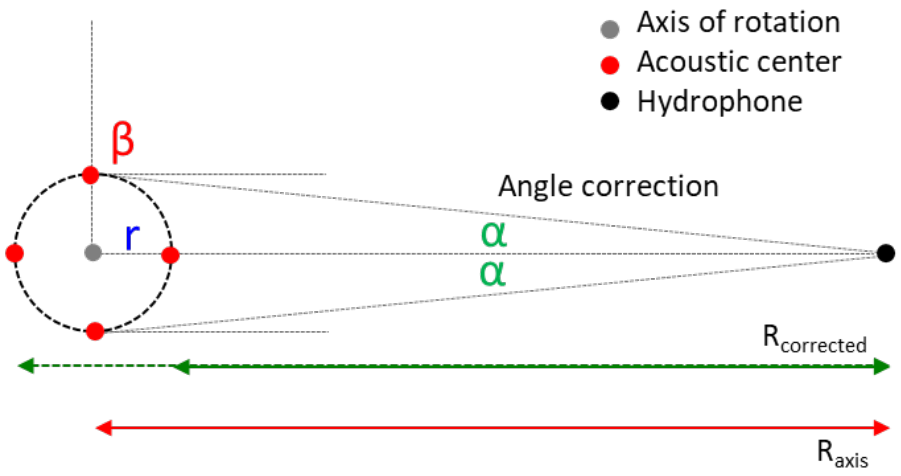

Figure 53. Correction Due to Axes Offset

D. RESULTS

Figure 54 and Figure 55 show the plotted results of the beam pattern measurements. The shown beam patterns are presented in the same orientation they had during the sea trials. Furthermore, the beam patterns show the normalized receive voltage (converted to decibels) for each five degree increment. The degree scale shows grazing angles, where positive angle are facing downward and negative angles upward.

1. X-axis

Figure 49 sketches how the tow body configurations were rotated around the x-axis. The x-axis is a relevant direction, since it represents sending and receiving range-request from and to targets at broadside.

In Figure 54, besides the beam pattern, a colored overlay is presented. This overlay presents which beams are relevant for estimating ranges at short (<200 m), medium (200 m-900 m) and long (>900 m) ranges, as discussed previously. Notice that the strongest beam in the September configuration is pointed fully downward. This is only relevant for very short ranges (<25 m) and not in accordance with the radiation patterns provided by Teledyne Benthos. The receive level in the more relevant beams (corresponding to medium and long range) show at least a 6 dB lower sensitivity. Notice as well that the variance in

the levels at relevant ranges is big (about 4 dB). There seem to be nulls present around 30 degrees downward grazing angles, which can still correspond to a very relevant range.

When compared to the April configuration the difference is immediately visible. The strongest beams of the transducer are now fully exposed and even 5dB stronger than the downward beam, which is similar to what was observed in the manufacturer's beam pattern. Within the relevant beams the variation is limited, about 1 dB. Only at beyond 30 degree grazing angles do the beam patterns start to significantly decline.

2. Y-axis

As mentioned before, the omni-directional part of the DAT-transducer is a ceramic ring. In normal circumstances, a ring would produce a symmetric beam pattern. No difference should be expected between rotations around the x-axis versus the y-axis. In this case, however the tow body is, over its full length, situated within the beam pattern. This was not the case for the rotation axis discussed in the previous section. The Y-axis rotation beam pattern is most relevant when targets are located in the forward and rear sections of the tow body.

Figure 55 shows again the beam pattern and the previously discussed overlay. Notice that the effect of the tow body result in a big decrease in receive levels compared to the main (down facing) beam. At medium ranges, the receive level is at least 10 dB less than the receive level straight down (90 degree). For longer ranges, this level rapidly decreases further to between -20 dB and about -25dB for maximum ranges.

In the April configuration's beam pattern, the effect of the tow body is very visible. The entire 'top half' of the main beams in Figure 54 are completely gone. The tow body even seems to act as a baffle, since the nulls, which were previously measured around 30 degrees, are now visible around 60 degrees. There is, however, still significant energy in the relevant beams, especially at shorter ranges. As we saw with the September configuration, the variation along the degree increments is far more significant than was observed during rotations around the x-axis. At long ranges, a 12 dB decrease is signal is observed.

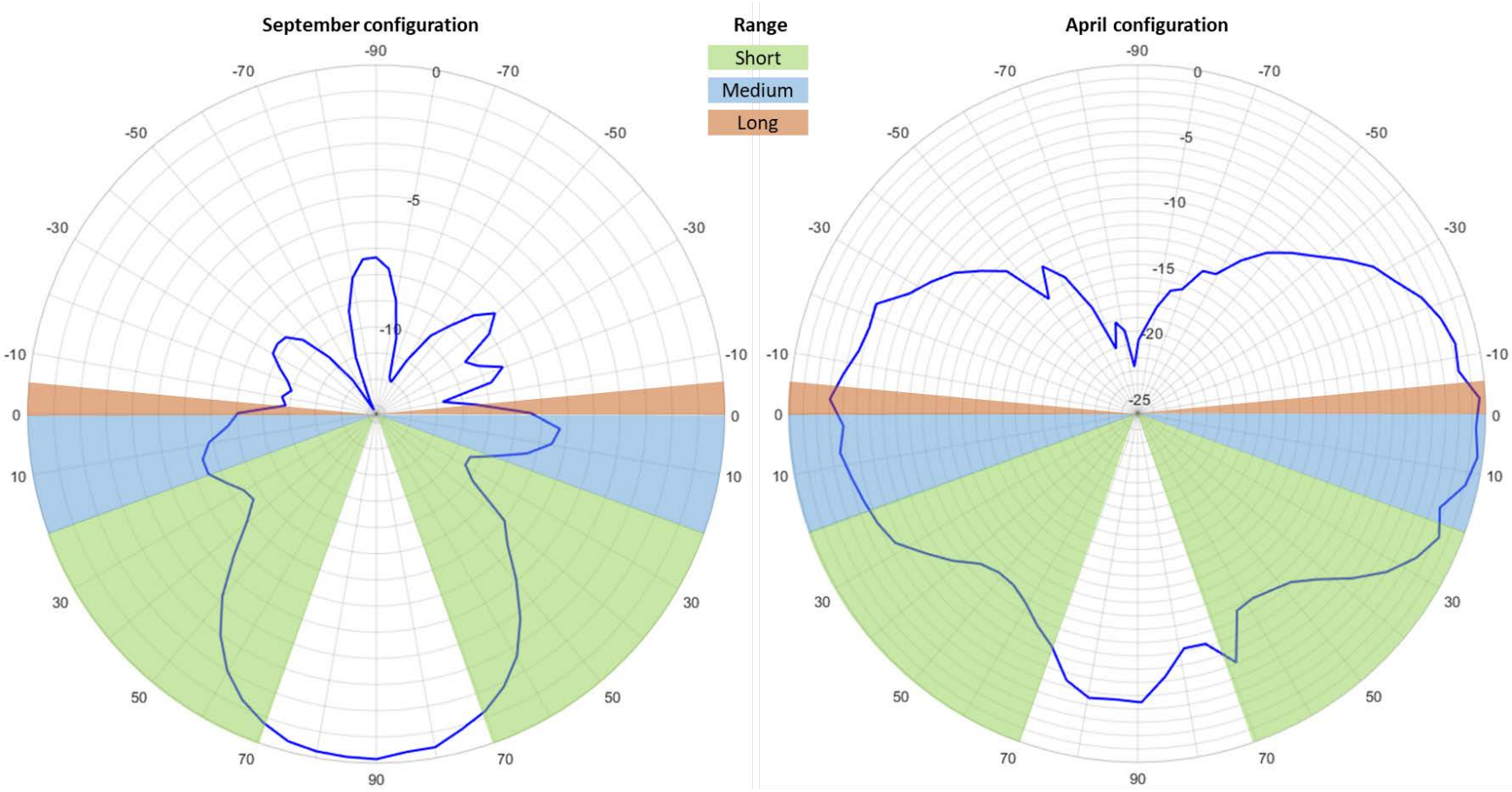

Figure 54. Vertical Beam Patterns for Rotation around the X-axis

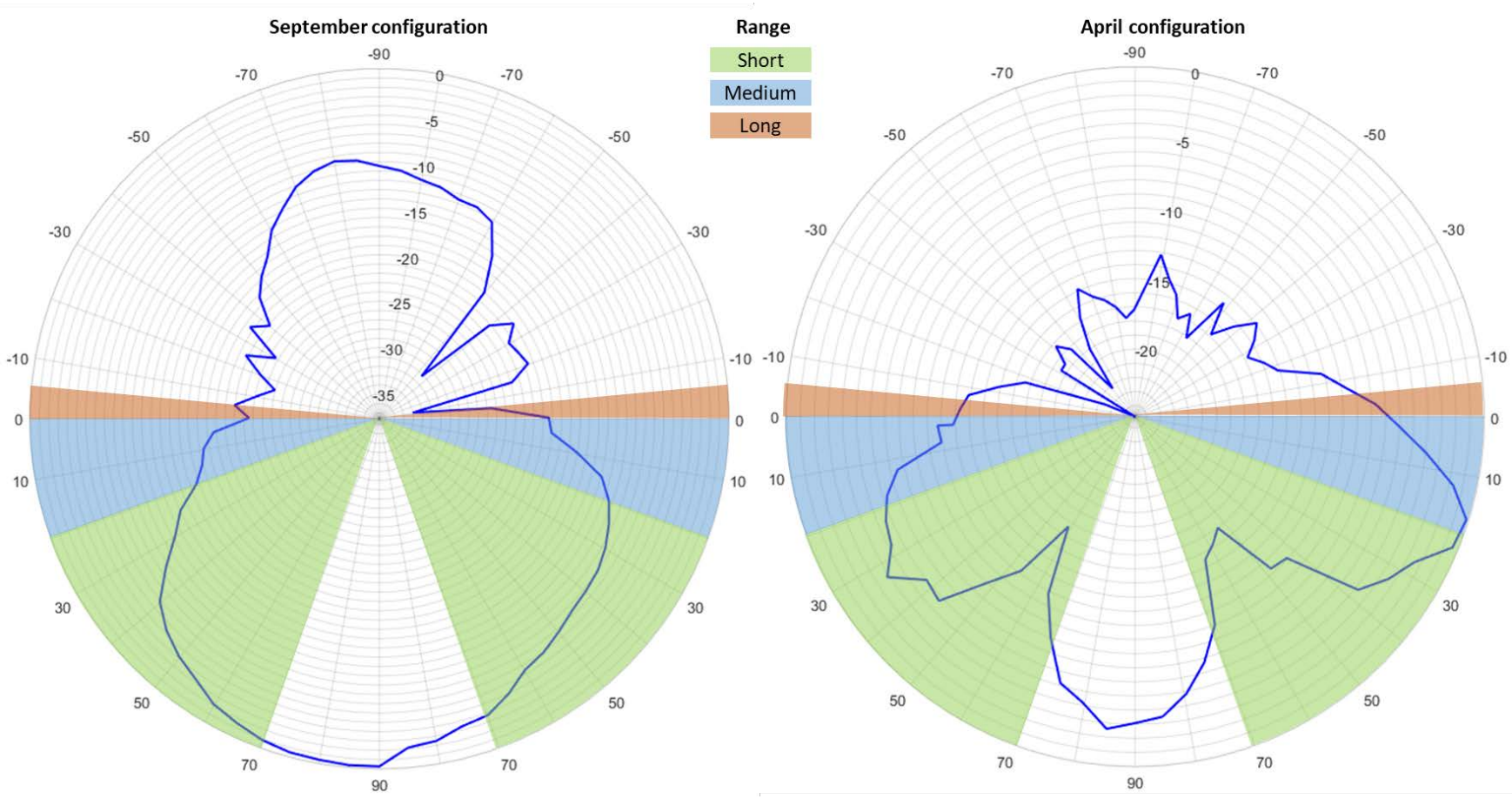

Figure 55. Vertical Beam Patterns for Rotation around the Y-axis

E. CONCLUSIONS

The discussion in the previous section provides very clear conclusions. First of all, based on the beam patterns, the April configuration should perform much better than the September configuration, especially at medium and long ranges. The April configuration should, at these ranges, perform almost an order better than the September configuration. Secondly, comparing rotation around the x- and y-axis, the tow body again hugely influences the beam patterns. Again, the effect should be most noticeable at medium and long ranges. At these ranges, it is highly desirable to maintain a broadside orientation towards the target. Thirdly, the manufacturer supplied beam patterns do (qualitatively) seem to fit the April configuration. The September configuration's beam pattern does not resemble the pattern provided by Teledyne Benthos. This again illustrates the huge influence the tow body potentially can have on the performance of the system. Therefore, very careful considerations should be made whenever a transducer is integrated in a tow body.

THIS PAGE INTENTIONALLY LEFT BLANK

VIII. CONCLUSIONS

As mentioned in Chapter I, the main objective of this thesis was to evaluate the role underwater acoustic modems can play in improving underwater navigation accuracy of submerged assets. Therefore, a specific system was thoroughly evaluated in a real world scenario. This final chapter will discuss the specific results found, using the Teledyne Benthos system, and build on these results to draw general conclusions. Besides these conclusions, several recommendations will be presented. While discussing these subjects, the research questions as formulated in Chapter I will be answered.

In Chapter V it was shown that, when an acoustic modem is properly configured, it is a very capable instrument to establish a range between two platforms. Especially when the location of one platform is very accurately known, the ranging routine in an acoustic modem can most probably improve the navigation of a UUV without interfering with the UUV's mission (e.g., surface to update the navigation by obtaining a GPS-fix). Ranging via acoustic modems can, for example, assist in updating the UUV's inertial navigation system. Examples of applications include a fixed bottom node, with accurately known position, or a (near) surface node with a GPS receiver, both exchanging ranges with a mobile unmanned platform.

In the same chapter, it was also shown that the ranging routine used by Teledyne Benthos could be improved. Presently the ranging routine estimates the range on its strongest arrival. As shown in Section V.C, the strongest arrival is, however, not always the direct path arrival. Even at relatively short ranges and in shallow water, the range difference between the strongest and first arrival can be 60 cm. Vio showed in his dissertation comparable results for more complicated scenarios. He proved that even bigger range corrections are possible [3]. Therefore, it is recommended to use the first arrival well above the noise level to estimate ranges between nodes.

Another way to improve the estimated range between two nodes is to take into account the refracted path instead of using the straight line approximation to establish the

horizontal range. This was also suggested by Vio [3], but is understood to require local measurements of the SSP.

In order to ensure successful range requests, the range between nodes should not be too large. It is highly recommended to use acoustic prediction models to establish the maximum expected operating range for a specific system. For the frequencies and system used in this thesis, the Bellhop ray tracing model proved to be useful.

As shown in this thesis, it seems possible to improve the maximum range at which successful range requests can be executed. In order to do so, multi-path arrivals from the second arrival group could be used. Further research would be required to successfully implement this. One major hurdle to overcome would be to establish, in real-time and at the modem-level, which path belongs to which arrival. As shown in several examples in Section V.C.2, Bellhop was able to accurately predict individual arrivals. However, the same section also shows that very accurate knowledge of the environment is required to do so. A first step to create this knowledge is to compare the (Bellhop) arrival predictions with the matched filter output and, therefore, improve the environmental data feeding into the prediction model. In order to use this approach, accurate initial conditions should be known. The most important initial conditions are the depth of the receiver and transmitter and the horizontal range between them.

As discussed in Chapter VI it is recommended to use (additional) depth, heading, roll and pitch sensors when operating a UUV. Understanding the way a UUV swims through the water column greatly assists in interpreting the results and errors in the obtained ranges.

This thesis also showed that the bearing accuracy, in real world scenarios using the acoustic modem under evaluation, was not yet at a level which enables it to improve UUV navigation. During the executed sea trials, part of the accuracy problem might have been associated with the specific system used. The conclusion is, however, that the bearing problem is far more complicated and bearing solutions acquired by acoustic modems should therefore be examined with great care before implementation in navigation solutions.

The beam pattern measurements in Chapter VII show the importance of carefully considering beam patterns while integrating a transducer into an unmanned underwater platform. The observed influence of the vehicle on the beam pattern was very significant. As a general rule, it seems that exposing the transducer section as much as possible will improve the radiated power and receive sensitivity. Especially at larger ranges, proper integration will ensure use of the full beam pattern of the transducer and therefore improve the signal to noise ratio (SNR) of range requests. A better SNR will subsequently improve the matched filter output. This would result in more successful range requests. More successful range requests will potentially provide a better range update rate and would therefore improve UUV navigation.

Another way to improve SNR of the range requests is to ensure the UUV maintains a broadside orientation towards the ranging beacon (in the case of this thesis' sea trials, the echo repeater). As shown in Chapter VII, the receive sensitivity at broad side was observed to be much greater than in the forward or rear sections of the vehicle. Especially at larger ranges, when smaller or negative grazing angles are required, the assessed effect will be significant.

THIS PAGE INTENTIONALLY LEFT BLANK

LIST OF REFERENCES

[1] D. R. Blidberg, “The Development of Autonomous Underwater Vehicles,” Autonomous Undersea System Institute, 2001. [Online]. Available: http://ausi.org/publications/ICRA_01paper.pdf

[2] Teledyne Benthos, ATM-900 Series Acoustic Telemetry Modems User Manual P/N M-270-26, Rev. F, North Falmouth, MA: Teledyne Benthos.

[3] R. P. Vio, “Improved UUV Positioning Using Acoustic Communications and a Potential for Real Time Networking and Collaboration,” Ph.D. dissertation, Dept. of Physics, Naval Postgraduate School, Monterey, CA, USA, 2017 [Online]. Available: https://calhoun.nps.edu/handle/10945/55517

[4] J. Borden, Manager Government Acoustic Systems at Teledyne Benthos, telephone conference, 9 February 2018.

[5] M. J. Hahn, “Undersea Navigation via Distributed Acoustic Communications Network,” M.S. Thesis Dept. of Physics, Naval Postgraduate School, Monterey, CA, USA, 2005 [Online]. Available: https://calhoun.nps.edu/handle/10945/2141

[6] J. Borden, email, 10 Januari 2018.

[7] F. B. Jensen, W. A. Kuperman, M. B. Porter and H. Schmidt, *Computational Ocean Acoustics*, 2nd ed., New York, NY: Springer, 2011.

[8] “Ocean Acoustics Library,” Heat, Light and Sound Research, Inc., [Online]. Available: http://oalib.hlsresearch.com/

[9] M. B. Porter, “The BELLHOP Manual and User’s Guide,” Heat, Light and Sound Research, 31 January 2011. [Online]. Available: http://oalib.hlsresearch.com/Rays/HLS-2010-1.pdf

[10] “Liquid Robotics - A Boeing Company,” Liquid Robotics, [Online]. Available: http://www.liquid-robotics.com

[11] E. Hamilton, “Geoacoustic Modelling of the Sea Floor,” *Journal of the Acoustical Society of America*, Vols. 68, no. 5, pp. 1313–1340, August 1980

[12] “Tides and Currents,” NOAA, September 2017. [Online]. Available: https://tidesandcurrents.noaa.gov/waterlevels.html?id=9413450.

[13] Harvard University, “A Summary of Error Propagation,” Fall 2007. [Online]. Available: http://ipl.physics.harvard.edu/wp-uploads/2013/03/PS3_Error_Propagation_sp13.pdf

[14] Federal Communication Commision, “Reference Points and Distance Computations,” 2011. [Online]. Available: https://www.gpo.gov/fdsys/pkg/CFR-2011-title47-vol4/pdf/CFR-2011-title47-vol4-sec73-208.pdf

[15] G. C. Cavell, *National Association of Broadcasters Engineering Handbook*, 11 ed., Focal Press / NAB, 2017.

[16] L. E. Kinsler, A. R. Frey, A. B. Coppens and J. V. Sanders, *Fundamentals of Acoustics* 4th ed., Hoboken, NJ: John Wiley & Sons, 1999.

[17] Space and Naval Warfare Systems Command, *Automated Acoustic Survey Quick Guide*, San Diego, CA.

INITIAL DISTRIBUTION LIST

1. Defense Technical Information Center
   Ft. Belvoir, Virginia

2. Dudley Knox Library
   Naval Postgraduate School
   Monterey, California